GFZ

POTSDAM

Helmholtz-Gemeinschaft

Fei-peng Zhang, Johann Wünsch, Tilo Schöne,
Tonie van Dam, Gerd Gendt, Mao-rong Ge

Vertical Crustal Motion at Tide Gauges Derived by analyzing GPS time series

Scientific Technical Report STR08/03

Vertical Crustal Motion at Tide Gauges Derived by Analyzing GPS Time Series

Fei-peng Zhang, Johann Wünsch

(Department of Geodesy and Remote Sensing, GeoForschungsZentrum Potsdam)

Tonie van Dam

(Physics and Material Research Unit, University of Luxembourg)

Gerd Gendt, Mao-rong Ge, Tilo Schöne

(Department of Geodesy and Remote Sensing, GeoForschungsZentrum Potsdam)

Abstract

This report studies the vertical crustal motion at tide gauges by analyzing GPS (Global Positioning System) height time series of about 370 GPS stations spanning 1994.0 to 2007.0. The procedure of generating a set of homogeneous GPS time series is described in detail. To estimate the vertical rate, the time series are modelled with seasonal (annual and semiannual) waves and step functions for jumps.

To improve the quality of the time series, the ocean tide loading (OTL) corrections are renovated by replacing the OTL corrections derived from new ocean tides model directly on the solutions without re-analyzing the GPS data. The algorithm of replacement of OTL corrections is derived in detail. To evaluate the effect of the error of OTL corrections, the aliased signal in daily solutions are analyzed theoretically.

To further improve the quality of GPS time series, atmospheric pressure loading (ATML) induced displacement is corrected to reduce color noise in the GPS time series. To stabilize the reference frame, the ATML corrections are applied on the loosely-constrained solutions before Helmert transformation. The linear regression analysis reveals that the GPS stations most influenced by ATML displacement are located in the northern hemisphere with latitudes higher than 30 degrees. The effect of ATML corrections on vertical rate estimates could reach 1 mm/a, which is already at the level of accuracy required by the oceanographic community.

When studying vertical crustal motion using GPS, the reference frame's stability is crucial. Therefore, this report studies the stability of the reference frame realized by the GPS solutions. The emphasis of the study is laid on scale factors. This study reveals that the scale factor of the reference frame realized implicitly by the GPS solutions has non-regular change accompanied by the update of the GPS constellation. This could be caused by inconsistent antenna phase center offset of satellite transmitters used in the data analysis.

Finally the vertical rates are derived by fitting the GPS time series based on the above mentioned improvements. While inspecting the GPS time series, the nonlinear and inter-annual variations in the time series are noticed. These time series need further closer inspection if they are to be used properly by the oceanographic community.

DOI: 10.2312/GFZ.b103-08037

Scientific Technical Report 08/03 Deutsches GeoForschungsZentrum GFZ

Contents

DOI: 10.2312/GFZ.b103-08037

Scientific Technical Report 08/03 Deutsches GeoForschungsZentrum GFZ

DOI: 10.2312/GFZ.b103-08037

List of Tables

DOI: 10.2312/GFZ.b103-08037

DOI: 10.2312/GFZ.b103-08037

List of Figures

DOI: 10.2312/GFZ.b103-08037

DOI: 10.2312/GFZ.b103-08037

DOI: 10.2312/GFZ.b103-08037

DOI: 10.2312/GFZ.b103-08037

DOI: 10.2312/GFZ.b103-08037

DOI: 10.2312/GFZ.b103-08037

1 Introduction

Global sea level change has been studied for several decades with increasing concern over its far-reaching effects on our planet. To precisely quantify the rate at which the sea level is changing, multidisciplinary efforts have been made including ground and space observations, ice mass transfer, ocean modelling and glacial isostatic adjustment. With their direct connection to sea level rise and long observation history, tide gauge records can uniquely benefit this study. One inevitable problem with using tide gauge records for studying sea level change is the effect of vertical crustal motion at tide gauge benchmarks, which would directly affect the result inferred from tide gauge records. A commonly used method is to model post-glacial rebound and make the correction on the tide gauge records. Nowadays, with its improved accuracy, continuous GPS has been becoming a promising approach to monitoring the vertical land motion at tide gauges. This probability motivated the launch of an IGS pilot project, TIGA, which is concentrating on monitoring the tide gauge benchmarks by continuous GPS with an accuracy of better than 1 mm/a. Within the frame of IGS TIGA Pilot Project and with financial support from the SEAL Project, 13 years of GPS data at tide gauges were analyzed at GFZ[50]. With these long-period high accuracy GPS solutions, it is possible to monitor the vertical crustal motion at globally distributed tide gauges with significant accuracy.

To gauge the uplift rate, we can consider two approaches[9]. One approach combines the normal equations from all solutions (e.g. spanning several years) and estimates site velocities for all stations together. The advantage of this approach is that the full covariance matrix is used, hence all correlations are taken into account. Aside from significant computational burden, its primary disadvantage is that any outlier or misfit of one site will affect the estimates of all the other sites. Another approach is to construct position time series for each site separately from daily (or weekly) solutions, and to obtain station motion rate by fitting the time series. The advantage of this approach is that it is easier to detect and handle the position outliers (e.g., from instrumental effects) of each time series. Any misfit of one time series (e.g., local nonseasonal variations or series offsets) will not affect the estimates of the other sites. The weakness of this approach is that the correlation between each time series is neglected. However, Zhang (1996) showed that these correlations are small. Considering that outliers and misfits may be the primary error sources affecting the motion rate estimates, we adopt the latter approach by constructing daily time series.

To get high accuracy GPS time series with less well-known signals and consequently to improve the velocity estimates from time series, some improvements could be carried out on the existing GPS solutions. In the scheme of GPS data processing for TIGA and SEAL projects[50], ocean tide loading model FES95.2 was used without considering long-period constituents. This can be improved by considering the effects of long-period constituents and even with the most state-of-the-art ocean loading model, e.g. GOT00.2 or FES2004. Additionally, atmospheric loading pressure displacements could be considered to improve the quality of GPS time series[44].

To accurately estimate the station vertical velocities, the scale stability of the

DOI: 10.2312/GFZ.b103-08037

reference frame is critical, since the long-term scale change could be interpreted as vertical motion of the ground stations. In this report, the stability of reference frame will also be studied.

DOI: 10.2312/GFZ.b103-08037

2 GPS time series

2.1 GPS solutions and construction of time series

2.1.1 GPS network and general procedure of time series construction

The data of about 370 GPS stations from 1994 to 2006 were analyzed at GFZ for TIGA and SEAL projects, among which about 180 stations are TIGA observing stations (TOS), and 335 stations have valid solutions. The geographical distribution of the analyzed GPS stations is illustrated in Figure 1. Note that in TIGA/SEAL cluster, some inland stations are also included for the purpose of:

1. stabilizing the reference frame;
2. stabilizing solutions, e.g. for ambiguity-fixing for which denser network is needed to bridge baselines;
3. supporting other studies, e.g. the north American network for studying Glacial Isostatic Adjustment (GIA).

For estimating station velocities, the time series approach is used. To generate daily GPS time series, the daily normal equations of cluster networks from [50] are used. The generation of daily time series is carried out in the following steps (illustrated in Figure 2):

- Combining daily cluster normal equations to get loosely constrained daily solutions in SINEX format;
- Aligning the loosely constrained daily solutions with a terrestrial reference frame (TRF), e.g. ITRF2000[1];
- Generating daily time series of station coordinates (X,Y,Z) in terrestrial reference system (TRS);
- Generating daily time series of station coordinate residuals (ΔX, ΔY, ΔZ) in TRS;
- Transforming the daily time series from TRS to local topocentric coordinate system, (Δe, Δn, Δu).

2.1.2 Loosely constrained daily solutions

At first, the cluster normal equations are combined to daily normal equations. Then, the daily normal equations are solved with loose constraints. The solutions of station coordinates and Earth rotation parameters (ERP) are written into SINEX files with full covariance matrix. While generating SINEX solutions, station coordinates are loosely

DOI: 10.2312/GFZ.b103-08037

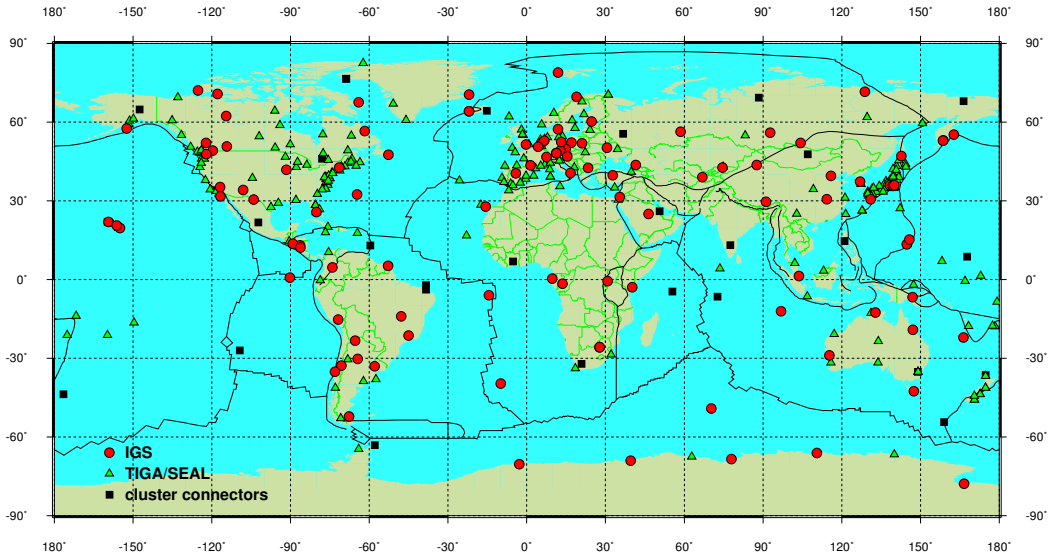

Figure 1: GPS network processed at GFZ for TIGA and SEAL. Some IGS stations that are used for TIGA purpose still marked as IGS sites.

constrained by specifying the stabilization factors s_i (see Eq. (18) of [50]) as 7 for all the stations.

The full SINEX files are bulky for our purpose due to their large size. For the networks of $25 \sim 260$ stations, the size of the SINEX files could be $3 \sim 38$ megabytes (MB). In the later stages, several operations will be applied directly on the SINEX files. This will require several copies for each SINEX file. For the daily SINEX files of more than a decade, each copy takes considerable storage space. Additionally, large SINEX files make the subsequent operations more time-consuming. To save storage space and to operate swiftly, the SINEX files are reduced to keep only the station coordinate estimates and the correlation information among the coordinate components of each station. The correlation information among stations is ignored. By the reduction, the file size can be reduced dramatically without losing information necessary for generating time series. For example, for the day 2006 309, the size of the SINEX file is reduced from 32.309 MB to 0.13 MB. After reduction, the original SINEX files could be archived.

2.1.3 Alignment with ITRF

The time series should be generated in a unified reference frame. However, the loosely constrained solutions are not in any reference frame since no reference stations are fixed while solving the daily normal equations. To generate homogeneous time series, the loosely constrained daily solutions are aligned with ITRF. The alignment is realized by transforming the daily solutions to ITRF by 7-parameter Helmert transformation as follows,

$$\begin{bmatrix} X \\ Y \\ Z \end{bmatrix}_{\mathrm{ITRF}} = \left(\begin{bmatrix} t_X \\ t_Y \\ t_Z \end{bmatrix} + \begin{bmatrix} 1 & r_Z & -r_Y \\ -r_Z & 1 & r_X \\ r_Y & -r_X & 1 \end{bmatrix} \cdot \begin{bmatrix} X \\ Y \\ Z \end{bmatrix}_{\mathrm{loosely}} \right) \cdot (1+s) \ , \qquad (1)$$

DOI: 10.2312/GFZ.b103-08037

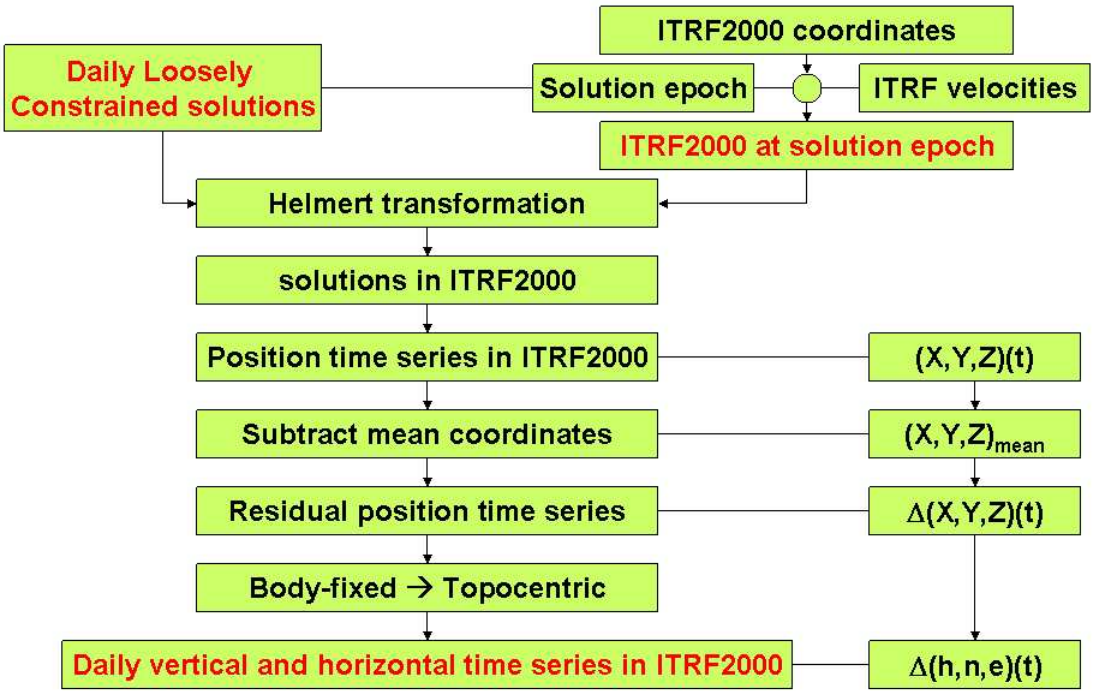

Figure 2: Procedure of forming GPS time series.

in which subscripts "ITRF" and "loosely" indicate the coordinates in ITRF and in loosely constrained frame in meters; t_X, t_Y, t_Z are translation components in meters; r_X, r_Y, r_Z are rotation angles round axes X, Y and Z in radian; s is the dimensionless scale factor. Here, we choose ITRF2000 as the reference frame. Totally, 111 globally distributed high-quality core stations (see figure 3) are used for estimating the 7 parameters. Before transformation, the reference station coordinates given in ITRF2000 are mapped to the epoch of the transformed daily solution by site velocities attached in ITRF2000 solution. The number of core stations used in Helmert transformation for each day are plotted in Figure 4. For the low number of stations shortly after 2003, there must be something wrong for those day. However, they do not dominate and distort the statistics.

2.1.4 Generation of GPS time series

The position time series $(X_i,\ Y_i,\ Z_i)^g$ for the station g is then constructed from the daily coordinates in ITRF2000 obtained above. Here, the subscript i indicates time in days. After subtracting the mean coordinate $(\overline{X},\ \overline{Y},\ \overline{Z})^g$ of the station g from its daily coordinate estimates $(X_i,\ Y_i,\ Z_i)^g$, we get a time series of position residuals $(\Delta X_i,\ \Delta Y_i,\ \Delta Z_i)^g$ in body-fixed reference system. Then, the time series in east, north

DOI: 10.2312/GFZ.b103-08037

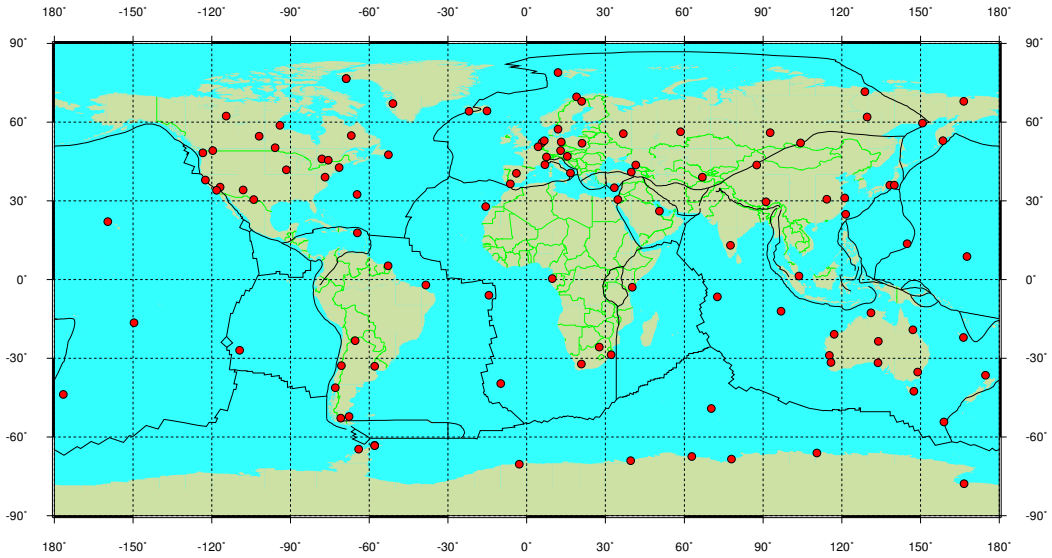

Figure 3: Selected reference stations for aligning solutions with reference frame ITRF2000.

and height components $(\Delta e_i,\, \Delta n_i,\, \Delta h_i)^g$ can be obtained by transforming the residual vector $(\Delta X_i,\, \Delta Y_i,\, \Delta Z_i)^g$ from body-fixed to the local topocentric coordinate system. The transformation formulae are as follows

$$\begin{bmatrix} \Delta e \\ \Delta n \\ \Delta h \end{bmatrix} = \begin{bmatrix} -\sin\lambda & \cos\lambda & 0 \\ -\cos\lambda\sin\phi & -\sin\lambda\sin\phi & \cos\phi \\ \cos\lambda\cos\phi & \sin\lambda\cos\phi & \sin\phi \end{bmatrix} \cdot \begin{bmatrix} \Delta X \\ \Delta Y \\ \Delta Z \end{bmatrix} = \Phi \cdot \begin{bmatrix} \Delta X \\ \Delta Y \\ \Delta Z \end{bmatrix}, \quad (2)$$

in which λ and ϕ are the station longitude and latitude, respectively. Here, the vertical direction is defined as the radial direction from Earth's center but not the normal direction of ellipsoid. Note that we are only interested in height variations which are not larger than a few centimeters and are thus insensitive to the definition of the local vertical direction.

The error information could be also transformed. According to the law of variance-covariance propagation, the correlation information among X, Y and Z is used to propagate the error of $(\Delta X,\, \Delta Y,\, \Delta Z)$ as the error of $(\Delta e,\, \Delta n,\, \Delta h)$ as follows

$$D_{\mathrm{enh}} = \Phi D_{\mathrm{xyz}} \Phi^T \ . \quad (3)$$

Here, D_{enh} and D_{xyz} are the covariance matrices for position residual vectors in topocentric and body-fixed coordinate systems, respectively; superscript T indicates transpose operation. D_{xyz} comes from the covariance block of a SINEX file.

Examples of the GPS height time series for stations ALBH and STJO are given in Figures 5 and 6. The time series are fitted using Least-Squares method with constant, linear trend, seasonal (annual and semi-annual) waves and identified offsets. The vertical rates in the figures are estimated from raw time series without editing any outliers.

DOI: 10.2312/GFZ.b103-08037

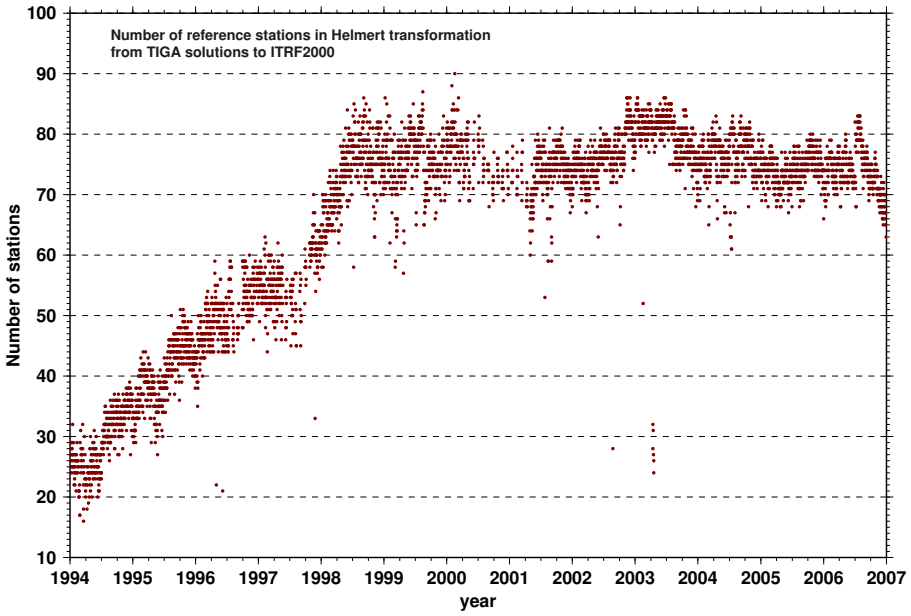

Figure 4: The number of core stations for each day in analysis used to align TIGA solutions to ITRF2000.

2.2 Statistical information about GPS time series

Some statistics are made to measure the quality of the GPS time series, including length, point density, and balance index of time series.

The length of a time series L_{TS} is defined as the years spanning from the first to the last data point. The length of a time series is critical in achieving a reliable linear trend estimate.

The density of a time series concerns data gaps. Normally a denser time series is more robust to derive a reliable linear rate. Here, the density of a time series is defined as

$$\rho_{\mathrm{TS}} = N_{\mathrm{DP}}/L_{\mathrm{TS}} \ , \tag{4}$$

in which N_{DP} is the number of daily data points, L_{TS} the length of time series in days.

The balance of a time series, which includes non-linear signals, is also important in achieving a reliable linear rate estimate, since the condensed part of the time series could dominate the estimation. To inspect the balance of the time series, we define here the balance index n_{BI} as

$$n_{\mathrm{BI}} = (N_{2\mathrm{h}} - N_{1\mathrm{h}})/N_{\mathrm{DP}} \ , \tag{5}$$

in which $N_{1\mathrm{h}}$ and $N_{2\mathrm{h}}$ are the numbers of data points before and after the middle point of the time series, i.e., first and second halves, respectively. A zero value of n_{BI} indicates an absolute balanced time series. A positive value of n_{BI} implies that the second half has more data points than the first half, and vice versa.

Table 7 in Appendix A (see page 70) lists the statistical parameters for the GPS time series generated in this study, including the starting and end date of the time

DOI: 10.2312/GFZ.b103-08037

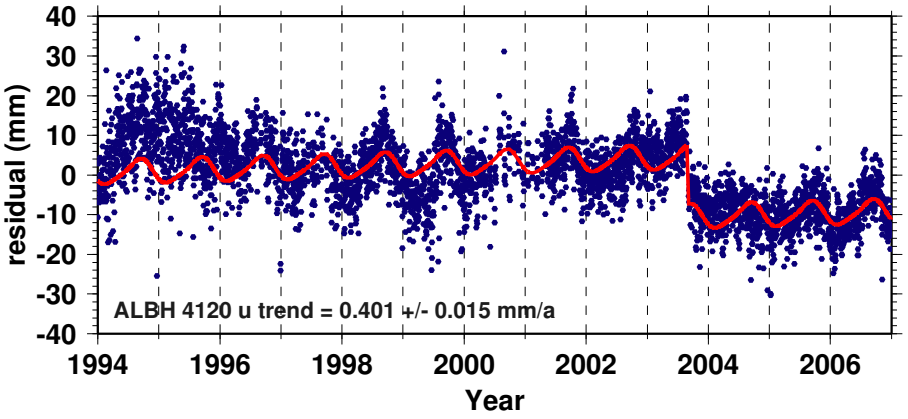

Figure 5: Height time series for GPS station ALBH (Albert Head; Victoria, Canada) derived from GFZ TIGA solution. NOTE: The vertical velocity demonstrated in the figure is estimated by applying identical weights for all the data points (same for the following illustration figures). The final vertical rates given in table 9 are taken from the final iteration after re-weighting the data points according to their fitting residuals.

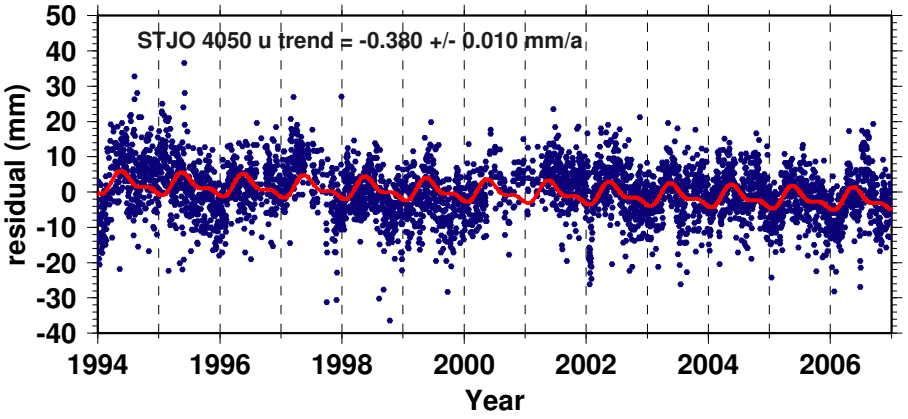

Figure 6: Height time series for GPS station STJO (St. John's; Newfoundland and Labrador, Canada) derived from GFZ TIGA solution.

series, the length of time series in years and days, the total number of daily data points, the density of time series, the numbers of data points before and after the middle point, the balance index of the time series.

2.3 Modelling the GPS time series

To estimate the vertical velocities of the GPS stations by fitting the GPS time series, the time series must be modelled properly. In this study, a GPS time series is modelled with seasonal waves including annual and semi-annual periods, offsets as step functions, constant bias and linear trend. This parameterization strategy is based on the following considerations.

Seasonal signals are obviously visible in most GPS height time series. An example

DOI: 10.2312/GFZ.b103-08037

is given in Figure 7 for station CAGL. As studied by Dong et al.[9], Zhang et al.[49] and Blewitt et al.[4], the seasonal waves should be modelled. Additionally, offsets exist in many GPS time series caused by antenna exchange, earthquake, and so on. An example is given in Figure 8 for station ALIC. These offsets can be modelled as step function.

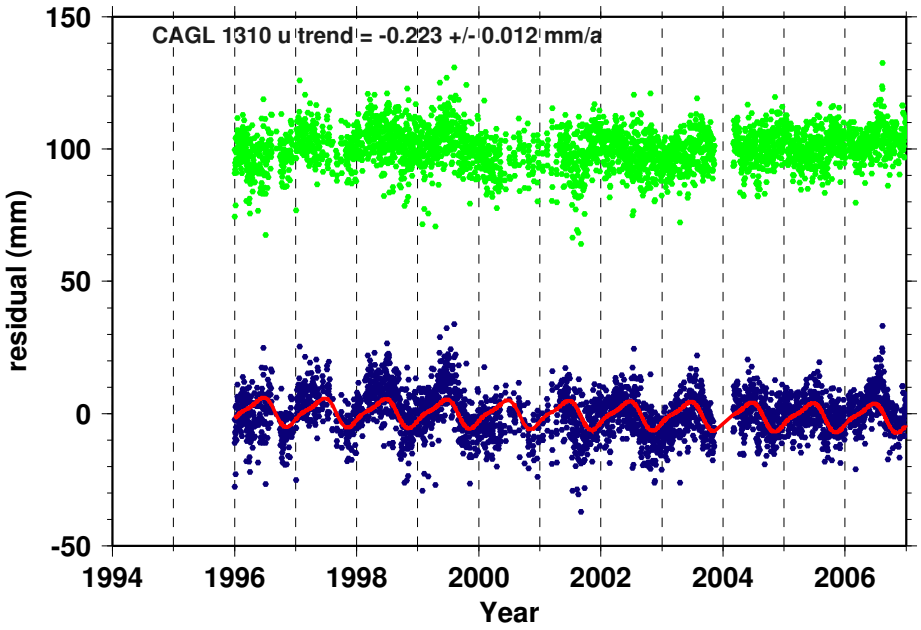

Figure 7: Fitting the height time series of the GPS station CAGL (Cagliari - Astronomic Station, Italy). Blue points: raw data; red line: fitted data; green points: fitting residuals (offset by 100 mm).

To see the influence of modelling seasonal waves, we can compare the estimated vertical velocities between the two cases: with and without modelling seasonal signals. The differences of the vertical rates estimated in the two cases are illustrated in Figure 9. The statistics are made with 271 GPS stations for which time series are longer than 3 years. The figure shows that for the two cases, the vertical rate estimates can differ within a range of 1 mm/a, which is at the same level of accuracy requirement for this study. Therefore, while estimating the linear rates, as a standard, we always fit the time series with seasonal waves, together with bias, linear trend and offset(s) parameters.

In fact, the signals in the GPS time series could not be fully modelled with the above specifications. In the section 5.4, the stations with non-linear, non-periodic, inter-annual signals are listed. For those stations, special studies are necessary to model the time series properly.

DOI: 10.2312/GFZ.b103-08037

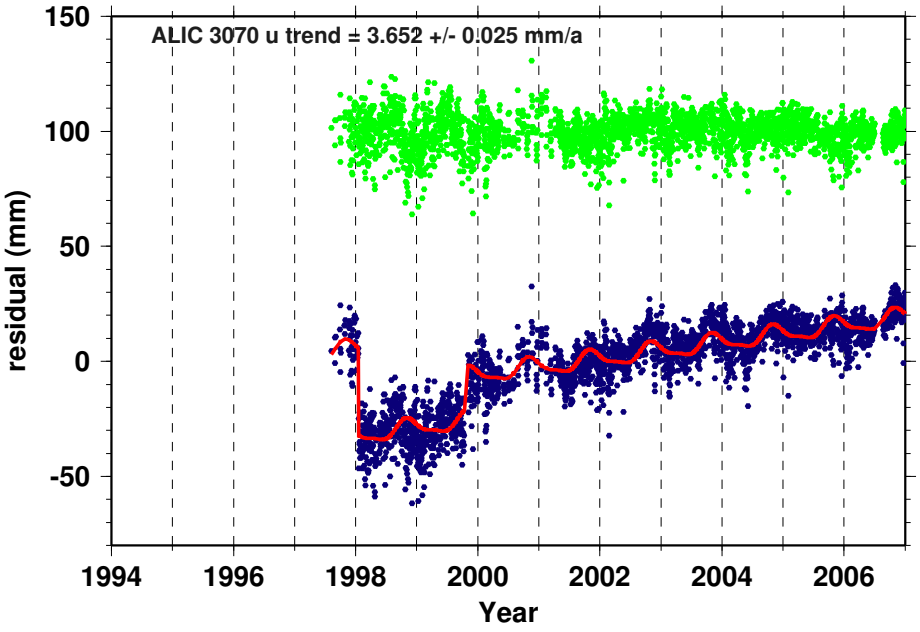

Figure 8: Fitting the height time series of the GPS station ALIC (Alice Springs; Northern Territory, Australia). Legend same as Figure 7.

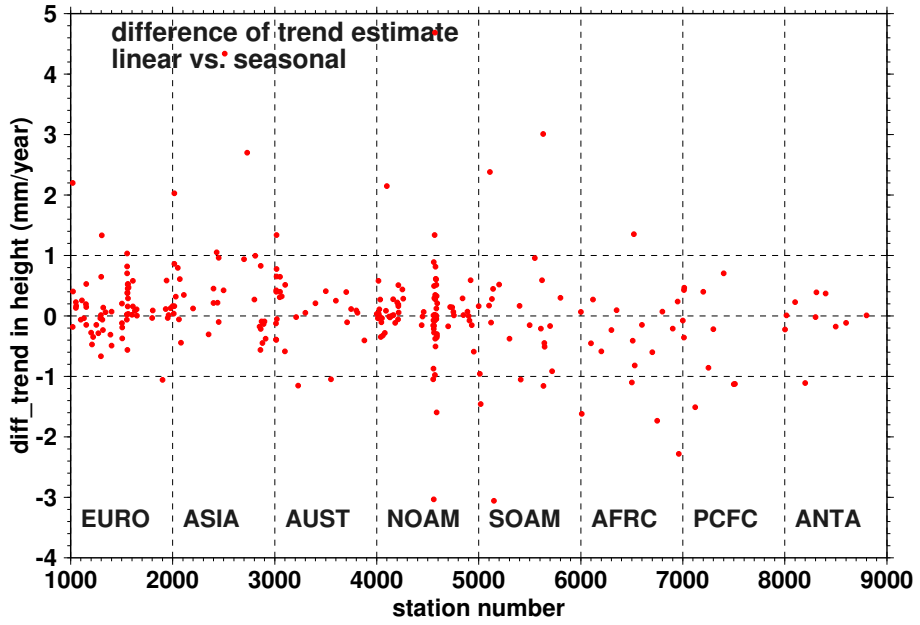

Figure 9: Differences of vertical rate estimates between the cases with and without modelling seasonal signals. Abscissa axis: station numbers (numbering in terms of tectonic plates, internally used by EPOS software for data analysis).

DOI: 10.2312/GFZ.b103-08037

3 Update ocean tide loading corrections

In the data processing for the solutions used in this study, the ocean tide loading correction on site displacement does not consider the long-period tidal constituents as mentioned in [50]. However, for a precise application such as monitoring the vertical motion of tide gauge benchmarks, these terms should be considered according to IERS standards[30]. Additionally, the present ocean loading correction is based on ocean tide model FES95.2, which is already not up to date. For high accuracy applications such as TIGA, applying the correction with a more state-of-the-art model is necessary.

3.1 General principle to apply or replace systematic correction on estimated station positions

Normally, the station position time series is obtained from a year-long data processing. As the procedure of data processing goes on, there may be new models developed to replace the old model, or there may be new physical phenomena that are modelled properly making it possible to employ into data reduction. To apply a new model correction or to replace the old one with a newer one, the most rigorous and straightforward way is to reprocess all the data. However, reprocessing the data consumes much time. A simple way to get the updated results quickly, is to operate directly on the existing solutions afterwards. However, this is not rigorous because station coordinates (especially height) correlate with several other parameters, such as phase ambiguities, satellite and receiver clocks, and tropospheric delay.

For convenient description, we take ocean loading displacement Δc and station coordinate P as example. In GPS data processing, while forming the equation of observation at epoch t_i, the ideal coordinate $P_{\text{ideal},i}$ without the effect of ocean tide loading is corrected by Δc_i to get the instantaneous position $P_{\text{instant},i}$ as follows

$$P_{\text{instant},i} = P_{\text{ideal},i} + \Delta c_i \ . \tag{6}$$

Then, $P_{\text{instant},i}$ is used to form the equation of observation. From the procedure of parameter estimation, we get the estimated value of P_{ideal}, namely $\hat{P}_{\text{ideal}}$, at a weighted time instant which is normally the mid of the data interval for GPS.

If a correction Δc is not applied in the equation of observation, and if the mean of $\{\Delta c_i, i = 1, \cdots, n\}$, $\overline{\Delta c}$, is not zero, which is probably the case for a periodic signal when the adjustment interval is not an integer multiple of the period, then the estimated value is approximately P_{instant}, noted as $\hat{P}_{\text{instant}}$. Our goal is to get the estimate of P_{ideal}, namely $\hat{P}_{\text{ideal}}$. If the estimation procedure has finished and we want to get $\hat{P}_{\text{ideal}}$ by applying the mean correction $\overline{\Delta c}$ on $\hat{P}_{\text{instant}}$, we have the following formula

$$\hat{P}_{\text{instant}} = \hat{P}_{\text{ideal}} + \overline{\Delta c} \ . \tag{7}$$

Accordingly,

$$\hat{P}_{\text{ideal}} = \hat{P}_{\text{instant}} - \overline{\Delta c} \ . \tag{8}$$

DOI: 10.2312/GFZ.b103-08037

Therefore, unlike the estimation procedure, in which the correction Δc is added to the theoretic value (or generally speaking, initial value), here, the correction Δc should be subtracted from the estimated P, namely $\hat{P}_{\rm instant}$, to get the ideal coordinate.

Replacing a correction $\Delta c_{\rm A}$ derived from model A with its replacement $\Delta c_{\rm B}$ from model B on the estimated value, is just like applying a correction of the difference $\Delta c_{\rm B} - \Delta c_{\rm A}$ in terms of the form of the formula (8). The following formulae hold:

$$\begin{aligned} \hat{P}_{\rm ideal,B} &= \hat{P}_{\rm instant} - \overline{\Delta c}_{\rm B} && (9)\\ &= \hat{P}_{\rm ideal,A} + \overline{\Delta c}_{\rm A} - \overline{\Delta c}_{\rm B} && (10)\\ &= \hat{P}_{\rm ideal,A} - (\overline{\Delta c}_{\rm B} - \overline{\Delta c}_{\rm A}) \ . && (11) \end{aligned}$$

3.2 Calculation of ocean loading displacement

According to IERS Conventions (2003)[30], the ocean tide loading displacement can be computed by the following formulae

$$\Delta x_{\rm OL} = (\Delta x_{\rm h}, -\Delta x_{\rm e}, -\Delta x_{\rm n})^T \tag{12}$$

$$\Delta x_c = \sum_{j=1}^{11} f_j A_{cj} \cos\left(\omega_j t + \chi_j + u_j - \Phi_{cj}\right), \ c = {\rm h},\ {\rm e},\ {\rm n} \tag{13}$$

where h, e, n indicate components height (h), east (e) and north (n). At present, the following 11 most significant tidal constituents are included. In ascending order, $j = 1, 2, \ldots, 11$ denote M_2, S_2, N_2, K_2, K_1, O_1, P_1, Q_1, M_f, M_m, S_{sa}. The ocean loading tables including amplitudes A_{cj} and phase angles Φ_{cj} could be obtained at the interactive ocean loading web provider http://www.oso.chalmers.se/∼loading/. In the tables, the positive directions for horizontal components are defined as west and south. Therefore, we take negative signs in Eq. (12) for the components $\Delta x_{\rm e}$ and $\Delta x_{\rm n}$. The time-dependent astronomical arguments $\omega_j t + \chi_j$ can be computed with subroutine ARG provided with IERS conventions[30]. Scale factor f_j and phase angle offset u_j for tide j depend on the mean longitude of the lunar ascending node N

$$N = 259^\circ.157 - 19^\circ.32818(Y - 1900) - 0^\circ.05295(D + I) \tag{14}$$

where Y is year in 4 digits, e.g. 1999; D is day of year elapsed since January 1st of the year Y, i.e. $D = 0$ at January 1st 0h; $I = {\rm int}[(Y - 1901)/4]$ is additional days for leap years. f_j and u_j can be calculated by formulae

$$\begin{aligned} f &= f_0 + f_1 \cos N + f_2 \cos(2N) + f_3 \cos(3N) && (15)\\ u &= u_1 \sin N + u_2 \sin(2N) + u_3 \sin(3N) \ \ \text{(in degrees)} && (16) \end{aligned}$$

The coefficients f_0, f_1, f_2, f_3, u_1, u_2, u_3 are listed in Table 1[43].

DOI: 10.2312/GFZ.b103-08037

Table 1: Amplitude scaling factors f and phase angle offset u (in degrees) for the required partial tides according to Doodson [1928, pp.274-275, table 25, 26 and 27][10].

Tide	f_0	f_1	f_2	f_3	u_1	u_2	u_3
M_2	1.0004	-0.0373	0.0002	0.0	-2.14	0.0	0.0
S_2	1.0	0.0	0.0	0.0	0.0	0.0	0.0
N_2	(see M2)						
K_2	1.0241	0.2863	0.0083	-0.0015	-17.74	0.68	-0.04
K_1	1.0060	0.1150	-0.0088	0.0006	-8.86	0.68	-0.07
O_1	1.0089	0.1871	-0.0147	0.0014	10.80	-1.34	0.19
P_1	1.0	0.0	0.0	0.0	0.0	0.0	0.0
Q_1	(see O1)						
M_f	1.0429	0.4135	-0.0040	0.0	-23.74	2.68	-0.38
M_m	1.0000	-0.1300	0.0013	0.0	0.0	0.0	0.0
S_{sa}	1.0	0.0	0.0	0.0	0.0	0.0	0.0

3.3 Selection of ocean loading models

For ocean tide loading displacement correction, GFZ IGS AC has been using Pagiatakis' software[33, 34] to calculate ocean loading coefficients based on the FES95.2 ocean tide model[24]. The scheme has two shortcomings. On the one hand, Pagiatakis' software sets fortnight component $M_{\rm f}$ to zero and does not include monthly component $M_{\rm m}$ and semi-annual component $S_{\rm sa}$. However, long-period components can degrade the accuracy of linear rate estimation especially in height component. On the other hand, the coefficient accuracy of diurnal and semi-diurnal constituents are also important. According to the study of Penna and Stewart[36], the residual semi-diurnal and diurnal signatures can result in aliased periodic signals with semi-annual and annual periods. In terms of the above considerations, it's necessary to update the ocean loading coefficients based on the state-of-the-art ocean tide models.

Some of the latest ocean tide models are probably better than the FES95.2 model. They are GOT00.2[40], NAO.99b[27], FES99[22], TPXO.5[12] and CSR4.0[11], though it's difficult to say which ocean tide model is the best for calculating ocean loading displacement. For some special regions, there may be no suitable global models (all of the above mentioned are global ocean tide models). For example, in the Amery Ice Shelf region (70E) at Antarctica, due to very little bathymetry information under the Amery Ice Shelf, including no information in the case of the southern 200 km, the coastline (grounding zone) definition in the Amery Ice Shelf is incorrect by 200 km in most models. Therefore regional ocean tide model is recommended for Antarctica by Matt King[28].

In deciding which ocean tide model, we make a simple comparison of the latest models. There is a brief description at web page
http://www.oso.chalmers.se/∼loading/tidemodels.html by Dr. H.-G Scherneck. In some ocean tide models, there are water areas that are missing. Among the latest 5 models, GOT00.2 and CSR4.0 are the only two models to include all the water areas.

DOI: 10.2312/GFZ.b103-08037

Therefore, we concentrate our selection between GOT00.2 and CSR4.0.

Both GOT00.2 and CSR4.0 are long wavelength adjustments of FES94.1[23] using TOPEX/Poseidon altimetry data. Unfortunately, CSR4.0 has spurious gridcells over land that have been removed using the grid of GOT00.2 as a mask. At the same time, GOT00.2 has been used to add extra tidal values in the Weddell and Ross Sea in the Antarctica. For the other tidal values below and above the 66S and 66N latitude (the limits of the TOPEX/Poseidon satellite), CSR4.0 becomes equal to FES94.1. GOT00.2 is different from FES94.1 in the polar region because ERS-1/2 data is used in the assimilation process. Therefore, from the development process of the models, we prefer to use GOT00.2 ocean tide model.

3.4 Evaluation of the difference between two ocean loading models for daily solution

The daily GPS solution is derived from the data spanning exactly one day. However, the periods of the diurnal and semi-diurnal ocean tide waves involved in ocean loading displacement have some differences from exact one or half day. Thus, the error of diurnal and semi-diurnal ocean loading coefficients cannot be averaged out in daily solutions. To evaluate the residual effects, we can derive the average of the differences for any constituents between two ocean loading models.

Let

$$c_i^1 = A_{ci}^1 \cos(\omega_i t - \Phi_{ci}^1) \ , \tag{17}$$
$$c_i^2 = A_{ci}^2 \cos(\omega_i t - \Phi_{ci}^2) \ , \tag{18}$$

in which c denotes the position components in height (h), east-west (e) and north-south (n); subscript $i = 1, \cdots, 8$ is one of the semi-diurnal and diurnal tidal constituents, i.e. M_2, S_2, N_2, K_2, K_1, O_1, P_1, Q_1; superscript 1 and 2 denote the two ocean loading models; A and Φ denote the amplitude and phase of a tidal constituent; ω_i is the angular velocity of ith constituent.

The difference of c_i^1 and c_i^2 can be derived as following.

$$\Delta c_i^{12} = c_i^1 - c_i^2 \tag{19}$$
$$= A_{ci}^1 \cos(\omega_i t - \Phi_{ci}^1) - A_{ci}^2 \cos(\omega_i t - \Phi_{ci}^2) \tag{20}$$
$$= A_{ci}^1 \left[\cos\omega_i t \cos\Phi_{ci}^1 + \sin\omega_i t \sin\Phi_{ci}^1\right] - A_{ci}^2 \left[\cos\omega_i t \cos\Phi_{ci}^2 + \sin\omega_i t \sin\Phi_{ci}^2\right] \tag{21}$$
$$= \left(A_{ci}^1 \cos\Phi_{ci}^1 - A_{ci}^2 \cos\Phi_{ci}^2\right) \cos\omega_i t + \left(A_{ci}^1 \sin\Phi_{ci}^1 - A_{ci}^2 \sin\Phi_{ci}^2\right) \sin\omega_i t \ . \tag{22}$$

Let T_i be the period of the ith constituent, then

$$\omega_i = \frac{2\pi}{T_i} \ . \tag{23}$$

DOI: 10.2312/GFZ.b103-08037

Let the data processing interval

$$T = 1 \text{ day},$$

the mean of Δc_i^{12} in one day can be written as

$$\begin{aligned}
\overline{\Delta c_i^{12}} &= \frac{1}{T}\int_0^T \Delta c_i^{12} \mathrm{d}t & (24)\\
&= \frac{1}{T}\int_0^T \left(A_{ci}^1 \cos\Phi_{ci}^1 - A_{ci}^2 \cos\Phi_{ci}^2\right)\cos\omega_i t \ \mathrm{d}t + \\
&\quad \frac{1}{T}\int_0^T \left(A_{ci}^1 \sin\Phi_{ci}^1 - A_{ci}^2 \sin\Phi_{ci}^2\right)\sin\omega_i t \ \mathrm{d}t & (25)\\
&= \frac{1}{T}\left(A_{ci}^1 \cos\Phi_{ci}^1 - A_{ci}^2 \cos\Phi_{ci}^2\right)\int_0^T \cos\omega_i t \ \mathrm{d}t + \\
&\quad \frac{1}{T}\left(A_{ci}^1 \sin\Phi_{ci}^1 - A_{ci}^2 \sin\Phi_{ci}^2\right)\int_0^T \sin\omega_i t \ \mathrm{d}t & (26)\\
&= \left(A_{ci}^1 \cos\Phi_{ci}^1 - A_{ci}^2 \cos\Phi_{ci}^2\right) C_i + \left(A_{ci}^1 \sin\Phi_{ci}^1 - A_{ci}^2 \sin\Phi_{ci}^2\right) S_i \ , & (27)
\end{aligned}$$

in which

$$\begin{aligned}
C_i &= \frac{1}{T}\int_0^T \cos\omega_i t \ \mathrm{d}t = \frac{1}{T}\int_0^T \cos\frac{2\pi t}{T_i} \ \mathrm{d}t = \frac{T_i}{2\pi T}\sin\frac{2\pi T}{T_i} \ , & (28)\\
S_i &= \frac{1}{T}\int_0^T \sin\omega_i t \ \mathrm{d}t = \frac{1}{T}\int_0^T \sin\frac{2\pi t}{T_i} \ \mathrm{d}t = \frac{T_i}{2\pi T}\left(1 - \cos\frac{2\pi T}{T_i}\right) \ . & (29)
\end{aligned}$$

For diurnal waves K_1, O_1, P_1, Q_1, let

$$T_i = (1 + \alpha_i)T \ , \tag{30}$$

where α_i is the difference factor of diurnal period to one day. Substitute Eq. (30) into (28) and (29) and then into Eq. (27), we can get the mean difference of displacement for position component c and diurnal tidal constituent i in one day as follows

$$\begin{aligned}
\overline{\Delta c_i^{12}}_{\text{diurnal}} &= \left(A_{ci}^1 \cos\Phi_{ci}^1 - A_{ci}^2 \cos\Phi_{ci}^2\right)\cdot\frac{1+\alpha_i}{2\pi}\sin\frac{2\pi}{1+\alpha_i} + \\
&\quad \left(A_{ci}^1 \sin\Phi_{ci}^1 - A_{ci}^2 \sin\Phi_{ci}^2\right)\cdot\frac{1+\alpha_i}{2\pi}\left(1 - \cos\frac{2\pi}{1+\alpha_i}\right) \qquad (31)
\end{aligned}$$

For semi-diurnal waves M_2, S_2, N_2, K_2, let

$$T_i = (1 + \beta_i)\frac{T}{2} \ , \tag{32}$$

where β_i is the difference factor of semi-diurnal period to half day. Substitute Eq. (32) into (28) and (29), and then into Eq. (27), we can obtain the mean difference of displacement for component c and semi-diurnal constituent i in one day as follows

$$\begin{aligned}
\overline{\Delta c_i^{12}}_{\text{semi-diurnal}} &= \left(A_{ci}^1 \cos\Phi_{ci}^1 - A_{ci}^2 \cos\Phi_{ci}^2\right)\cdot\frac{1+\beta_i}{4\pi}\sin\frac{4\pi}{1+\beta_i} + \\
&\quad \left(A_{ci}^1 \sin\Phi_{ci}^1 - A_{ci}^2 \sin\Phi_{ci}^2\right)\cdot\frac{1+\beta_i}{4\pi}\left(1 - \cos\frac{4\pi}{1+\beta_i}\right) \qquad (33)
\end{aligned}$$

DOI: 10.2312/GFZ.b103-08037

Table 2: Spectral characteristics of ocean tidal constituents.

tide	frequency ($^\circ/h$)	period (day)	α / β	alias period (day)
M2	28.984104	0.51752505	0.03505011 (β)	14.76529
S2	30.000000	0.50000000	0.00000000 (β)	∞
N2	28.439730	0.52743117	0.05486234 (β)	9.61372
K2	30.082137	0.49863479	-0.00273042 (β)	182.62172
K1	15.041069	0.99726954	-0.00273046 (α)	365.23899
O1	13.943036	1.07580587	0.07580587 (α)	14.19159
P1	14.958931	1.00274545	0.00274545 (α)	365.23899
Q1	13.398661	1.11951485	0.11951485 (α)	9.36716
Mf	1.098033	13.6607916		
Mm	0.544375	27.5545350		
Ssa	0.082137	182.621717		

Eqs. (31) and (33) can be used to evaluate the difference in displacement correction due to diurnal and semi-diurnal constituents between two ocean loading models.

To evaluate the model differences, the periods of the tides should be known. Table 2 gives the frequencies and periods of the relevant tidal constituents[29]. Here, we compare the ocean tide models FES95.2 which has been used by GFZ IGS AC, and GOT00.2 which is selected as the replacement. From Eqs. (31) and (33), we can calculate the mean differences of each constituent in one day for all stations. Table 3 gives the ranges of daily mean displacement differences for the semi-diurnal and diurnal constituents in height, east-west and north-south components. The lower rows of Table 3 give the range of the summation of mean differences of each constituents and the related stations.

3.5 Aliased signal in daily solutions

Besides S_2, neither semidiurnal nor diurnal constituent has exact half day or one day period. Therefore, the mis-modelled displacements of these tidal constituents can not be averaged out in daily GPS solutions due to the phase-residual parts from half or one day. Then, these residual parts can be aliased as some long-period signals. The principal alias period can be calculated from the change of tidal phase over the data processing interval T, 1 day. The phase change of a given tidal constituent i with period T_i is (following the equations (25) and (26) in [35])

$$\Delta\phi_i = \frac{2\pi T}{T_i} \ , \quad \Delta\phi_i \in (-\pi, \pi) \ , \tag{34}$$

and the resulting principal alias period T_i' is then

$$T_i' = \left| \frac{2\pi T}{\Delta\phi_i} \right| \ . \tag{35}$$

DOI: 10.2312/GFZ.b103-08037

Table 3: Stations with significant correction differences between two sets of ocean loading coefficients based on ocean tide models FES95.2 and GOT00.2. The lower rows are station names and GFZ internal numbers with the largest differences.

	$\overline{\Delta h_i^{12}}$ (mm)		$\overline{\Delta e_i^{12}}$ (mm)		$\overline{\Delta n_i^{12}}$ (mm)	
tide	min	max	min	max	min	max
M2	-1.73	1.63	-0.33	0.38	-0.25	0.29
S2	-0.00	0.00	-0.00	0.00	-0.00	0.00
N2	-0.36	0.53	-0.10	0.12	-0.10	0.13
K2	-0.01	0.01	-0.00	0.00	-0.00	0.00
K1	-0.06	0.05	-0.02	0.01	-0.01	0.01
O1	-1.13	1.41	-0.27	0.24	-0.23	0.24
P1	-0.02	0.02	-0.01	0.01	-0.00	0.00
Q1	-0.23	0.44	-0.07	0.07	-0.05	0.07
total	-1.76	3.00	-0.38	0.60	-0.28	0.57
name	vene	fort	will	mali	whit	fort
numb	1305	5200	4214	6300	4260	5200

For a diurnal constituent, the phase change is

$$\Delta\phi_i = \frac{2\pi T}{(1+\alpha_i)T} = \frac{2\pi}{1+\alpha_i} \ . \tag{36}$$

Setting $\Delta\phi_i$ into the interval $(-\pi, \pi)$ yields

$$\Delta\phi_i = \frac{2\pi}{1+\alpha_i} - 2\pi = \frac{-\alpha_i}{1+\alpha_i} 2\pi \ . \tag{37}$$

Then, the principal alias period for a diurnal constituent is

$$T_i' = \left| \frac{2\pi T}{\Delta\phi_i} \right| = \left| \frac{1+\alpha_i}{\alpha_i} \right| T \ . \tag{38}$$

For a semidiurnal constituent, the phase change is

$$\Delta\phi_j = \frac{2\pi T}{(1+\beta_j)\frac{T}{2}} = \frac{4\pi}{1+\beta_j} \ . \tag{39}$$

Setting $\Delta\phi_j$ into the interval $(-\pi, \pi)$ yields

$$\Delta\phi_j = \frac{4\pi}{1+\beta_j} - 4\pi = \frac{-\beta_j}{1+\beta_j} 4\pi \ . \tag{40}$$

The principal alias period for semidiurnal constituent can be then obtained as

$$T_j' = \left| \frac{2\pi T}{\Delta\phi_j} \right| = \left| \frac{1+\beta_j}{2\beta_j} \right| T \ . \tag{41}$$

DOI: 10.2312/GFZ.b103-08037

The calculated alias periods from equations (38) and (41) are listed in column 5 of Table 2. The aliased signals can be seen clearly from Figure 10 for tidal constituents M_2, N_2, O_1 and Q_1. It's not obvious for constituents K_2, K_1 and P_1 because of small amplitudes. The daily mean is obtained from time series of ocean loading displacements from GOT00.2 model with sampling rate of 30 minutes.

It should be mentioned that the aliasing problem can also be induced from the viewpoint of sampling. Nyquist-Shannon sampling theorem[32] states that, when converting from an analog signal to digital (or otherwise sampling a signal at discrete intervals), the sampling frequency must be greater than twice the highest frequency of the input signal in order to be able to reconstruct the original perfectly from the sampled version. If the sampling frequency is less than this limit, then frequencies in the original signal that are above half the sampling rate will be "aliased" and will appear in the resulting signal as lower frequencies.

The GPS coordinate time series are derived from discrete 24-hour solutions. It's just like sampling the ocean loading signals in a 24-hour interval. Under this scheme, residual semi-diurnal and diurnal crustal tide signatures are under-sampled, resulting in aliased periodic signals in the coordinate time series[9, 21, 36]. The aliased frequency of a sinusoidal signal may be computed for a given sampling interval using the following equation[19, 36]:

$$f' = \left| f - \frac{1}{T} \langle f \cdot T + 0.5 \rangle \right| \tag{42}$$

where f' is the aliased frequency, f is the original frequency of the signal, T is the sampling interval which is 24 hours in our case, $|\cdot|$ takes the absolute value of the argument, and $\langle \cdot \rangle$ returns the largest integer less than or equal to its argument.

In fact, equation (42) is just the generalized form of equations (38) and (41). This can be proved as follows. Let

$$I = \langle f \cdot T + 0.5 \rangle \ . \tag{43}$$

I is the nearest integer number of cycles for a sinusoidal signal in the sampling interval T. It holds

$$\begin{aligned} I &= 1 \quad \text{for diurnal, and} \\ I &= 2 \quad \text{for semidiurnal} \end{aligned}$$

in the sense of daily sampling. Then, equation (42) can be written as

$$f'_i = \left| f_i - \frac{1}{T} \right| \quad \text{for diurnal, and} \tag{44}$$

$$f'_i = \left| f_i - \frac{2}{T} \right| \quad \text{for semidiurnal .} \tag{45}$$

Since

$$f_i = \frac{1}{T_i} \ , \tag{46}$$

then, for diurnal constituents, equation (44) can be written as

$$\frac{1}{T'_i} = \left| \frac{1}{T_i} - \frac{1}{T} \right| \ . \tag{47}$$

DOI: 10.2312/GFZ.b103-08037

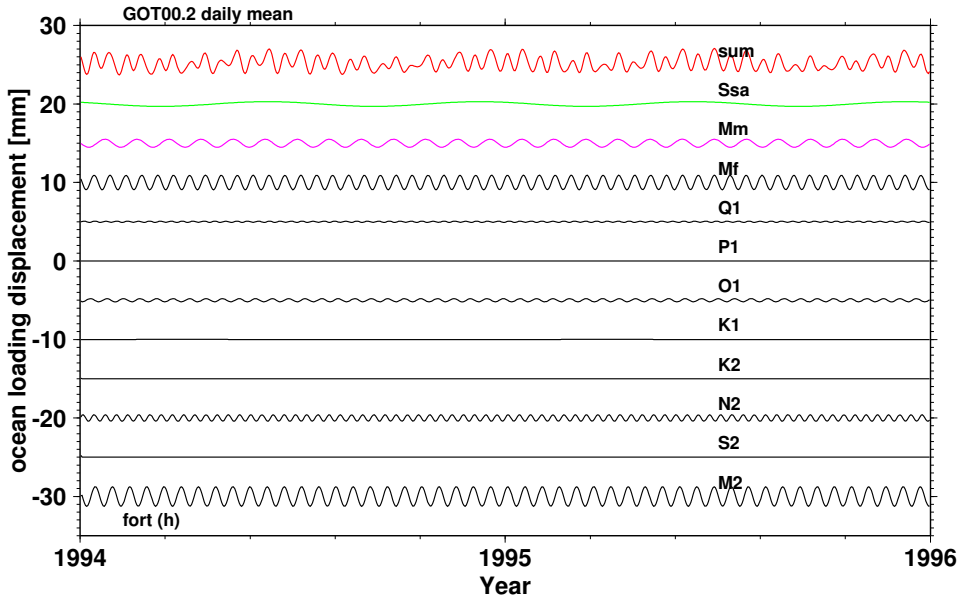

Figure 10: Daily mean of ocean loading displacements in height for GPS site FORT (Fortaleza, Brazil). In the figure, 'fort(h)' denotes height component for the station FORT. For clearer visibility, the time series for each constituent are shifted consecutively by ±5 mm.

Substituting equation (30) into above equation yields

$$\frac{1}{T_i'} = \left| \frac{1}{(1+\alpha_i)T} - \frac{1}{T} \right| \tag{48}$$

$$= \left| \frac{-\alpha_i}{(1+\alpha_i)} \right| \frac{1}{T} \tag{49}$$

Reverse the formula, equation (38) can be obtained exactly.

For semidiurnal constituents, the proof procedure is similar.

$$\text{Eq. (45)} \implies \frac{1}{T_i'} = \left| \frac{1}{T_i} - \frac{2}{T} \right| \tag{50}$$

$$\text{Eq. (32)} \implies \frac{1}{T_i'} = \left| \frac{2}{(1+\beta_i)T} - \frac{2}{T} \right| \tag{51}$$

$$= \left| \frac{-\beta_i}{1+\beta_i} \right| \frac{2}{T} \tag{52}$$

It can be seen that equation (52) is exactly the reciprocal form of equation (41). Thus, the equivalence of the two approaches of deriving aliased frequencies are proved.

3.6 Replacement of the ocean loading correction on solutions with new model

Based on the consideration in section 3.1, we can replace the correction of ocean loading displacement derived from ocean tide model FES95.2 with the one from new ocean tide

DOI: 10.2312/GFZ.b103-08037

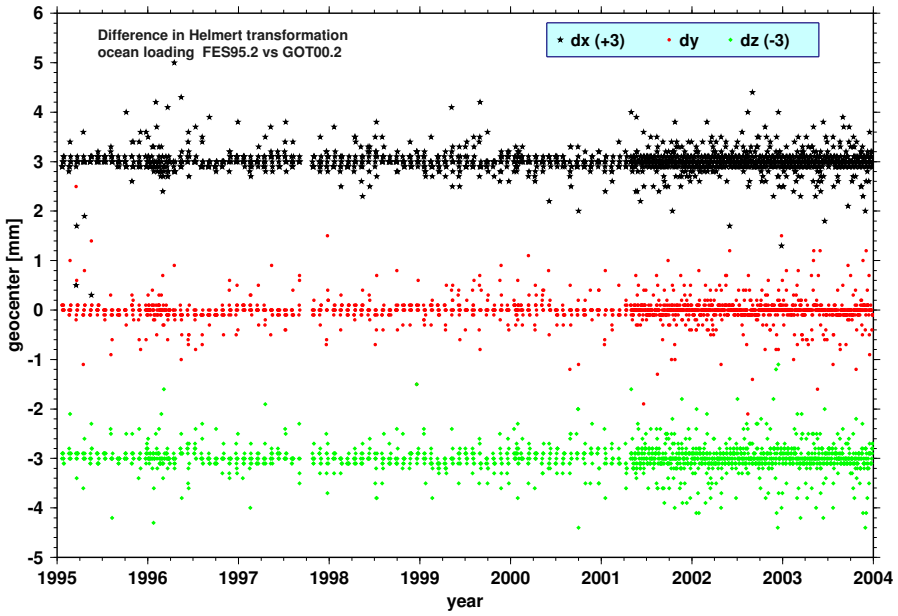

Figure 11: Difference between two sets of Helmert transformation parameters while aligning the station coordinate solutions from different ocean loading model FES95.2 and GOT00.2 to ITRF2000 (difference of geocenter parameters).

model GOT00.2. To realize this replacement, we calculate the ocean loading corrections every 30 minutes and get the daily mean for the two ocean loading models. Then, we simply subtract the daily mean difference of $\overline{\Delta c}_{\text{new}} - \overline{\Delta c}_{\text{old}}$ from the daily coordinate solutions. In doing so, we apply the new ocean loading corrections (approximately) for all the existing solutions.

When we generate station position time series, we first align the solution with ITRF2000 by Helmert 7-parameter similarity transformation. For the solutions with ocean loading correction from FES95.2 ocean tide model (old model), we can get a series of Helmert transformation parameters (3 geocenter offsets, 3 rotation angles, 1 scale factor). For the solutions with GOT00.2 ocean loading corrections, we can get another series of 7 parameters. Then, we can examine the differences between the two series of Helmert transformation parameters. Figures 11, 12, 13 give these differences. Figure 13 also gives the difference of the number of reference stations which are automatically selected during iterations in Helmert transformation.

How does the different ocean loading model affect the position time series? As an example, Figure 15 gives the series of the difference between the two sets of position time series by using ocean loading models FES95.2 and GOT00.2 for GPS site CHUR. To see the details, Figure 15 is zoomed into Figure 16 for three years and Figure 17 for one year. From Figure 16, we can clearly see the period of semiannual in height component. From Figure 17, we can see the period of fortnight modulated on a monthly wave.

DOI: 10.2312/GFZ.b103-08037

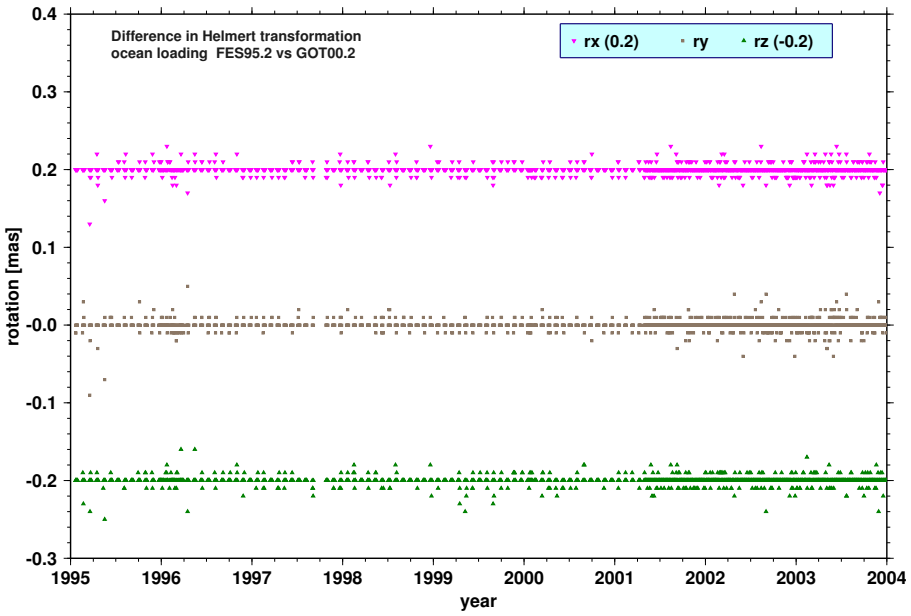

Figure 12: Difference between two sets of Helmert transformation parameters while aligning the station coordinate solutions from different ocean loading model FES95.2 and GOT00.2 to ITRF2000 (difference of rotation parameters).

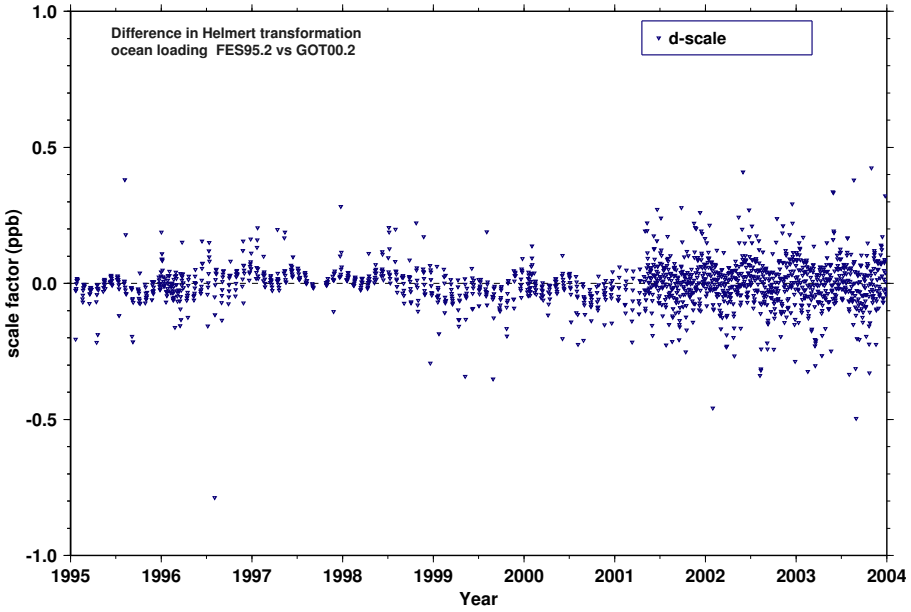

Figure 13: Difference between two sets of Helmert transformation parameters while aligning the station coordinate solutions from different ocean loading model FES95.2 and GOT00.2 to ITRF2000 (difference of scale factors).

DOI: 10.2312/GFZ.b103-08037

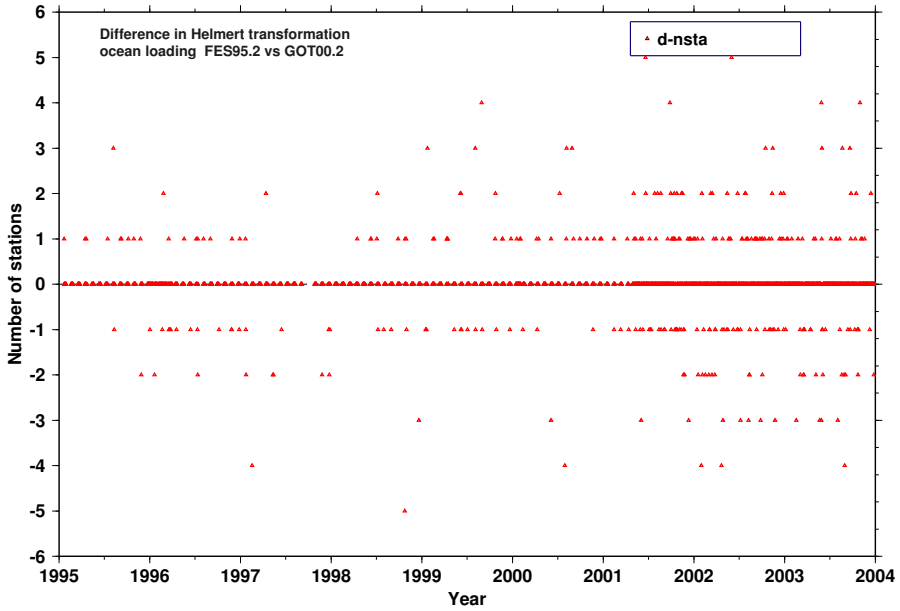

Figure 14: Difference between two sets of Helmert transformation parameters while aligning the station coordinate solutions from different ocean loading model FES95.2 and GOT00.2 to ITRF2000 (difference of number of reference stations).

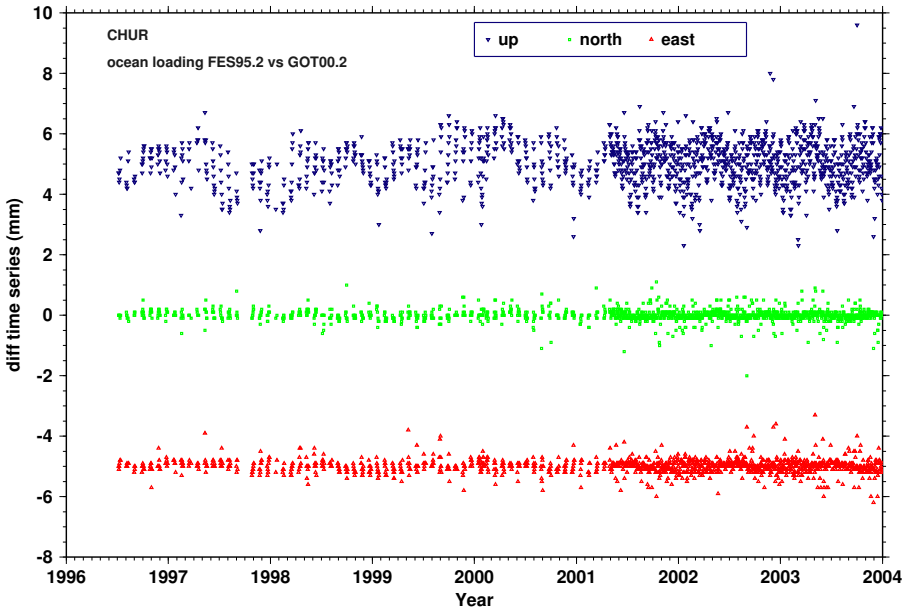

Figure 15: Difference between two sets of position time series by using ocean loading models FES95.2 and GOT00.2. Taking GPS station at Churchill as example. Up and east components are shifted by 5 and -5 millimeters respectively to make the plots readable.

DOI: 10.2312/GFZ.b103-08037

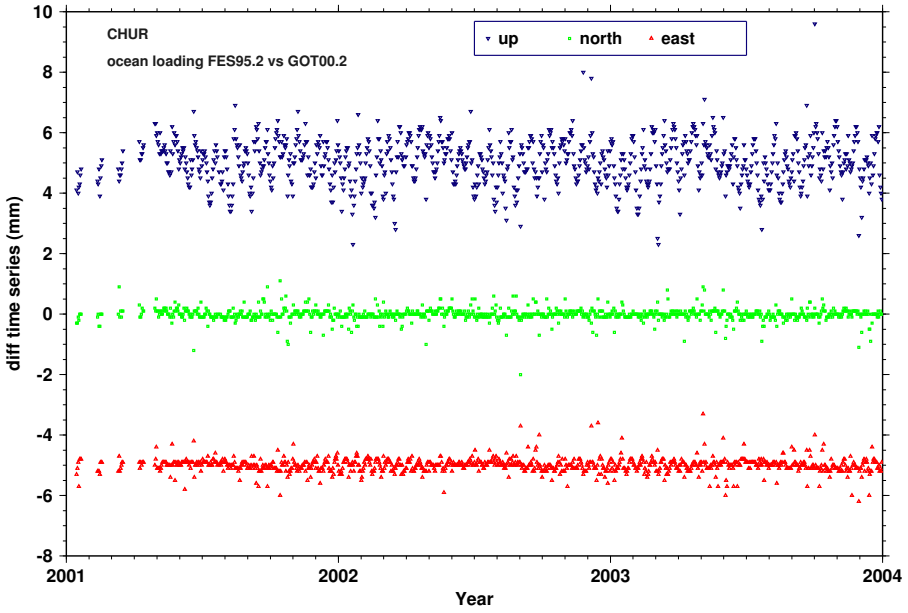

Figure 16: Zoom of Figure 15 in the interval 2001-2004.

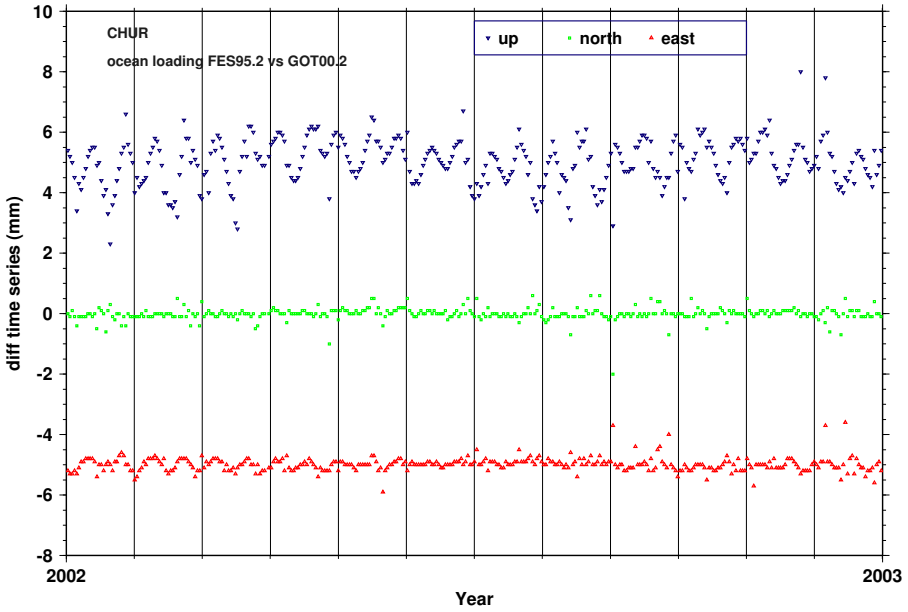

Figure 17: Zoom of Figure 15 in the interval of 2002-2003.

DOI: 10.2312/GFZ.b103-08037

4 Effect of atmospheric pressure loading (ATML)

4.1 ATML induced displacement

The atmospheric mass redistribution can deform the Earth's crust by up to 20 mm vertically and 3 mm horizontally[41, 45]. With the improvement of measurement precision and analysis models, this signal becomes detectable by the modern space geodetic techniques[45, 25, 44, 37]. The studies on interpreting the geodetic observed seasonal height variations[26, 9, 49] show that ATML displacement can partially account for the observed station height variation, especially the seasonal variation. The studies by van Dam et al.[44], Brondeel and Willems[5] show that removing the modelled ATML displacement from GPS coordinates reduces the variances of vertical position residuals for about 65% of the investigated stations, most of which are inland. The same variance reduction ratio is also found for baselines by van Dam et al.[44].

Figure 18 gives an example of ATML height time series at GPS station BAHR. The time series shows very significant seasonal fluctuations.

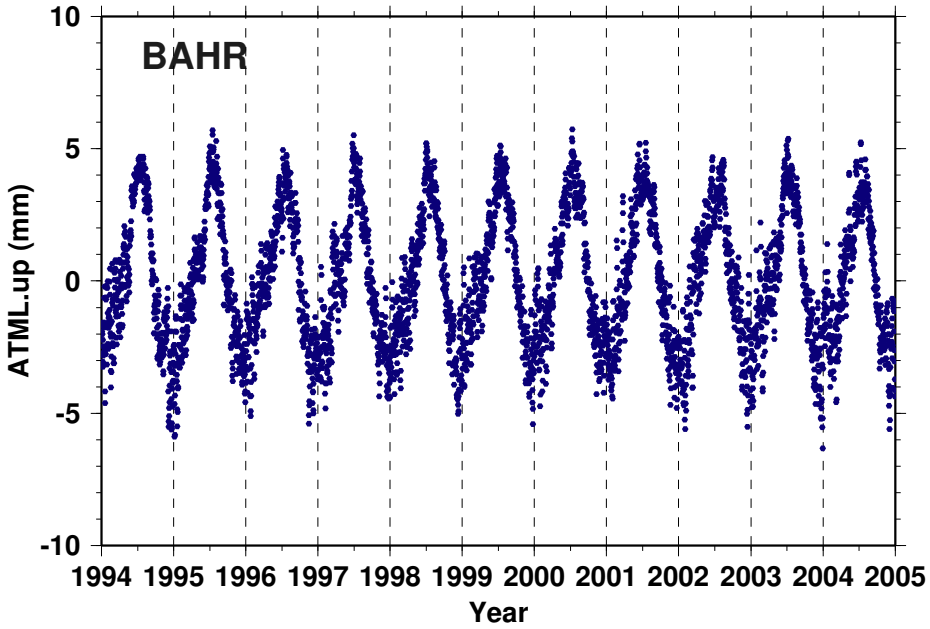

Figure 18: Time series of atmospheric loading induced vertical displacement at GPS station BAHR (Bahrain; Manama, Bahrain).

Figure 19 plots together the ATML induced vertical displacements and GPS estimated height variations at GPS station IRKT.

4.1.1 Calculation of six-hourly ATML displacement

The forward model of station displacement is created using global suface atmospheric pressure convolved with mass loading Green's Functions [13]. The method was first outlined in [45]. Only deviations from that method will be described here.

DOI: 10.2312/GFZ.b103-08037

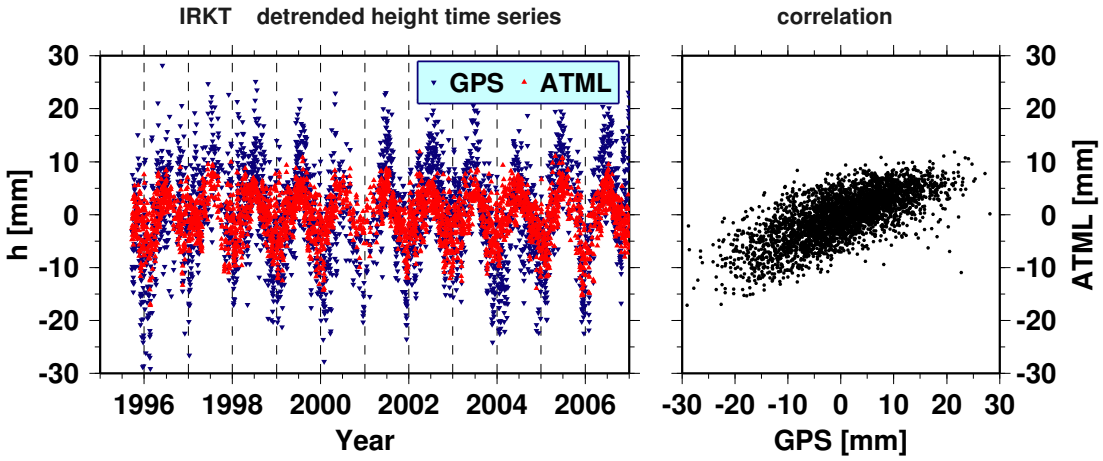

Figure 19: Left panel: time series of atmospheric loading induced vertical displacement and GPS estimated height variations at GPS station IRKT (Irkutsk; Siberia, Russia). Right panel: the correlation between ATML and GPS height time series, with abscissa axis as GPS height residual and vertical axis the ATML height at the same time as the GPS height. A positive rate of slope denotes a positive correlation.

The input atmospheric pressure data is the National Center for Environmental Prediction surface pressure. This data is provided on a $2.5° \times 2.5°$ global grid at 6 hourly intervals. We account for the pressure load over the ocean using the modified inverted barometer as described in [45]. The ocean land mask has a resolution of 0.25° and is derived from ETOPO5[31].

4.1.2 Generation of daily ATML time series from six-hourly time series

The ATML time series are 6-hourly data points at 0, 6, 12, 18 o'clock each day. However, the GPS time series are daily points. To apply the ATML corrections to GPS solutions, we average the 6-hourly ATML displacement values to daily values. For each day, the daily mean is calculated as follows

$$\overline{h}_{\mathrm{ATML\ daily}} = \frac{1}{4}(\frac{1}{2}h_{\mathrm{ATML\ 0h}} + h_{\mathrm{ATML\ 6h}} + h_{\mathrm{ATML\ 12h}} + h_{\mathrm{ATML\ 18h}} + \frac{1}{2}h_{\mathrm{ATML\ 24h}}) \quad (53)$$

4.2 Linear regression analysis between atmospheric loading and GPS time series

For the height time series, we can make a linear regression between GPS and atmospheric loading as follows

$$h_{\mathrm{ATML}}(t_i) = B + T \cdot h_{\mathrm{GPS}}(t_i), \quad i = 1, 2, \cdots, N \quad (54)$$

in which $h_{\mathrm{ATML}}(t_i)$ indicates atmospheric loading induced vertical motion (in millimeters) at epoch t_i, h_{GPS} the GPS measured height variation, B the intercept of the regression line, T the trend of the regression line, namely the amplitude ratio. In this

DOI: 10.2312/GFZ.b103-08037

case, B tells if there is any systematic bias between atmospheric and GPS time series. T tells how much the atmospheric loading displacement contribute to the GPS measured vertical motion.

The correlation between atmospheric loading induced displacement time series and detrended GPS observed position time series can be measured by the linear correlation coefficient r (also called the product-moment correlation coefficient, or *Pearson's* r) given by the formula (see [39] equation (14.5.1)):

$$r = \frac{\sum_{i=1}^{N}(x_i - \overline{x})(y_i - \overline{y})}{\sqrt{\sum_{i=1}^{N}(x_i - \overline{x})^2}\sqrt{\sum_{i=1}^{N}(y_i - \overline{y})^2}} \quad , \tag{55}$$

given $(x_i, y_i), i = 1, \ldots, N$ are the pairs of quantities composing the two sets of time series. The accuracy of r can be measured by the formula

$$f_r = \frac{1 - r^2}{\sqrt{N-1}} \; . \tag{56}$$

The significance level can be tested by t statistic. We implement this hypothesis test by using MATLAB© function *corrcoef*.

Table 8 in Appendix B (see page 79) gives the parameters obtained from the above linear regression analysis between GPS and atmospheric loading time series for the analyzed stations. These parameters include the number of data points, the correlation coefficient and its standard deviation, the significance factor (1 for significant; 0 for non-significant), and the amplitude ratios.

The correlation coefficients are illustrated in Figure 20, and the amplitude ratios (or admittances) in Figure 21. In Figures 20 and 21, the size of a color-filled circle indicates correlation coefficient. The filling color indicates level of correlation and significance in terms of a 99% confidence level, yellow for positive correlation and significance, orange for positive correlation and non-significance, pink for negative correlation. Plus sign '+' indicates core stations used for TRF alignment using Helmert transformation.

Figure 20 shows that for most stations, the correlations are significant in terms of a significance level of 99%. Most of the large correlations appear in high latitude regions. Figure 21 shows that large amplitude ratios appear mainly in high latitude regions in the northern hemisphere. From these two figures, we can preliminarily conclude that the ATML contributions in GPS estimated height displacements are significant and mostly in northern hemispheric high latitude regions with $\phi > 30°$.

4.3 Two approaches to applying ATML corrections and their different effects on the vertical site velocities

Since the ATML displacements were not corrected on-line in the observation model during data processing, they have to be corrected in an off-line mode. There are two ways to apply off-line ATML corrections that are illustrated in Figure 22. A straightforward way is to apply the ATML corrections onto the GPS height time series which

DOI: 10.2312/GFZ.b103-08037

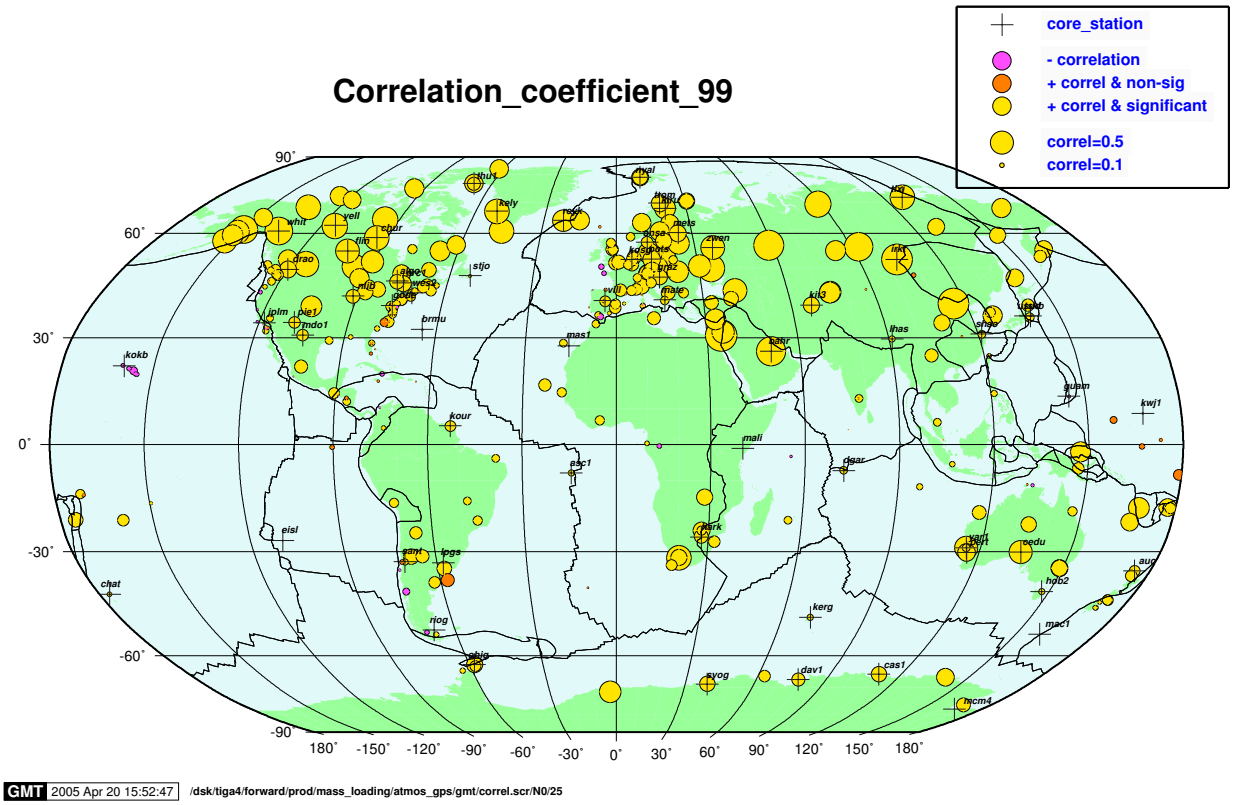

Figure 20: Correlation between ATML induced and GPS estimated height time series.

is named approach 1 in Figure 22. However, considering that the ATML displacements are not globally homogeneous, the modelling error due to ATML may also affect the reference frame's stability of the GPS time series, which is realized via the alignment of the loosely constrained GPS solutions with ITRF. To compensate for this effect, another approach (named approach 2 in Figure 22) is preferred for applying the ATML corrections directly on the coordinate solutions before the reference frame alignment.

Considering that approach 2 is more complicated than approach 1, the eventual benefit of using approach 2 should be evaluated to see if it is necessary to use the more complicated approach. To assess the necessity, we can compare the vertical site velocities derived by applying the two approaches individually. Figure 23 shows the differences of the vertical linear rates derived by applying the ATML corrections in two approaches. From the figure we can see that applying the ATML corrections on the solutions and on the time series can create differences in the vertical rates generally in the level of sub-mm/a. The large differences can even reach the level of mm/a. For precise geodynamic applications like TIGA, which requires an accuracy of better than 1 mm/a, such levels of difference should be taken into account.

DOI: 10.2312/GFZ.b103-08037

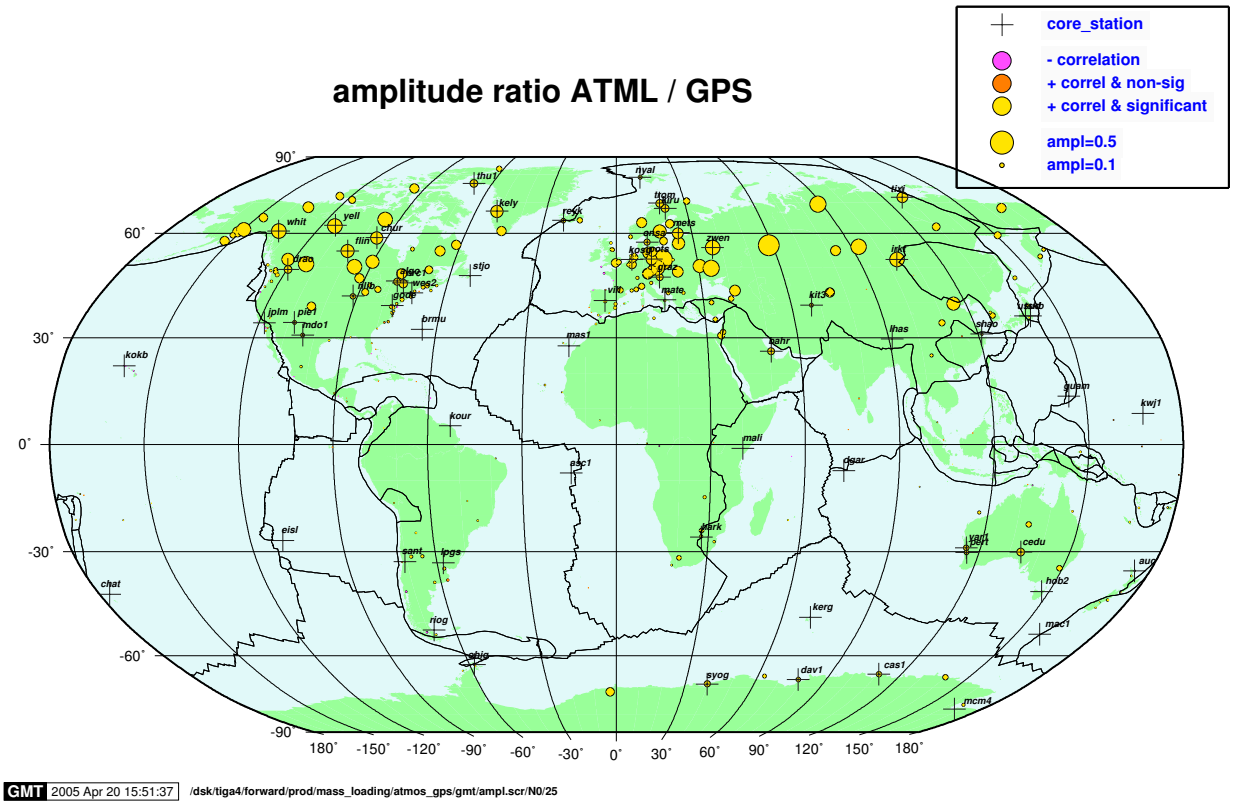

Figure 21: Amplitude ratios between ATML induced and GPS estimated height time series (ATML/GPS).

4.4 Effect of atmospheric loading on stability of reference frame

As mentioned above, approach 2 can improve the stability of the reference frame realized by alignment via Helmert transformation. This raises an interesting question: how significantly does ATML affect the stability of the reference frame of the GPS time series? To inspect this effect, we compare the seven transformation parameters between the two cases, without and with ATML corrections. For each case, we can get a time series of 7 parameters (3 geocentric translation, 3 rotation angles, 1 scale factor) used to transform the TIGA solutions to ITRF.

First, let us compare the geocentric translation parameters (see Figure 24, the data points for x and z components are shifted by 10 mm in the plot). We can see that the differences are generally within 1 mm level with insignificant seasonal variations. Some large differences appear in early years which are mainly caused by fewer stations (the numbers of core stations for the days in analysis are illustrated in Figure 4). The time series are fitted with bias, trend, annual and semi-annual waves. The estimated parameters are listed in Table 4. For the purposes of TIGA and SEAL projects, which concentrate mostly on the linear trend, the effect of ATML corrections on the linear trend of geocentric variation would be especially concerned. However, the level of 0.01 mm/a linear trend in geocentric translation can surely be neglected in light of the 1

DOI: 10.2312/GFZ.b103-08037

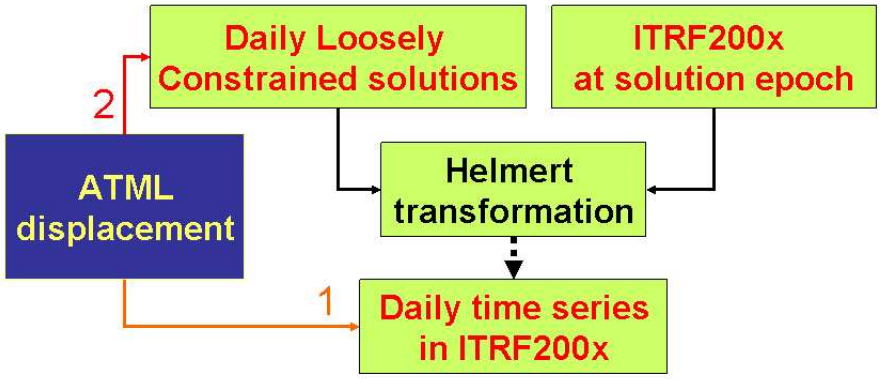

Figure 22: Two possible approaches to applying ATML corrections.

mm/a of accuracy requirement for the height variations for studying sea level change.

Table 4: Estimated parameters by fitting the time series of differences of the 3 geocentric translation parameters with and without ATML corrections applied to TIGA solutions.

parameters	x	y	z
Trend (mm/a)	0.006	-0.006	-0.010
Amp-ann (mm)	0.095	0.040	0.129
Amp-semi-ann (mm)	0.043	0.086	0.125
Bias (mm)	-0.004	0.014	-0.012

Let us now compare the rotation parameters which are illustrated in Figure 25. For convenient plotting, the data points for x and z components are shifted by 0.2 mas. The figure shows that the amplitude of the rotation angles are generally about 0.02 mas in each component, which corresponds to about 0.6 mm horizontally on ground surface. This could be ignored without significant effect considering two aspects of ground. On one hand, the current accuracy level for horizontal components are about 5 mm, therefore one tenth of the accuracy range is not significant. On the other hand, TIGA and SEAL projects concentrate mainly on the height component while rotation parameters mainly affect horizontal station positions.

Finally, let us compare the scale factors which are illustrated in Figure 26. The figure shows that the peak-to-peak differences are about 0.6 ppb, which correspond to 3-4 mm in height at Earth's surface. The fitting parameters listed in Table 5 show that the linear trend of scale factors is very small and can be ignored.

The comparison implies that ATML corrections do not affect the long-term stability of the reference frame. Does this mean that the ATML corrections also do not affect the estimates of vertical velocities? The following section attempts to explore this effect.

DOI: 10.2312/GFZ.b103-08037

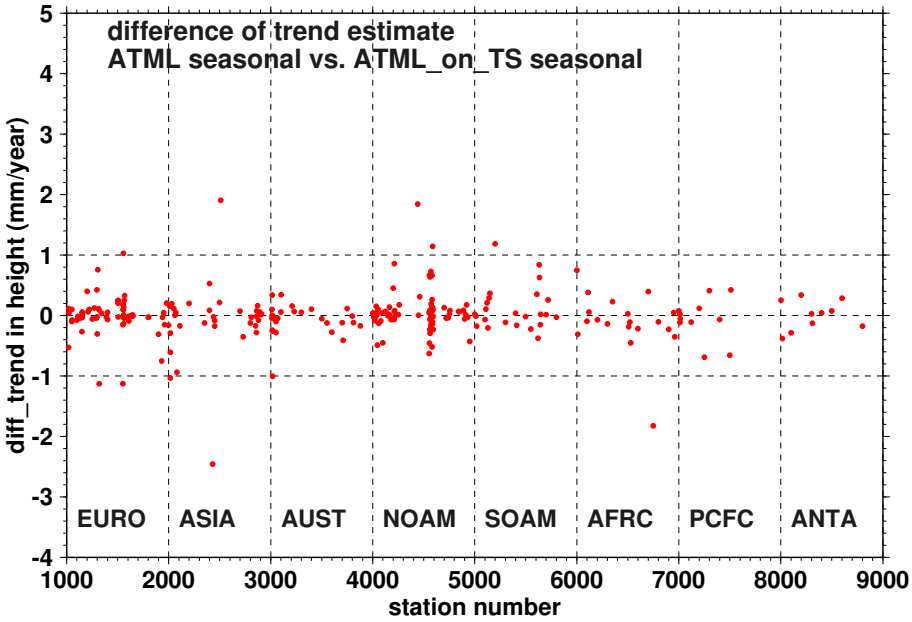

Figure 23: Differences of vertical rates derived by applying two approaches to ATML corrections.

Table 5: Estimated parameters by fitting the time series of differences of the scale factors with and without ATML corrections applied to TIGA solutions.

parameters	scale
Trend (ppb/a)	0.003
Amp-ann (ppb)	0.025
Amp-semi-ann (ppb)	0.019
Bias (ppb)	0.010

4.5 Effect of ATML on vertical rate estimates

4.5.1 Differences of vertical rate estimates with and without ATML corrections

This section will inspect the influence of the ATML corrections on the vertical rate estimation. We compare the vertical rate estimates for all the stations derived from two cases: without and with ATML corrections. In both cases, the same scheme of time series fitting is used as mentioned in section 2.3. Figure 27 illustrates the differences of vertical rate estimates between the two cases for all the stations with longer than 3 years of time series. In the figure, the stations are grouped in terms of tectonic plates. The figure shows that with corrections of ATML on solutions, the estimated vertical rates can differ in the level of sub-mm/a. This level of effects is already critical for studying sea level changes which require better than 1 mm/a accuracy. The figure also shows that the vertical rate differences are obviously rather globally than geographically correlated.

DOI: 10.2312/GFZ.b103-08037

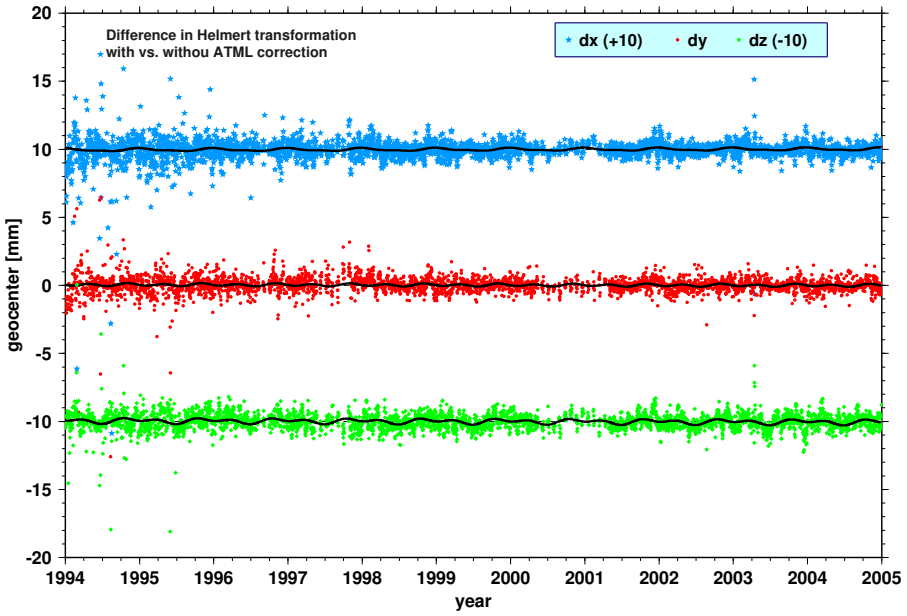

Figure 24: Differences of geocentric translation parameters out of the 7 parameters used to align TIGA solutions to ITRF2000.

4.5.2 Inspection of linear trend in ATML time series

Considering that ATML corrections do not affect the long-term stability of the reference frame, a question is raised: where do such large differences in vertical rates come from? Do they come from the ATML time series?

To answer this question, let us first determine whether the ATML time series themselves have linear trends. We sample the ATML time series by picking the data points which have corresponding GPS solutions at the same day. The sampled ATML time series for all the stations for statistic are fitted to estimate linear rates. Figure 28 gives the estimated vertical trends from the sampled ATML time series. We see that the linear trends of ATML time series are not significant compared with the vertical rate differences given in Figure 27. Note that the ATML time series are sampled against the corresponding GPS time series, which are not evenly distributed in time space. Since the linear trends are not significant, we can easily draw a conclusion that the uneven sampling of ATML time series does not affect vertical rate significantly.

4.5.3 Effects of ATML correction on estimation of seasonal parameters

Then let us inspect the influence of ATML corrections on the seasonal signal estimates. Figures 29 and 30 illustrate the effects of ATML corrections on the estimated amplitudes of annual and semi-annual waves. In the figures, the data points are the differences of amplitudes estimated with and without applying ATML corrections (ATML case subtracts non-ATML case). The figures show that ATML corrections affect seasonal amplitudes in millimeter level. For annual waves, the amplitudes for 97 of 271 stations (35.8%) are increased, and for 174 stations (64.2%) decreased. For semi-annual

DOI: 10.2312/GFZ.b103-08037

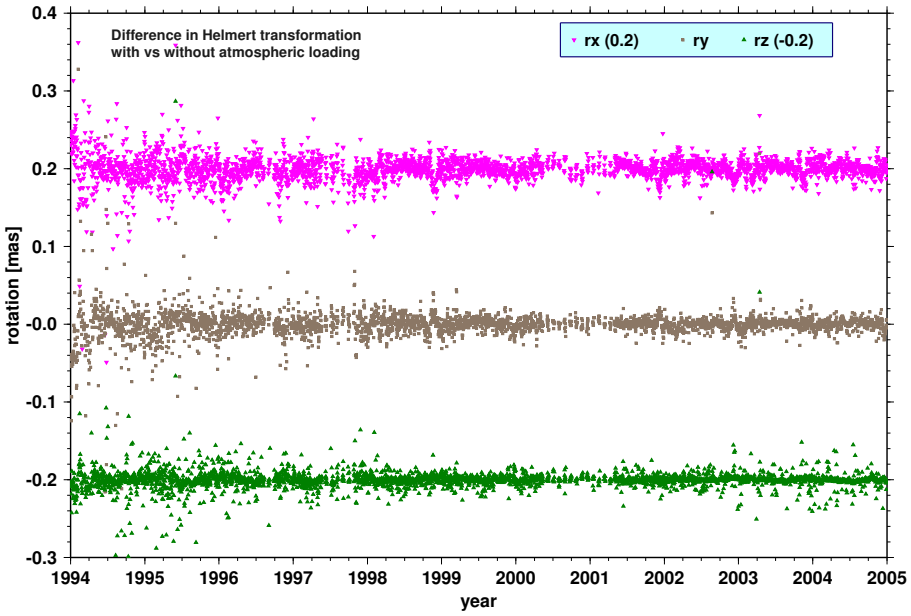

Figure 25: Differences of rotation parameters out of the 7 parameters used to align TIGA solutions to ITRF2000.

waves, the amplitudes of 120 stations (44.3%) are increased, and 151 stations (55.7%) decreased. Generally, the estimated amplitudes of seasonal waves are decreased for most stations after applying ATML corrections. It could be expected that the effects on seasonal parameter estimates would affect the vertical rate estimates indirectly since these parameters are correlated in a least-squares estimator. This indirect effect could be further evaluated via covariance analysis method.

4.5.4 Dependency of ATML effects on the quality of time series

Here we measure the quality of the GPS time series by three quantities: length, density, and balance index.

Normally, the linear rate estimate from a shorter time series is more sensitive to additional corrections. In Figure 31, the differences of estimated vertical rates between the cases with and without ATML corrections are plotted against the lengths of the GPS time series. From the figure we see that, in general, the longer a time series is, the smaller the vertical rate difference is.

Figure 32 gives the trend differences between the above mentioned two cases against the densities of the GPS time series. The figure implies that in general, ATML corrections have a smaller effect on a denser time series. However, the statistical correlation is not so obvious, probably because of the relative completeness of the time series.

Figure 33 plots the differences of vertical rates between the two cases: with and without ATML corrections, against the balance indices of all the stations under statistic. The figure shows that some large rate differences correspond to large imbalance indices. However, the statistical correlation is not generally obvious. This is probably

DOI: 10.2312/GFZ.b103-08037

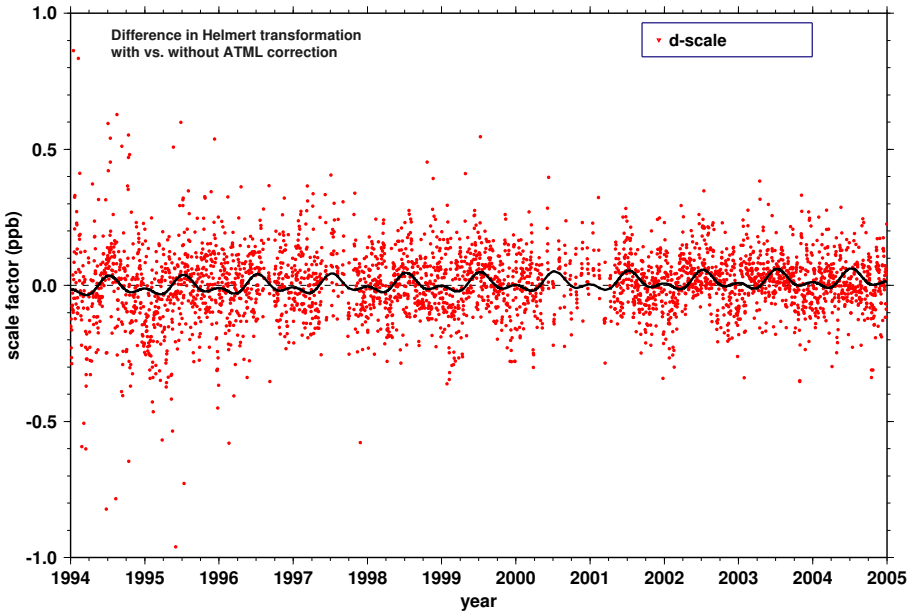

Figure 26: Differences of scale factors out of the 7 parameters used to align TIGA solutions to ITRF2000.

due to the fact that most GPS time series are relatively steady and of good quality.

DOI: 10.2312/GFZ.b103-08037

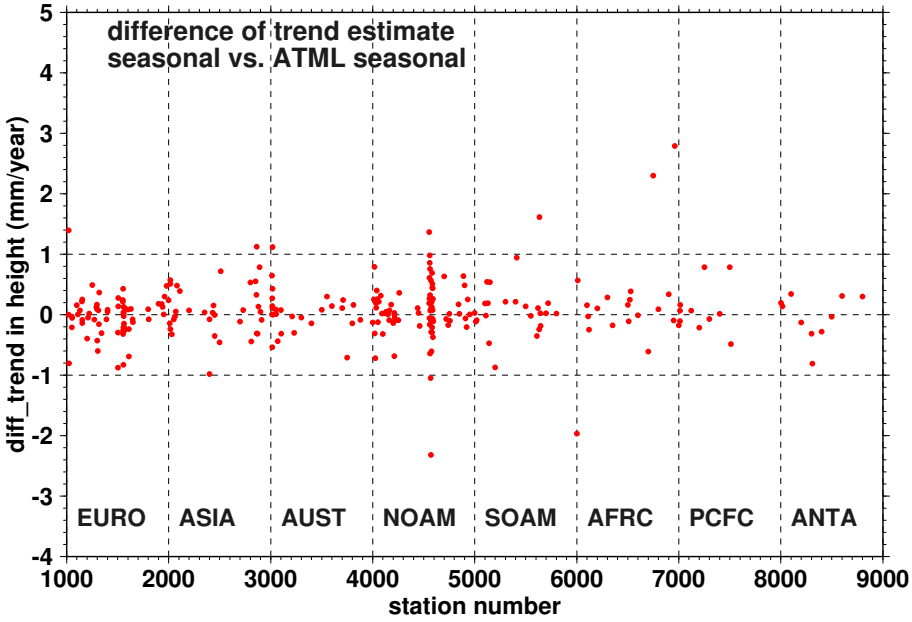

Figure 27: Differences of vertical rate estimates (with vs without applying ATML corrections).

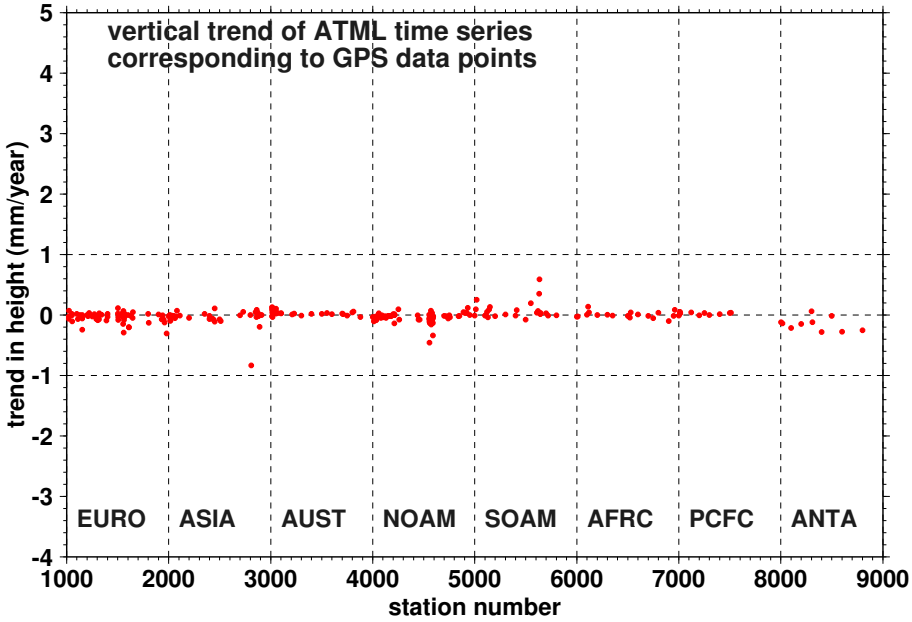

Figure 28: Vertical rates of ATML time series for the stations with longer than 3 years of GPS time series.

DOI: 10.2312/GFZ.b103-08037

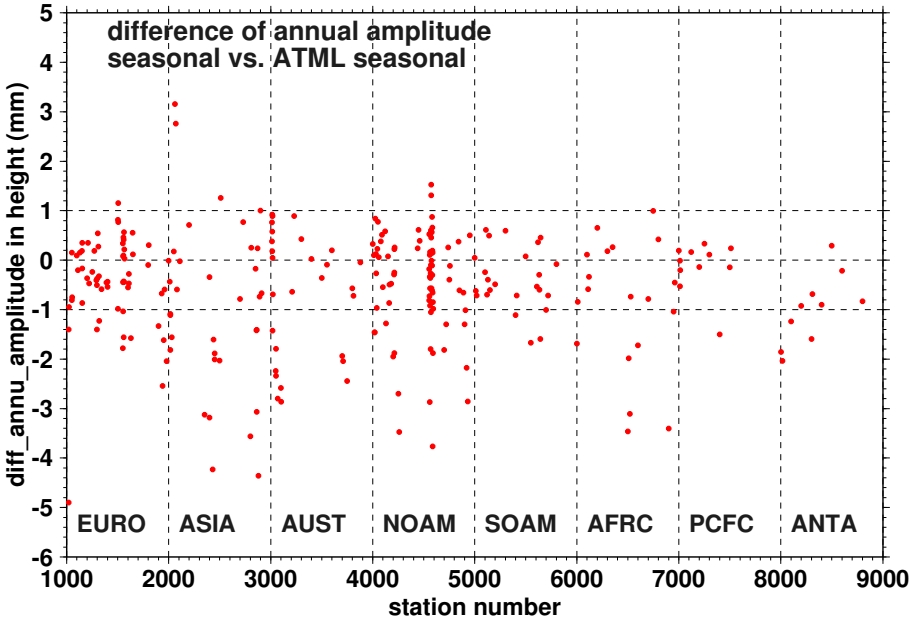

Figure 29: Differences of annual amplitude estimates with and without ATML corrections (for the stations with longer than 3 years of GPS time series).

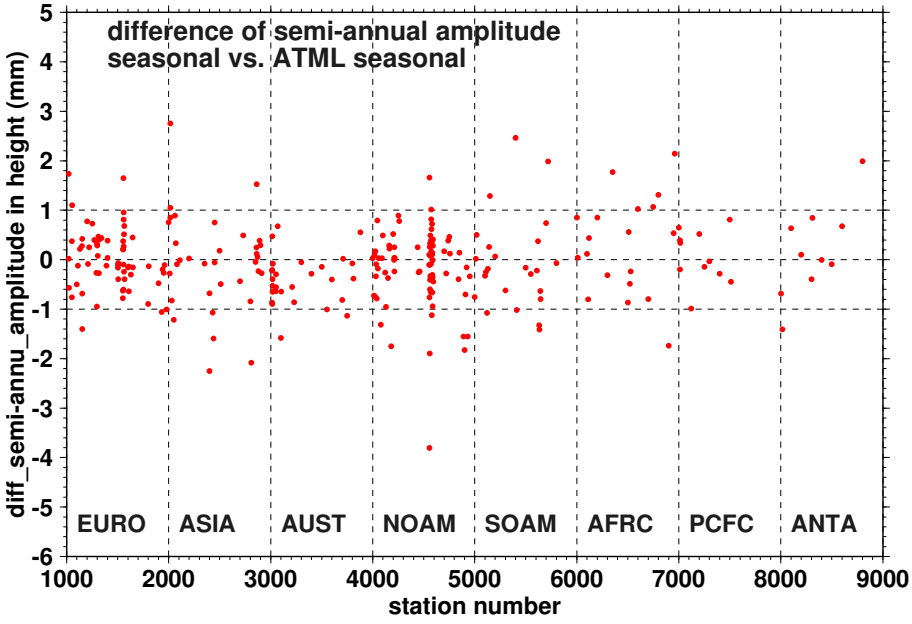

Figure 30: Differences of semi-annual amplitude estimates with and without ATML corrections (for the stations with longer than 3 years of GPS time series).

DOI: 10.2312/GFZ.b103-08037

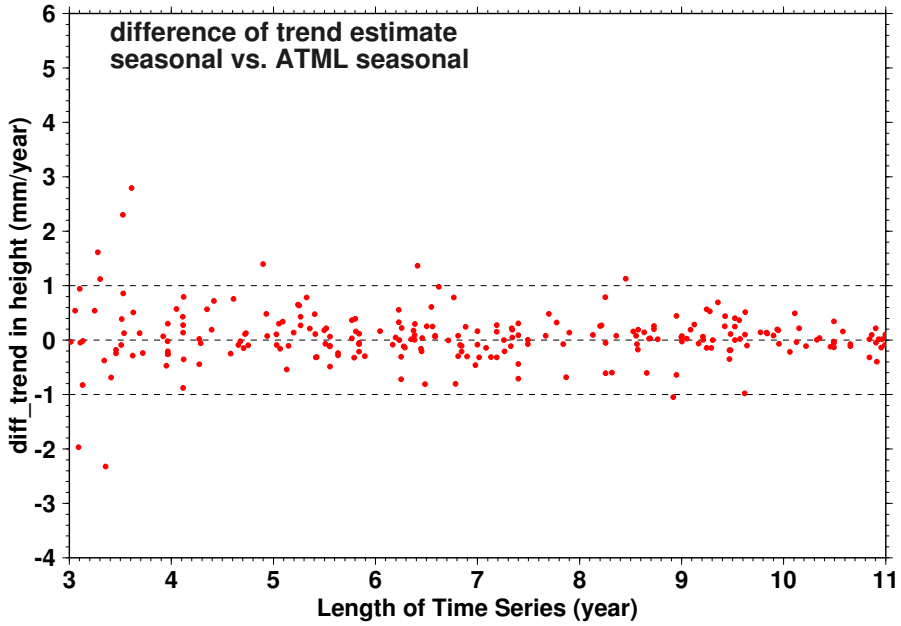

Figure 31: Differences of vertical rate estimates with and without ATML corrections against length of time series.

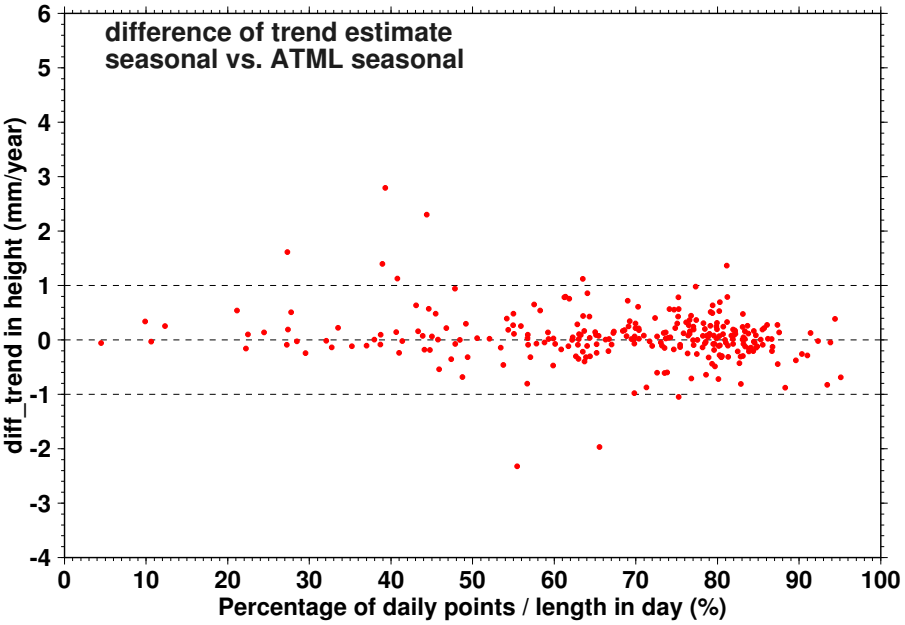

Figure 32: Differences of vertical rate estimates with and without ATML corrections against density of time series.

DOI: 10.2312/GFZ.b103-08037

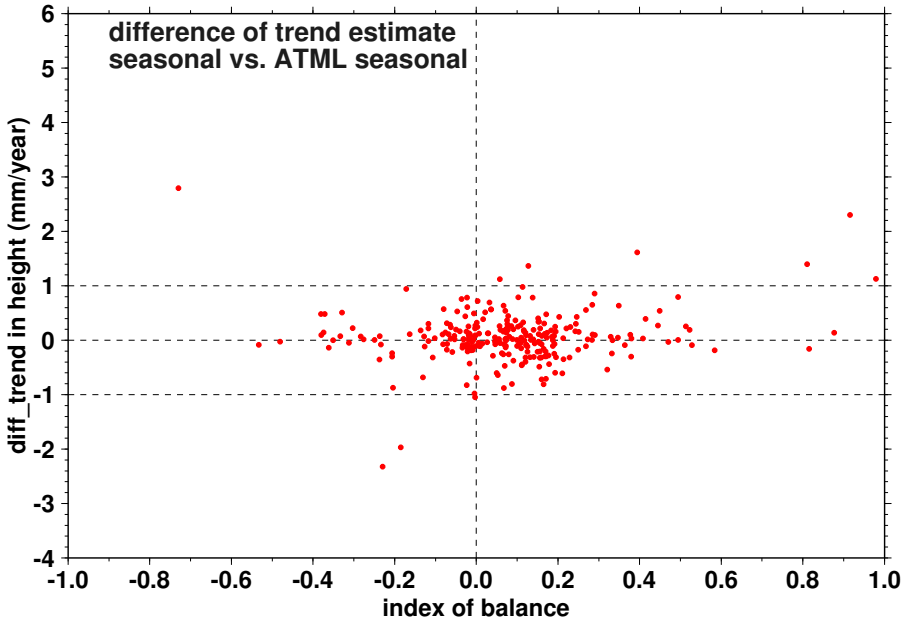

Figure 33: Differences of vertical rate estimates with and without ATML corrections against balance index of time series.

DOI: 10.2312/GFZ.b103-08037

5 Estimation of vertical velocities from height time series

This section attempts to estimate vertical velocities by analyzing GPS time series. Meanwhile horizontal velocities are also estimated to verify the quality of the time series and the procedure of velocity estimation. During the time series analysis, identification of offsets in time series is an important step in ensuring the reliability of the linear rate estimation.

5.1 Final procedure to form GPS time series for linear rate estimation

The time series are generated with the approaches described in section 2 after updating ocean tide loading (OTL) corrections (see section 3) and applying atmospheric pressure loading displacement (ATML) corrections (see section 4). Figure 34 demonstrates the summarized procedure used to form the final GPS time series for estimating vertical and horizontal velocities. In addition to Figure 2, updating OTL corrections and applying ATML corrections are also included in the flowchart.

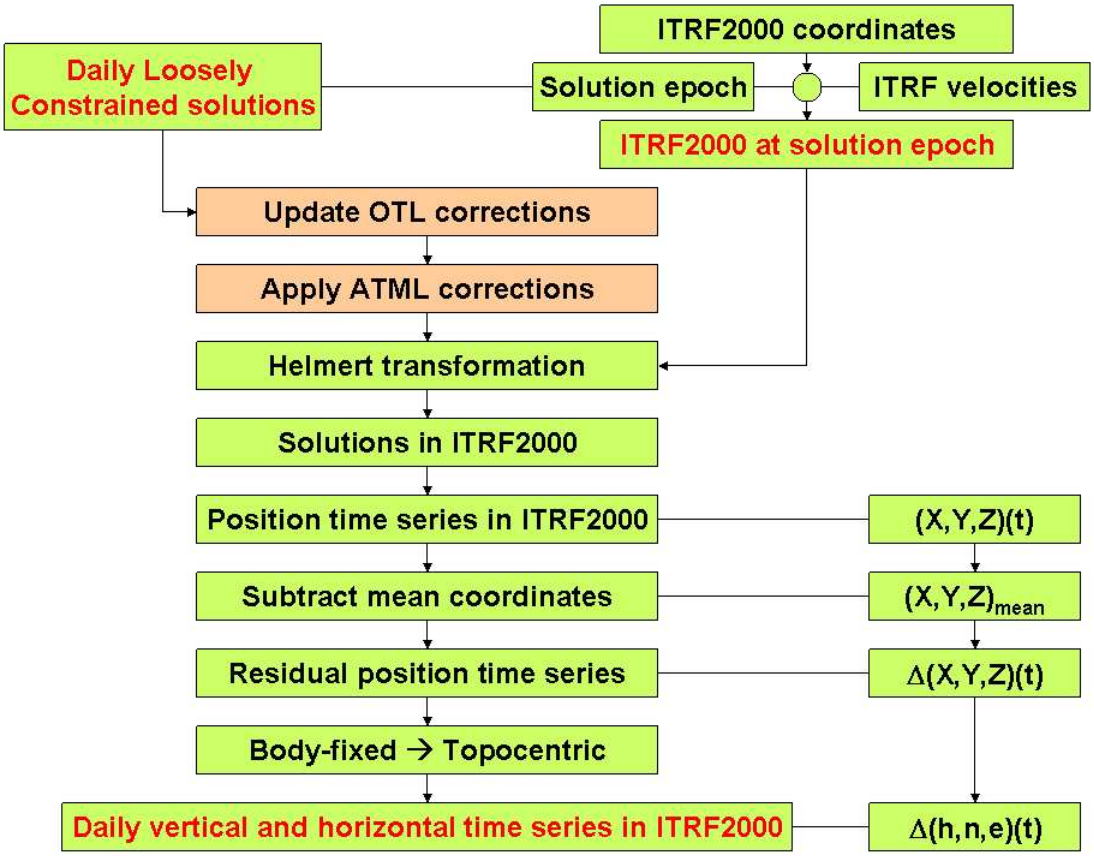

Figure 34: Summarized procedure of forming GPS time series for vertical rate estimation.

DOI: 10.2312/GFZ.b103-08037

5.2 Identification of offsets in GPS time series

Offsets in time series may contaminate the estimation of linear rates. Therefore, any offsets should be identified and modelled as step functions. In this study, the offsets in height time series are identified manually. The identified time series offsets for a station are recorded into a so-called 'jmptbl' file which is used to model potential step functions during time series fitting.

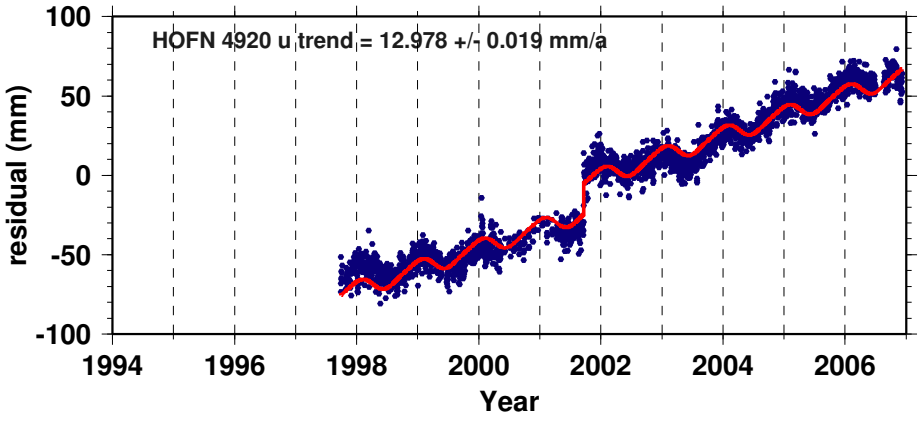

Figure 35: Offset in the height time series at GPS station HOFN (Hoefn, Iceland).

The identification of offsets in height time series can be aided from other perspectives. Sometimes, the offset in height time series is not so obvious. In such a case, it can be confirmed by inspecting the horizontal time series. The obvious horizontal offsets can help to locate the offsets in height time series. Some offsets are caused by hardware exchanges. For example, Figure 35 shows an offset at GPS station HOFN caused by the antenna exchange at September 21, 2001 recorded in IGS log file of the station. The time series offset reveals that the reported new antenna height value is deviated by about 31.8 mm. Additionally, there is an offset table for IGS stations maintained by IGS. This table can be also used as a reference to identify offsets.

Sometimes 'common-mode' offsets happen repeatedly in the time series of several stations. Normally, this kind of offsets is caused by an abnormally behaving reference station used for aligning solutions to ITRF. Such station(s) has to be identified manually to remove the corresponding offsets.

Note that the more offsets are modelled, the weaker the vertical rate estimates are. Therefore, time series offsets should be flagged very carefully and as infrequently as possible. For the small pieces of outliers, it's normally better to exclude them from the time series before carrying out estimation.

5.3 Estimation of horizontal and vertical velocities of GPS stations

The velocities are estimated with the method described in section 2.3. To obtain robust estimates, the data points are re-weighted according to their fitting residuals

DOI: 10.2312/GFZ.b103-08037

to get robust estimates by reducing the influences of the outliers. The estimation procedure carries out iteratively by replacing the *a priori* standard deviations of the data points with the posteriori residuals from the last estimation. Thus, the outliers are automatically lower weighted. To avoid ill-conditioned normal equation caused by an infinite weight, the minimum standard deviation is taken as 1 mm. The convergence criteria are 1 μm for all the solved-for parameters. This estimation procedure can effectively avoid the impact of the outliers and ensure a reasonable result.

To reduce the influence of the outliers, an approach was also tried by removing the outliers by a criterion of 3σ. However, the solutions could become unstable while fewer and fewer data points are kept. The instability could be also caused by improper modelling of some time series. Therefore, the re-weighting approach has been finally used for robust velocity estimation. The estimated velocities in vertical, east and north components are given in Table 9 in Appendix C (see page 84). Standard deviations of the estimates are also given in the table.

Figure 36 demonstrates the horizontal velocities estimated by this study. To verify the estimated velocities, the horizontal velocities from this study and ITRF2000, from this study and NNR-NUVEL-1A model are plotted in figures 37 and 38 in pairs for comparison. The comparison between this study and ITRF2000 shows that for most compared stations, the horizontal velocities are quite consistent with ITRF2000, except stations PIMO, BILI and INEG. The time series of these stations from this study are illustrated in Figures 39 - 42. Based on the quality of the time series, we are confident with the estimated velocities from this study. The comparison between this study and NNR-NUVEL-1A shows that for most compared stations, the horizontal velocities are quite consistent, except some stations located at plate boundary regions. This could be partly caused by the inaccurate division of the plate boundaries used in the NNR-NUVEL-1A plate velocity model.

Estimated vertical velocities are demonstrated in figure 45. For clarity, the regions with crowded symbols are zoomed out in figure 46 for North America, figure 47 for Europe, figure 48 for the region around Australia, figure 49 for New Zealand.

5.4 Nonlinear and inter-annual vertical motion

For quite a few stations, the long-term trends are not linear and also not periodic. We call such behavior inter-annual variations. For such stations, one should be cautious when using the estimated linear vertical rates derived in this study. The stations with outstanding inter-annual variations in our study include: ALBH, ALGO, AMC2, BAHR, BAKO, BARH, BILI, BJFS, CABL, CEDU, COCO CREU, DAEJ, DAV1, DRAO, DUBO, FAIR, FLIN, FORT, GODE, GOLD, GRAS, HARV, HNPT, HOB2, HOLM, JPLM, KELS, KELY, KIT3, KOSG, LHAS, MAC1, MAG0, MAS1, MCM4, MDO1, MKEA, NPRI, NYA1, NYAL, ONSA, OUSD, PALM, PGC5, PIE1, PLO3, POTS, PRDS, REYK, RIOG, SAG1, SEAT, SFER, SIO3, SOL1, THTI, TID2, TIDB, TIXI, TORP, TRO1, TSKB, UCLU, UNSA, URUM, USNA, USUD, VARS, VESL, VILL, VIMS, WES2, WHIT, ZIMM, in total, 75 stations. Height time series for these stations are demonstrated in Appendix D. For these stations, further studies should

DOI: 10.2312/GFZ.b103-08037

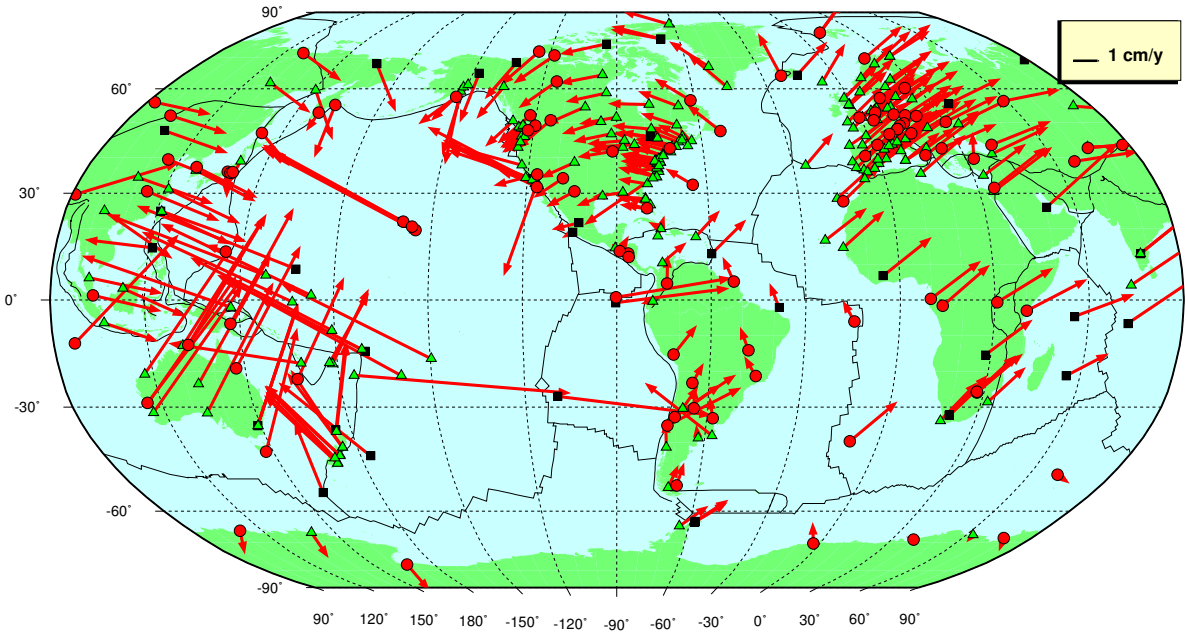

Figure 36: Horizontal velocities of the analyzed GPS stations for TIGA in the ITRF2000 from data spanning 1994.0-2007.0 (from this study).

be carried out to properly model the inter-annual variations. The idea of linear-trend analysis diagram used by Wolf et al.[48] might be a feasible way to analyze the linear trends of some of these stations.

DOI: 10.2312/GFZ.b103-08037

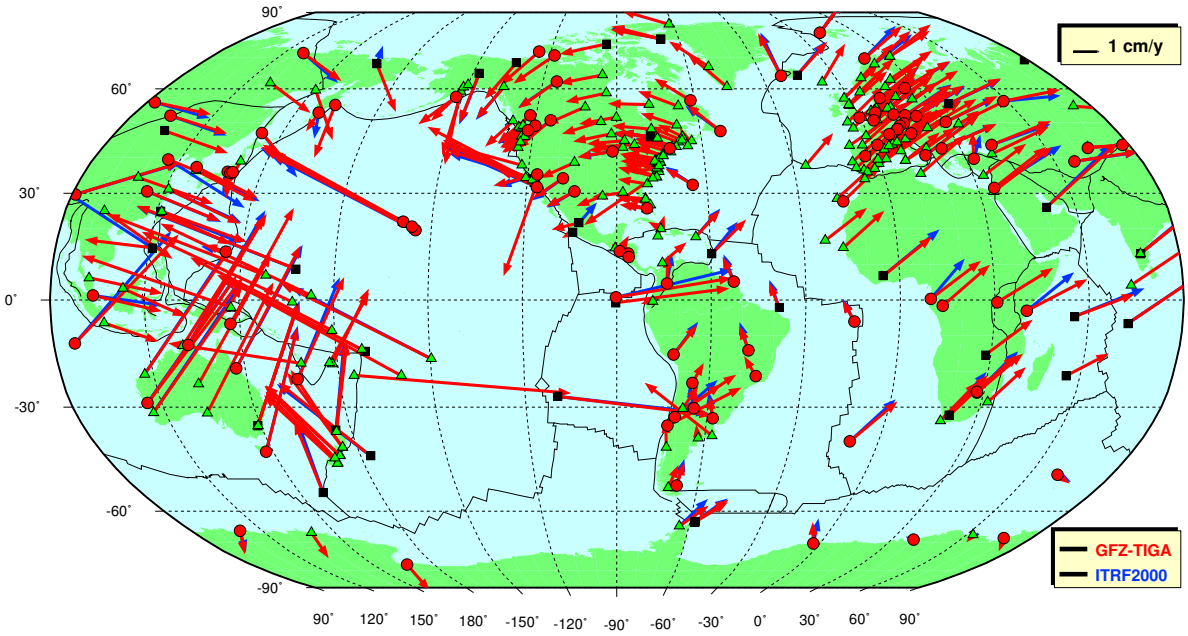

Figure 37: Comparison of horizontal velocities from this study with ITRF2000.

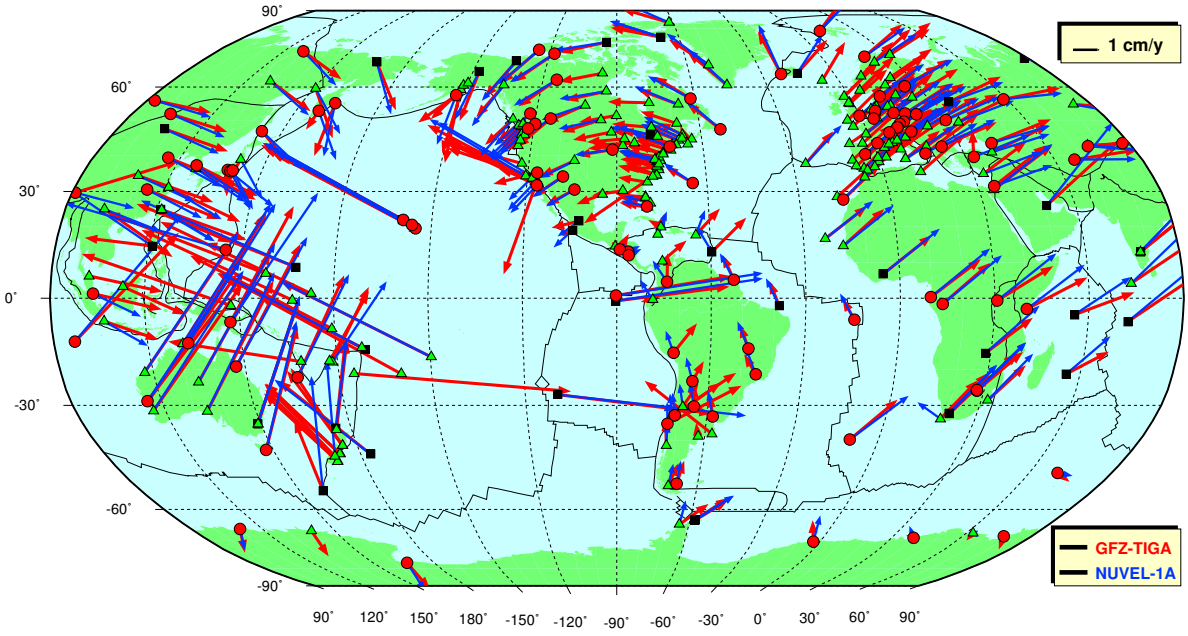

Figure 38: Comparison of horizontal velocities from this study with NNR-NUVEL-1A model.

DOI: 10.2312/GFZ.b103-08037

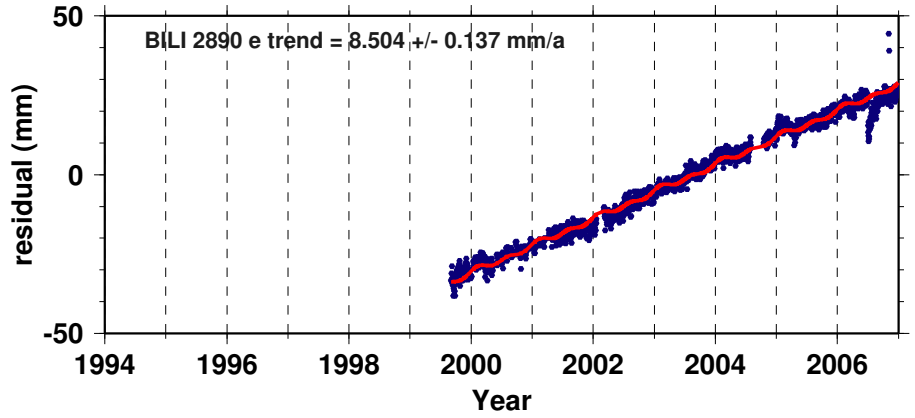

Figure 39: East-component time series of the station BILI, of which the horizontal velocity is significantly different from ITRF2000.

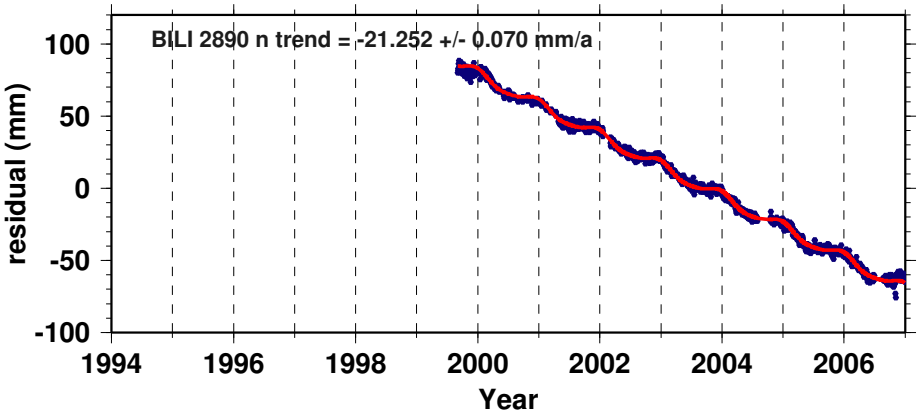

Figure 40: North-component time series of the station BILI, of which the horizontal velocity is significantly different from ITRF2000.

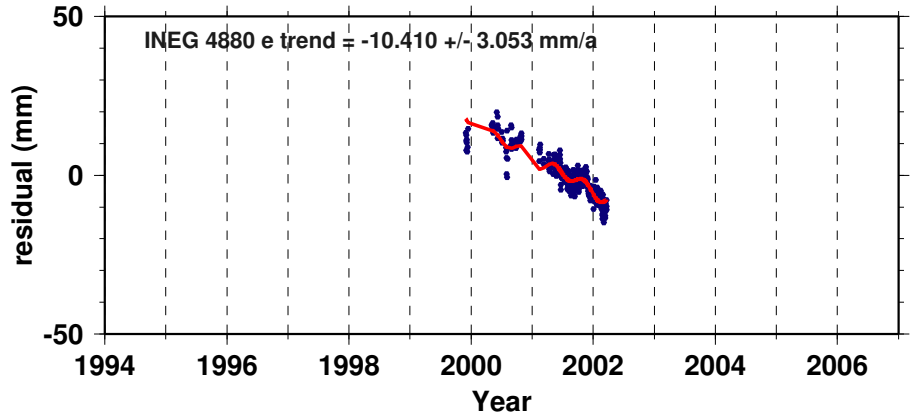

Figure 41: East-component time series of the station INEG, of which the horizontal velocity is significantly different from ITRF2000.

DOI: 10.2312/GFZ.b103-08037

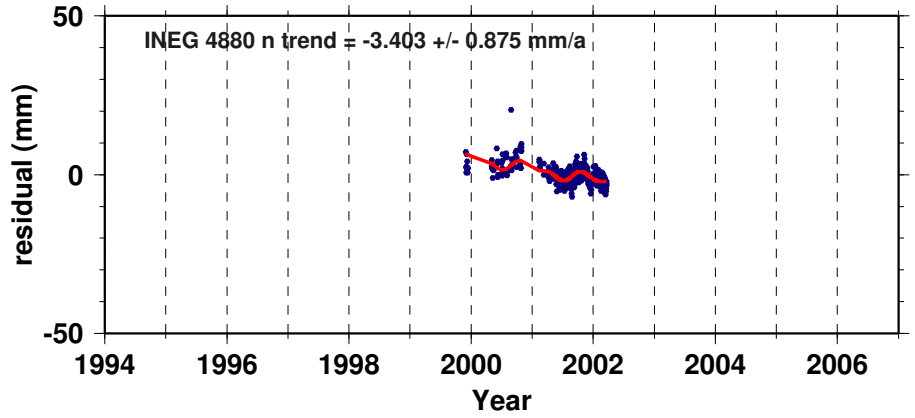

Figure 42: North-component time series of the station INEG, of which the horizontal velocity is significantly different from ITRF2000.

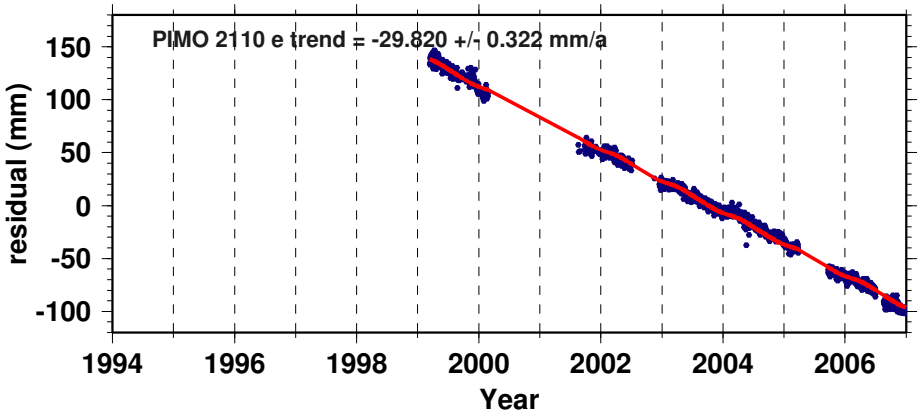

Figure 43: East-component time series of the station PIMO, of which the horizontal velocity is significantly different from ITRF2000.

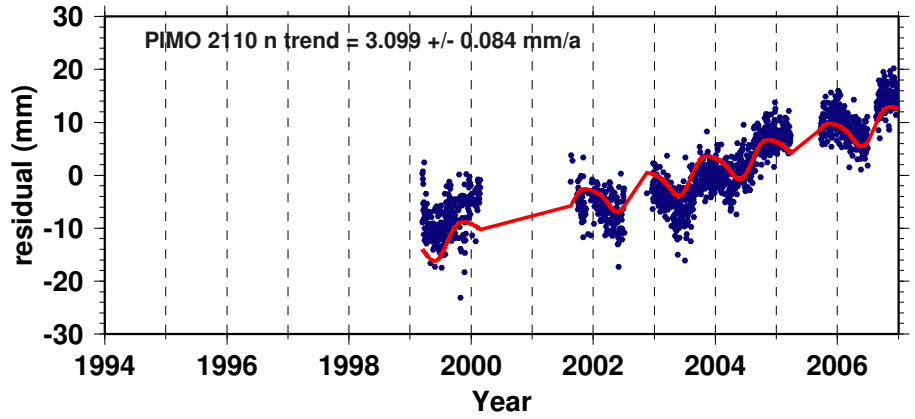

Figure 44: North-component time series of the station PIMO, of which the horizontal velocity is significantly different from ITRF2000.

DOI: 10.2312/GFZ.b103-08037

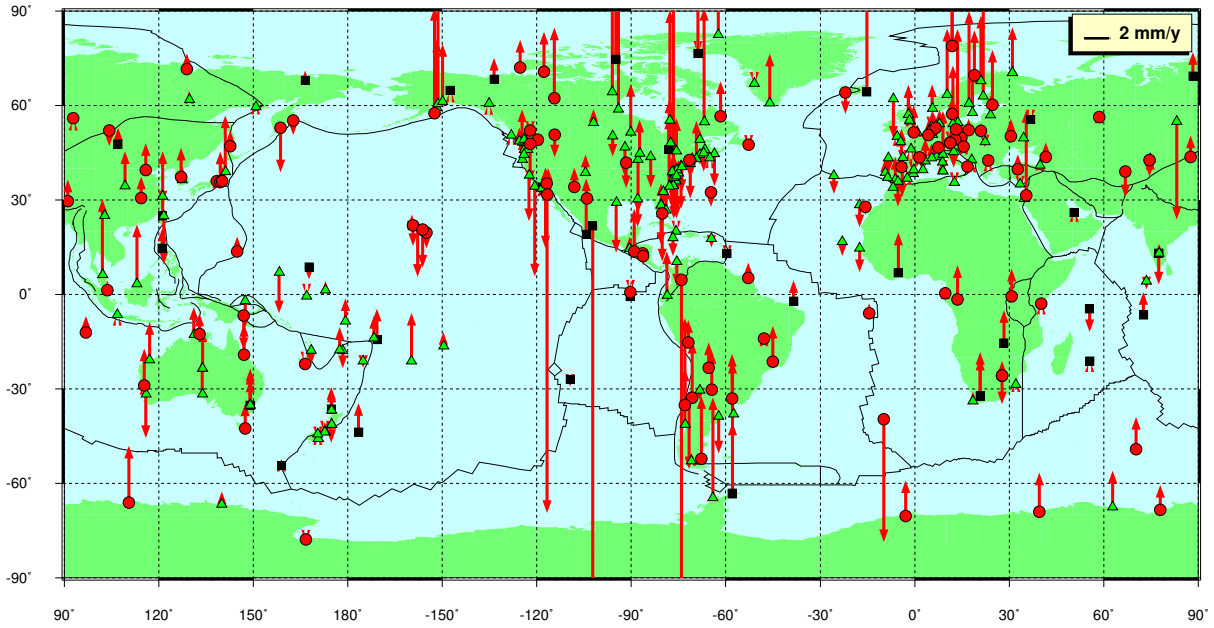

Figure 45: Vertical velocities of the analyzed GPS stations for TIGA/SEAL in the ITRF2000 from data spanning 1994.0-2007.0.

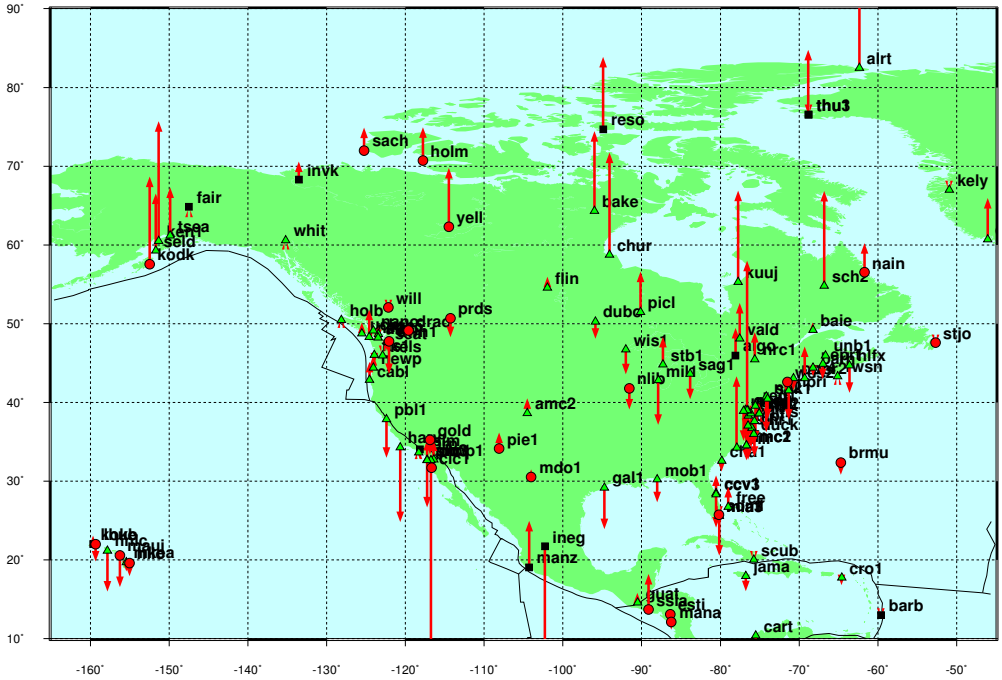

Figure 46: Vertical velocities of the analyzed GPS stations at North America.

DOI: 10.2312/GFZ.b103-08037

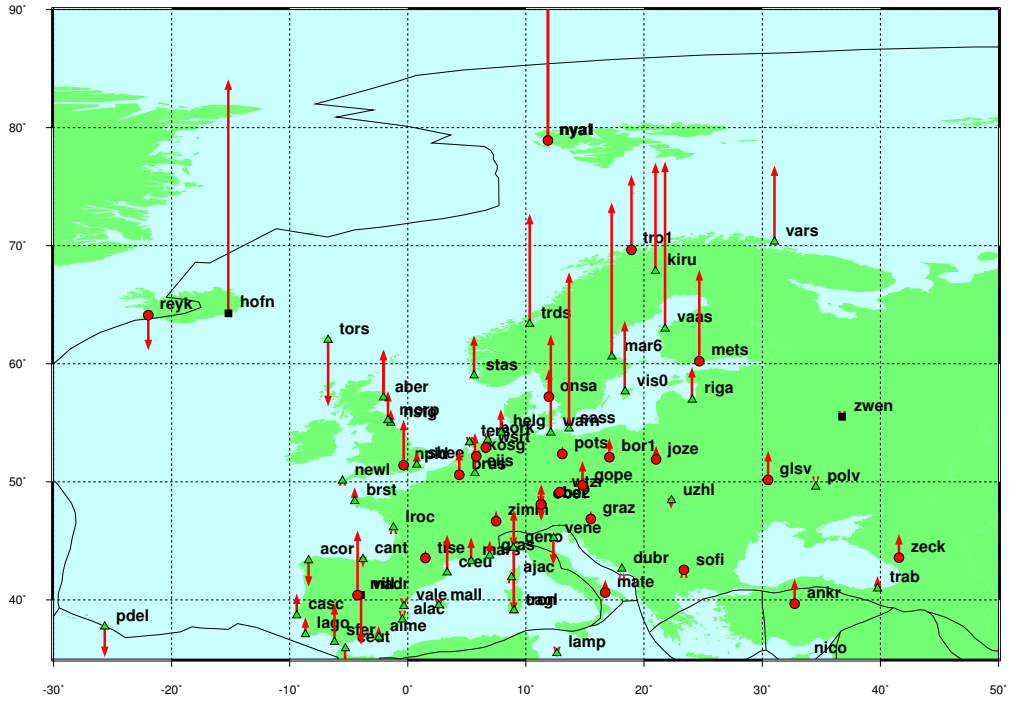

Figure 47: Vertical velocities of the analyzed GPS stations at Europe.

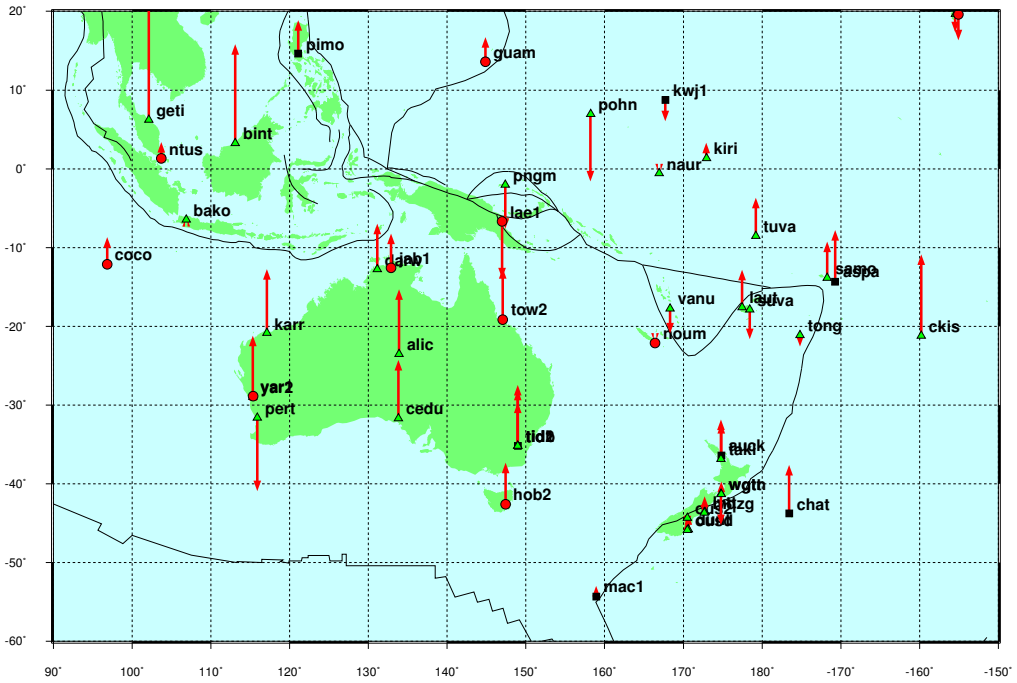

Figure 48: Vertical velocities of the analyzed GPS stations around Australia.

DOI: 10.2312/GFZ.b103-08037

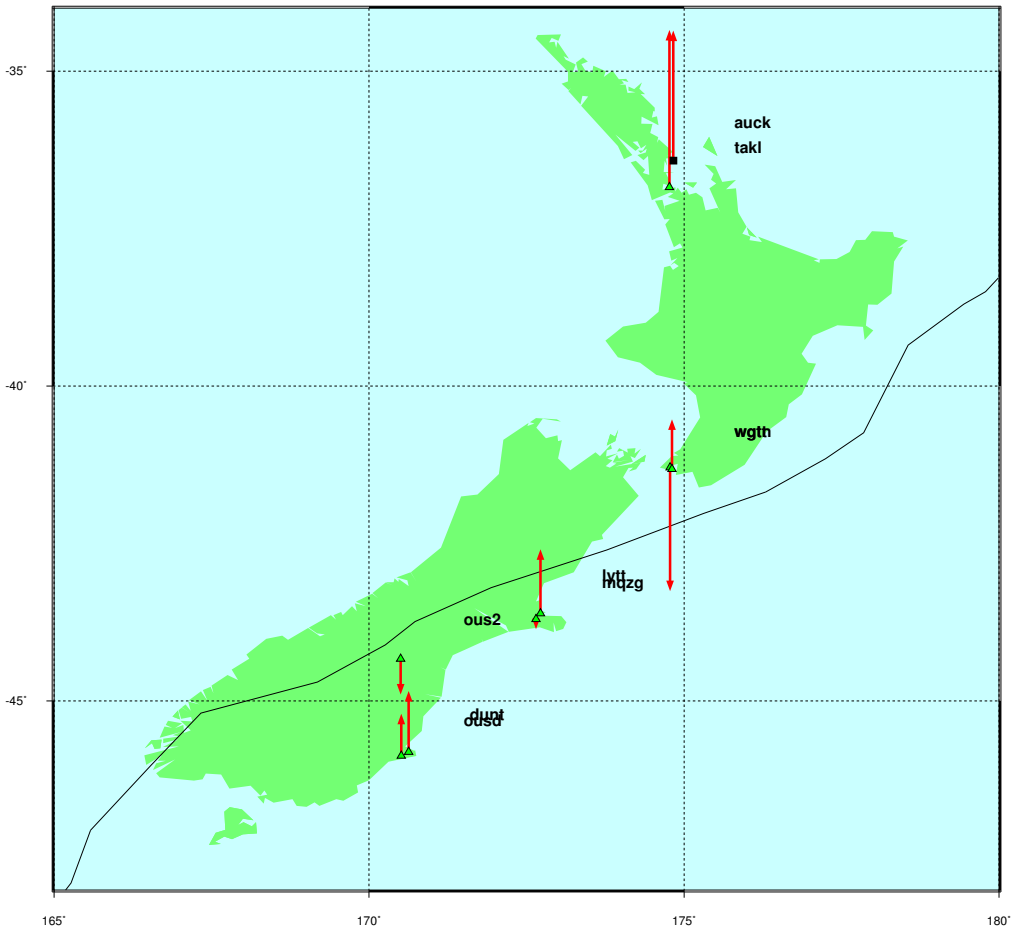

Figure 49: Vertical velocities of the analyzed GPS stations at New Zealand.

DOI: 10.2312/GFZ.b103-08037

6 The stability of GPS inferred reference frame

Monitoring vertical land motion is essentially sensitive to the stability of the to-be-aligned terrestrial reference frame (TRF), especially the long-term stability of the TRF scale. Therefore, close attention should be paid to the stability of the to-be-aligned TRF. While aligning the daily GPS solutions with ITRF2000 by 7-parameter similarity transformation, we can get the time series of transformation parameters, including 3 translation parameters (Fig. 50), 3 rotation parameters (Fig. 51), and 1 scale factor (Fig. 52). The time series of the transformation parameters can be used to inspect the stability of the GPS inferred reference frame compared to ITRF2000.

6.1 Translation parameters

Approximately, the loosely constrained solutions are in a center-of-mass (CM) terrestrial reference frame. To balance the mass redistribution of the surface fluid, the center of network defined by a set of ground stations (e.g. the origin of ITRF) moves around the center of mass in the terrestrial inertial coordinate system. Translation parameters, the shift of the origin of coordinate system of the solution to a specified reference system (e.g. ITRF), represent the motion of the Earth's center.

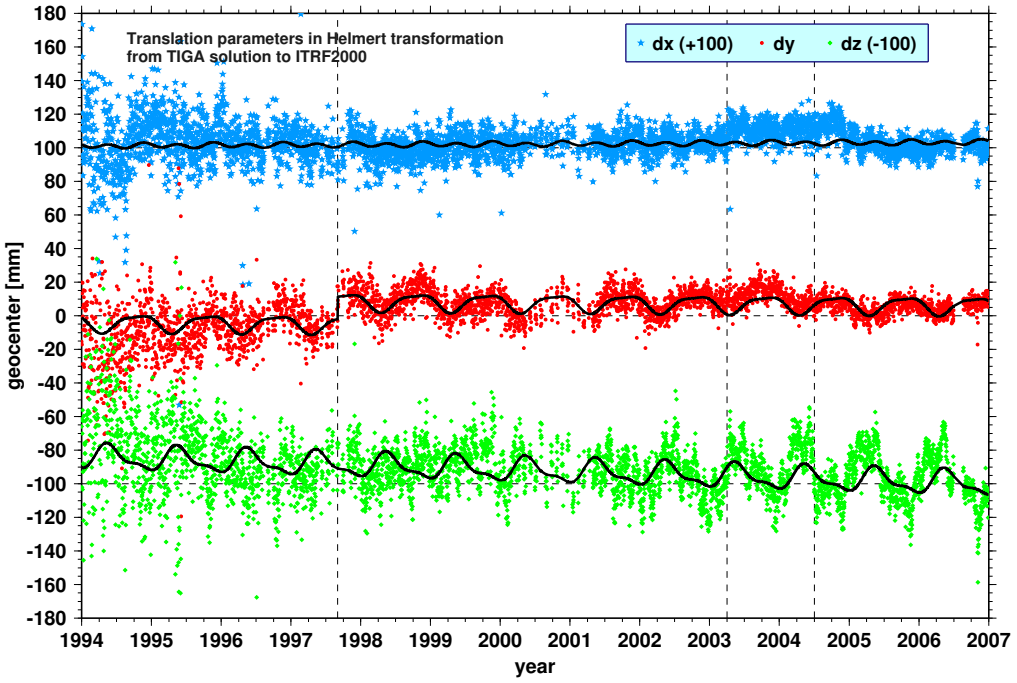

Figure 50: Time series of translation parameters in Helmert transformation from TIGA GPS solutions to ITRF2000. Solid black lines are fitting with a constant bias, linear trend, annual and semi-annual wave.

The time series of translation parameters (Figure 50) show obvious seasonal variations, especially in y and z components. The seasonal signals mainly come from the surface mass redistribution, including the effects of atmosphere, ocean, global surface

DOI: 10.2312/GFZ.b103-08037

water and snow, melting glaciers and changing sea level[8]. The significant seasonal signal in z-component may reflect the asymmetry of land-ocean distribution in the northern and southern hemispheres. The larger scatter in z-component may reflect the sparse coverage of reference stations in polar regions. The seasonal variation in y-component is obviously regular, reflecting the global land-ocean distribution[8]. For example, the well-known significant seasonal surface water storage variations in Siberia and Amazon areas derived e.g. by the high resolution (temporal and spatial) gravity model time series, and the significant seasonal atmospheric loading variations in American and Asian continents (see the global distribution of correlation coefficients between GPS and atmospheric loading induced vertical displacement, Figure 20) may mostly contribute to the seasonal signal in y-component.

Compared to the early years, the translation parameters become more stable since 1998 due to the increasing number of high-quality reference stations as shown in Figure 4. According to Eq. (1), the amplitude of the translation parameters is also correlated with the scale factor. If the estimated scale factor $s < 0$, the estimated translation parameters will be amplified. Contrariwise, a positive s will reduce the estimated translation parameters. Comparing Figure 50 and 52, we can see this correlation generally. From 1994.0 to 1997.0, the scale factors are much less than zero and the scatter of the translation parameters are also larger. Later on, the scatter is reduced as the scale factor becomes larger and larger.

Some offsets are visible in the time series of translation parameters. At 2003.25 as marked in Figure 50, there are obvious offsets in x and z components. At 2004.5, another offset occurs in z component. Coincidently, at 2003.25, a Block IIR satellite (PRN 21, SVN 45) was launched and a Block II (PRN 21, SVN 21) was decommissioned, at 2004.5, a Block IIR satellite (PRN 23, SVN 60) was launched and a Block IIA (PRN 23, SVN 23) was decommissioned. The change of the constellation may not cause significant geocentric variation unless the antenna offsets of these two newly launched Block IIR satellites are remarkably biased from their true values, since other launches of Block IIR satellites do not correspond to any significant geocentric offset. Offset also occurs in x and especially y component around 1997.67, while the number of reference stations has a turning point (see Fig. 4). This effect may come from the uneven distribution of the global network at that time, especially around x-z and y-z coordinate planes due to the land-ocean distribution. This is possible to be proved by statistics of the number of reference stations along x-z and y-z coordinate planes. From 1997.67, the geocenter becomes very stable, especially the y component after the offsets. This may be caused by the increase of the number of stations since this time, as a uniformly distributed reference network would balance the realization of the geocenter.

The linear trend $(\dot{x}_\mathrm{c},\ \dot{y}_\mathrm{c},\ \dot{z}_\mathrm{c})$ of the geocentric motion can be directly expressed as the linear vertical motion of a ground site located at latitude ϕ and longitude λ as follows

$$\dot{h} = \dot{x}_\mathrm{c} \cos\lambda \cos\phi + \dot{y}_\mathrm{c} \sin\lambda \cos\phi + \dot{z}_\mathrm{c} \sin\phi \ . \tag{57}$$

To estimate the linear geocentric motion, the translation parameter time series are fitted with a constant bias, a linear trend, an annual and a semi-annual wave by

DOI: 10.2312/GFZ.b103-08037

the same weighted least-squares estimator as used in section 5.3. Concerning the seasonal waves, the initial epoch is taken as MJD 51909. To obtain robust estimates, the estimation procedure carries out iteratively by replacing the *a priori* standard deviations of the data points with the posteriori residuals from the last estimation. Thus, the outliers are automatically lower weighted. To avoid ill-conditioned normal equation caused by an infinite weight, the minimum standard deviation is taken as 1 mm. The convergence criteria are 1 μm for all the solved-for parameters. This estimation procedure can effectively avoid the impact of the outliers and result in a reasonable result.

The estimated parameters are listed in Table 6. For the y-component, a jump at 1997.67 is fitted as a step-function. The estimated jump is 13.4 mm. This changes the estimate of the linear rate significantly from 0.382 to -0.256 mm/a. The small z-component linear rate indicates that the solutions are relatively stable in z-component.

The linear rate of the translation parameter time series may imply the evolution of the network. After the solutions have been translated to ITRF2000 origin, these linear rates would not affect the estimate of the motion rate of a ground site from position time series, which is homogeneously expressed in a unified reference frame. However, since the translation parameters are estimated from a finite set of stations in a sense of least squares, they may be deteriorated by bad stations, or by the uneven distribution of reference stations, especially in the early years of IGS activities, in which few stations were established in the southern hemisphere.

Table 6: Fitted parameters of the Helmert transformation parameters (translation parameter and scale factor).

	const.	linear	annual		semi-annual	
	bias	(a^{-1})	amp.	phase	amp.	phase
Trans. x (mm)	2.3	0.165	0.6	344.25°	1.3	277.08°
Trans. y (mm)	5.3	0.382	4.1	290.72°	1.1	7.42°
with jump	-6.0	-0.256	5.0	289.32°	1.4	20.14°
Trans. z (mm)	7.3	-1.228	6.5	142.86°	2.6	242.14°
Scale factor (ppb)	0.5	0.373	0.22	30.20°	0.05	183.04°

6.2 Rotation parameters

Only a very marginal effect could be expected for the rotation parameters on the vertical positioning. Therefore, only the time series of the rotation parameters are demonstrated here in Figure 51 to observe the stability of the orientation of the GPS reference frames implied in the solutions. Figure 51 shows that the orientation is generally rather stable except for the rotation around Z axis in the years 2003 and 2004. The reason of the instability has yet to be studied.

DOI: 10.2312/GFZ.b103-08037

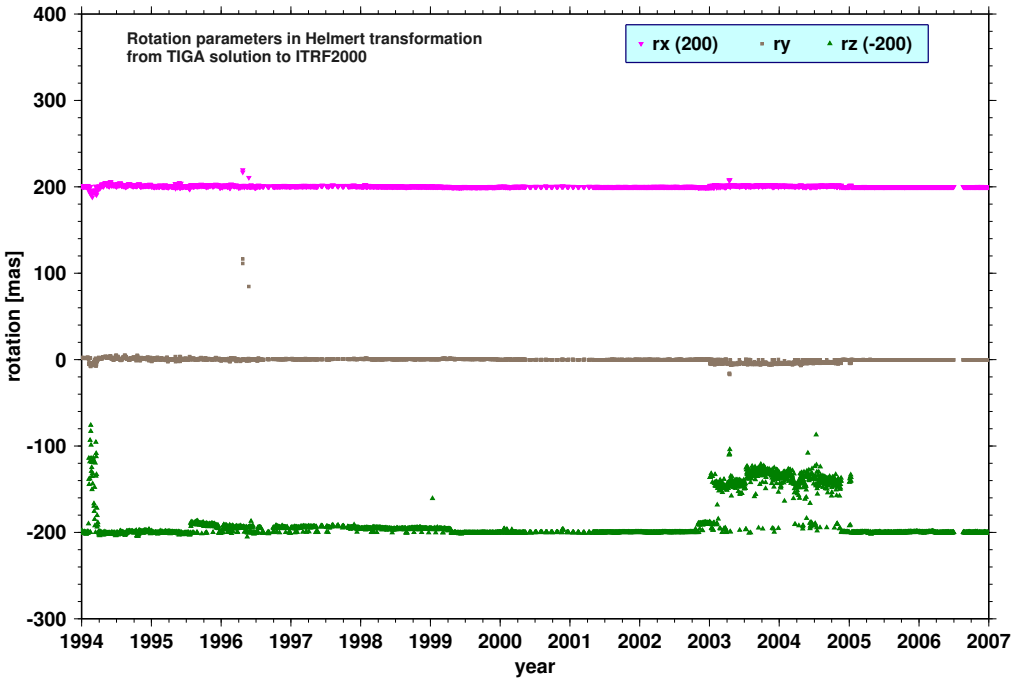

Figure 51: Time series of rotation parameters in Helmert transformation from TIGA GPS solutions to ITRF2000.

6.3 Scale factors

From Eq. (1), a positive scale factor means a smaller scale of our solution compared to ITRF2000. Figure 52 shows that the scale of our solutions is not around a constant, but becoming smaller and smaller in a nonlinear way accompanied by an inter-annual variation. In general, the variation of the scales can be classified as five phases as separated in Figure 52 by vertical rasters in solid lines at 1996.75, 1999.75, 2001.15 and 2004.0. In the two phases, 1996.75-1999.75 and 2001.15-2004.0, the scales of the solutions are relatively stable, with nearly constantly 0.5 ppb larger and 1 ppb smaller. In the other three phases, 1994.0-1996.75, 1999.75-2001.15 and 2004.0-present, the scales of the solutions decrease rapidly as indicated by the increasing scale factors.

The long-term scale change in the period of 1994.0-1996.75 may be correlated with the increasing number of reference stations during this time period (see Fig. 4).

The obviously larger negative scale factors during 1994.216-1994.5, which indicate a larger scale of the solution, are most likely caused by a wrong antenna offset of the newly launched Block IIA satellite (PRN6, SVN36) during the early phase of data analysis using this satellite. Since the file of satellite information used in data analysis has been updated periodically, this hypothetical error might have been corrected. Unfortunately, the SINEX files have not included the block of satellite antenna offset and therefore we have no chance to prove this suspicion by checking the history of used satellite antenna offset by inspecting the SINEX files. Hopefully, this suspicious error has been fixed and this scale change will not occur any more in future reanalyzed solutions.

DOI: 10.2312/GFZ.b103-08037

During the period from 1997.82 to 1998.10, the scale is obviously biased. This may be caused by the wrong recognition of a newly launched Block IIA satellite (PRN 8, SVN 38) as a Block IIR during the period from MJD 50753 (1997.84) to MJD 50900 (1998.24) (marked in Figure 52), while the satellite antenna offset was set at 1.6764 m but not 1.0229 m which is used for Block IIA satellites. This has been proved by a test analysis based on the normal equations. The problem should disappear during the reprocessing since the satellite antenna offset table has been carefully refined.

To interpret the scale variations, the status of the satellite constellation is also plotted in Figure 52 described with the number of satellites in Block types. From the figure we can see the correlation of the scale variation with the numbers of satellites of the Block types, especially the strong correlation with the number of Block IIR satellites. In the period of 1999.75-2001.15, the scale changed rapidly. Coincidentally, five Block IIR satellites were deployed, one Block I, three Block II and one Block IIA satellites were decommissioned. The rapid scale reduction in the period after 2004.0 is also accompanied by the latest climax of satellite constellation update, while three Block II and three Block IIA were replaced by seven Block IIR satellites.

The study by Zhu et al.[52] showed that the error in GPS satellite phase center offsets (PCO, position of transmitter phase center with respect to center of mass) will induce an improperly defined reference scale of the GPS solution. Usually, the PCO value of a flying satellite is poorly known due to the varying environmental condition in the space, even when they are calibrated in laboratory before launch. Due to improperly determined PCO values, the evolution of GPS satellite constellation will consequently cause a scale variation. We can tentatively conclude from the strong correlation of scale change and the deployment of Block IIR satellites, that the PCO values of Block IIR satellites are the worst determined compared to other block types. In fact, since the first launch of Block IIR (PRN14, GPS-41) at Dec. 6, 2000, the PCO of Block IIR satellites were never solved properly until this study. During the early period after the first Block IIR satellite was deployed, the IGS ACs tried to estimate the PCO value from real data. From the estimate, despite CODE, all other ACs got negative PCO values. As a compromise, a random median value of 0 m was adopted by most ACs but not JPL. From the rapid scale change of our solutions, we can say that this randomly adopted official PCO value by IGS ACs may be unrealistic. We hope that the new estimation of the PCO values will give more reasonable solutions[14].

Additionally, seasonal variations are also visible. This is mainly because the ITRF2000 did not consider the seasonal deformation of the geodetic network.

Although the vertical crustal motions of this study are estimated within ITRF2000, it is still worthwhile to have a budget estimation about the effect of GPS inferred reference scale on estimating vertical rates. From the linear rate of scale factors estimated in this study (see Table 6), a rate of 0.373 ppb/a corresponds to a linear vertical rate of about 2.3 mm/a. This effect is already far beyond the accuracy requirement of better than 1 mm/a of this study. Therefore, it is necessary to align the GPS solutions to ITRF2000 for studying the vertical crustal motion.

DOI: 10.2312/GFZ.b103-08037

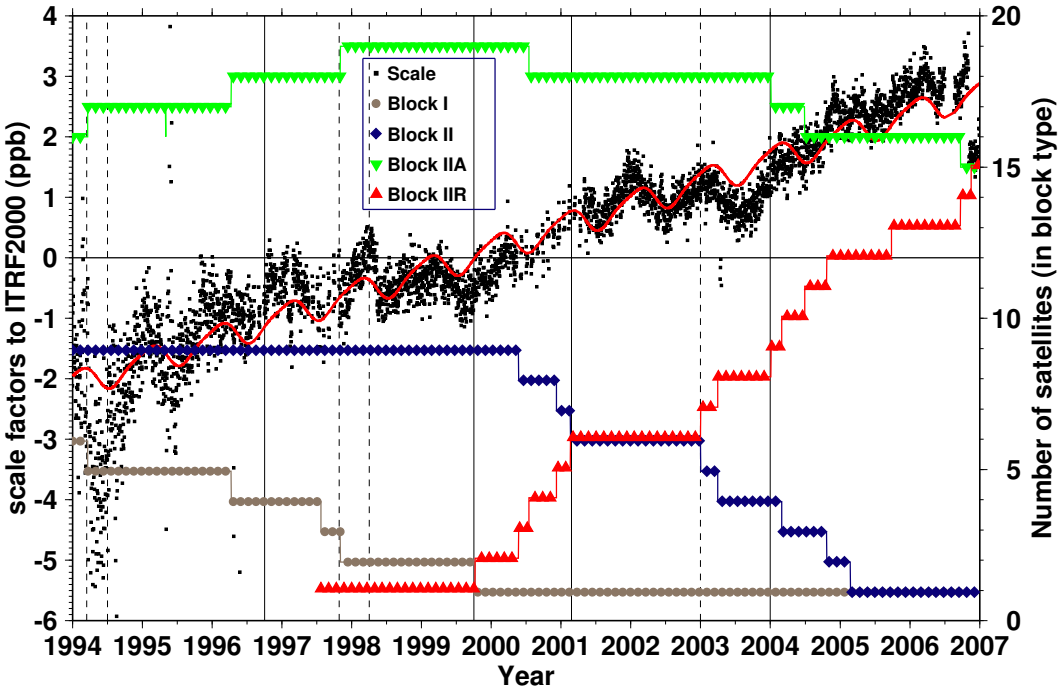

Figure 52: Scale factor variation in Helmert transformation from TIGA GPS solutions to ITRF2000, accompanied by the number of GPS satellites of each Block type and estimated satellite phase center offset for each Block IIR satellite.

DOI: 10.2312/GFZ.b103-08037

7 Summary and outlook

7.1 Summary

This report aims to study the vertical motion at tide gauges by analyzing GPS time series. The daily GPS time series are constructed by aligning the loosely constrained daily solutions with ITRF2000. To estimate vertical velocities, the position residual time series in cartesian system are transformed to local topocentric system including propagation of covariance information. To evaluate the quality of the time series, some statistics are taken concerning the density and balance of the time series which may relate to the deviation of the vertical rate estimates. While estimating the vertical rate, the time series are modelled with seasonal waves besides constant offset and linear rate. The offset within time series is modelled as step function.

The update of model corrections, especially of the ocean tide loading (OTL) corrections, is covered in this report. This is motivated by the old FES95.2 OTL model used in the data analysis without considering the constituents M_f, M_m and S_{sa}, while more modern OTL models are already available with complete 11 constituents conventionally used by the community. In this report, the FES95.2 OTL model is replaced with the GOT00.2 model by directly operating on the solutions without analyzing raw data. While finalizing this report, more modern OTL models (e.g. FES2004) have become available. This method can easily be applied to other models. The aliasing due to error in OTL models is discussed.

To improve the quality of the GPS time series, the corrections of atmospheric pressure loading (ATML) displacement are applied. Linear regression analysis shows that for most GPS stations, the GPS and ATML height time series are correlated with a high confidence level. The ATML contributions appear mostly for northern hemispheric sites with latitude $> 30°$. To stabilize the reference frame, the ATML corrections are applied before the time series are aligned with ITRF2000.

The effect of ATML on stability of reference frame is studied by comparing the 7 transformation parameters with and without applying ATML corrections. The comparison shows that the ATML effects on geocenter can be 2 mm by peak-to-peak. The effect on geocentric trend can be 0.01 mm/a, which would be completely transferred into vertical trend estimates. The seasonal amplitude of geocentric motion can reach 0.1 mm. For geocenter, the most significant effects are on the Z-component, which might be more sensitive due to the significant inhomogeneous distribution of the GPS sites in northern and southern hemispheres. The ATML effects on frame rotations can reach 0.2 mas peak-to-peak. However, the rotations would not affect the vertical rate estimate significantly. The ATML effect on reference scale can be 0.5 ppb in the sense of scattering. However, the long-term stability of the reference scale is not affected significantly, only 0.003 ppb/a corresponding to only 0.02 mm/a.

Meanwhile, the ATML effect on vertical rate estimates could reach 1 mm/a, which is equivalent to the accuracy requirement of the TIGA/SEAL project. This effect could not be explained either directly by the vertical trend of the ATML time series itself, or indirectly by the effect on the stability of the reference frame. The ATML effect

DOI: 10.2312/GFZ.b103-08037

on vertical rate estimates is also inspected against the quality of the GPS time series, e.g. the length, the density and the balance. The inspection shows that the longer and denser time series are less affected. However, the correlation between ATML effects and the time series quality are not significant to explain the effect. Most likely, the effect comes from the correlation between the modelled parameters while the seasonal parameters are affected simultaneously.

The vertical rates are estimated from analyzing the GPS height time series in ITRF2000 after updating OTL corrections and applying ATML corrections. Before the final estimation, the offsets in time series have to be identified completely to avoid deviated estimates. For validation purposes, the horizontal velocities are also estimated to compare with ITRF2000 and NNR-NUVEL-1A models. The comparison shows that our solutions coincide with ITRF2000 and NNR-NUVEL-1A generally very well. The vertical rate estimates are still not validated by ITRF2000. In general, ITRF2000 has shorter GPS solutions (till 2000.0) than ours. With longer time series and ATML corrections, our vertical rate estimates should be more reliable than ITRF2000.

Nonlinear and inter-annual behaviors of the GPS time series are noticed in this report. For about 75 GPS stations, the height time series do not develop linearly. In this report, these stations are simply listed with illustrations of their height time series for further study.

The stability of reference frame, especially for the scale, is crucial for studying the vertical motion. This report inspected the time series of Helmert transformation from TIGA GPS solutions to ITRF2000 and found that the scale factors of our solutions vary non-regularly. This non-regular scale factor development is found to be correlated with the update of the GPS constellation. The reasonable interpretation is that inconsistent phase center offsets of the GPS satellite transmitter antennae are used.

7.2 Outlook

Since the study in this report, there have been some important developments in GPS data analysis concerning the models, algorithms and conventions. The key developments are as follows:

- Absolute antenna PCO/PCV models have conventionally replaced the relative PCO/PCV models. According to the study by Cardellach et al. (2007), the vertical error caused by satellite antenna PCO/PCV cannot be solved by 7-parameter transformation. Therefore, it is necessary to re-estimate the 3-D site velocities with re-analyzed GPS solutions.

- More modern reference frame ITRF2005, which is compatible with the absolute antenna PCO/PCV models, has been published and widely used within the community[2]. Additionally, ITRF2005 has included the contribution of more than five years of data since the release of ITRF2000. Therefore, ITRF2005 should provide a more stable reference frame for this study.

- More modern OTL model such as FES2004 has become available. Additionally,

DOI: 10.2312/GFZ.b103-08037

for the first time, applying correction for the motion of the center-of-mass of the solid Earth is recommended.

- New scheme of ambiguity fixing has been implemented in EPOS software which is able to fix about 97% of ambiguities[15].

- New algorithm of parameter elimination has been implemented in EPOS software which is able to analyze much larger network in one single solution[16].

Considering the above mentioned developments, it is very necessary to re-analyze the whole data set to get homogeneous time series. At the moment of finalizing this report, the re-analysis has started and some preliminary solutions are now ready for the first inspection.

The mechanism of the ATML effect on the vertical rate estimates is still not very clear. To understand why the ATML corrections affect the vertical rate estimates so significantly, a covariance analysis might help, given the assumption that other solved-for parameters like seasonal waves would affect the vertical rate indirectly.

For the detection of jumps in the time series, some algorithms could be introduced to make the procedure automatic and reliable. One approach, though a diffuse one, is to apply the continuous wavelet transform.

The vertical rate estimates could be further validated with ITRF2005. However, ITRF2005 has a geocentric drift of 1.8 mm/a relative to ITRF2000[2]. Therefore, one should be cautious of the selection of an ITRF for this study since the drift of the origin would be interpreted as vertical and horizontal rates of the ground stations.

Finally, the feedback from sea level study using the GPS vertical rate estimates is also important to further inspect the GPS time series in more detail. It is important to keep in mind that the goal of this study is to study the eustatic sea level change combining the relevant technologies, such as satellite altimetry, tide gauges and so on.

DOI: 10.2312/GFZ.b103-08037

8 Glossary

Abbreviation	Name
AC	Analysis Center
ATML	Atmospheric Pressure Loading
CODE	Center for Orbit Determination in Europe
EPOS	Earth Parameters and Orbit determination System
ERP	Earth Rotation Parameter
GFZ	GeoForschungsZentrum
IGS	International GNSS Service
ITRF	International Terrestrial Reference Frame
mas	milli arc second
MJD	Modified Julian Date
mm/a	millimeter per year
PCO	Phase Center Offset
PCV	Phase Center Variation
ppb/a	part-per-billion per year
SEAL	Sea Level Change: An Integrated Approach to Its Quantification
SINEX	Solution INdependent EXchange format
TIGA	GPS Tide Gauge Benchmark Monitoring - Pilot Project
TOS	TIGA Observing Station
TRF	Terrestrial Reference Frame
TRS	Terrestrial Reference System

9 Acknowledgments

It is difficult to properly acknowledge all those responsible for the work described here. Nevertheless, we would like to express our sincere appreciation to Mr. Thomas Nischan, Mrs. Waltraud Sommerfeld, and Mrs. Gerda Beeskow who technically supported the data processing which provided GPS solutions for the time series analysis described in this report. The plotting utilities *gmtmap* and *gmt2d* developed by Thomas Nischan based on *GMT*© are used. The maps for correlation analysis parameters between GPS and ATML (Fig. 20, 21) were initially made by Mrs. Gerda Beeskow with the data provided by this study. Kind appreciation is also extended to Dr. Galina Dick for her extensive discussion and selfless sharing of knowledge and experience from her work for the Real Time Troposphere project based on the same software package EPOS, to which she has also extensively contributed. The re-analysis of TIGA GPS data will be carried out by Dr. Sergei Rudenko based on the upgraded EPOS software and models. The review by Mr. Jonathan Davies on the draft of this report has significantly improved the wording towards native English. Mrs. Yaqin Li has helped editing the report to speed up the publication. We may not have referenced all the relevant publications in this technical report. This does not mean that the authors do not regard them as important; we simply prefer not to review all the relevant contributions. This work is carried out under the contract of the project SEAL which is granted with strategy funding (No.

DOI: 10.2312/GFZ.b103-08037

2000/13) by the Hermann von Helmholtz Association of German Research Centres (HGF), and the project TIGA which is under the frame of IGS activity. The ocean tide loading program used in the data processing is written by Dr. S. D. Pagiatakis.

DOI: 10.2312/GFZ.b103-08037

A Statistical parameters of the GPS time series

This section gives the statistical parameters for the GPS time series generated in this study (see Table 7). In the table, the 1st and 2nd columns are the IGS 4-char station name and the internal station numbers used in data analysis. The 3rd and 4th columns are the starting and end date of the time series. The 5th and 6th columns are the length of time series in years and days. The 7th column is the total number of daily data points. The 8th column is the density of time series. The 9th and 10th columns are the numbers of data points before and after the middle point. The 11th, i.e. the last column, is the balance index of the time series.

Table 7: Statistical information about GPS time series.

name	No.	yd_from	yd_to	L_{TS}/y	L_{TS}/d	N_{DP}	ρ_{TS}	N_{1h}	N_{2h}	n_{BI}
ABER	1153	1998.261	2006.365	8.3	3027	1274	42.1	512	762	0.20
ACOR	1551	1999.237	2006.365	7.4	2686	2089	77.8	925	1164	0.11
AIS1	4730	1998.025	1998.026	0.0	2	2	100.0	1	1	0.00
AJAC	1552	2000.323	2006.342	6.1	2212	1614	73.0	780	834	0.03
ALAC	1553	1999.215	2006.365	7.4	2708	2195	81.1	1022	1173	0.07
ALBH	4120	1994.001	2006.365	13.0	4748	4185	88.1	2068	2117	0.01
ALGO	4000	1994.001	2006.365	13.0	4748	4203	88.5	2068	2135	0.02
ALIC	3070	1997.220	2006.365	9.4	3433	2824	82.3	1227	1596	0.13
ALME	1554	2001.014	2006.359	5.9	2172	1985	91.4	958	1027	0.03
ALRT	4770	2003.034	2006.365	3.9	1428	1382	96.8	679	703	0.02
AMC2	4130	1998.294	2006.365	8.2	2994	2602	86.9	1125	1477	0.14
ANKR	1020	1995.176	2006.333	11.4	4176	2058	49.3	1138	920	-0.11
ANP2	4551	2001.172	2006.214	5.1	1869	137	7.3	95	42	-0.39
AOML	4840	1997.324	2004.095	6.4	2328	1911	82.1	891	1020	0.07
AREQ	5300	1994.037	2006.365	12.9	4712	3273	69.5	1785	1488	-0.09
ARTU	1980	1999.219	2006.364	7.4	2703	2354	87.1	1031	1323	0.12
ASC1	5700	1996.112	2006.053	9.8	3595	1980	55.1	1043	937	-0.05
ASPA	7130	2004.046	2006.349	2.8	1035	934	90.2	453	480	0.03
AUCK	3800	1995.261	2006.365	11.3	4123	3564	86.4	1563	2000	0.12
BAHR	6500	1996.175	2006.365	10.5	3844	3272	85.1	1399	1873	0.14
BAIE	4013	2003.063	2006.365	3.8	1399	1040	74.3	357	682	0.31
BAKE	4215	2003.063	2006.365	3.8	1399	980	70.1	314	665	0.36
BAKO	2910	1998.063	2006.365	8.8	3225	2567	79.6	1042	1524	0.19
BAN2	2720	2003.193	2006.365	3.5	1269	917	72.3	598	318	-0.31
BARB	5110	1997.333	2001.015	3.1	1144	367	32.1	205	162	-0.12
BARH	4020	1998.275	2006.351	8.2	2999	2530	84.4	1160	1369	0.08
BAY2	4210	1998.057	2004.158	6.3	2293	807	35.2	353	454	0.13
BILI	2890	1999.247	2006.365	7.3	2676	2176	81.3	976	1200	0.10
BINT	2016	1999.032	2002.260	3.6	1325	368	27.8	244	123	-0.33
BISH	2399	1996.161	2006.022	9.6	3515	2257	64.2	1003	1254	0.11

DOI: 10.2312/GFZ.b103-08037

Table 7: (*cont.*)

name	No.	yd_from	yd_to	L_{TS}/y	L_{TS}/d	N_{DP}	ρ_{TS}	N_{1h}	N_{2h}	n_{BI}
BJFS	2880	1999.294	2006.365	7.2	2629	2088	79.4	940	1147	0.10
BOGT	5400	1994.311	2006.365	12.2	4438	2426	54.7	870	1556	0.28
BOR1	9048	2002.317	2006.365	4.1	1510	1475	97.7	731	744	0.01
BORK	9638	2000.323	2003.036	2.2	810	671	82.8	279	392	0.17
BRAZ	5500	1995.063	2006.353	11.8	4309	2569	59.6	1008	1561	0.22
BRMU	4850	1994.001	2006.365	13.0	4748	3944	83.1	2011	1933	-0.02
BRST	1270	1998.304	2006.031	7.3	2650	1825	68.9	839	986	0.08
BRUS	1130	1994.001	2006.365	13.0	4748	3350	70.6	1859	1491	-0.11
CABL	4552	1997.242	2006.365	9.3	3411	2953	86.6	1349	1603	0.09
CAGL	1310	1996.001	2006.365	11.0	4018	3262	81.2	1436	1826	0.12
CANT	1555	2001.014	2006.365	6.0	2178	1968	90.4	912	1056	0.07
CART	5150	2000.035	2003.054	3.1	1116	236	21.1	65	171	0.45
CAS1	8200	1994.186	2006.365	12.5	4563	3612	79.2	1517	2095	0.16
CASC	1556	1998.197	2006.365	8.5	3091	2436	78.8	1022	1413	0.16
CCV1	4553	1996.038	199.001	2.9	1070	634	59.3	341	293	-0.08
CCV3	4554	1998.216	2006.365	8.4	3072	2581	84.0	1185	1396	0.08
CEDU	3710	1998.044	2006.365	8.9	3244	2603	80.2	1085	1518	0.17
CEUT	1557	2001.319	2006.341	5.1	1849	1550	83.8	864	685	-0.12
CFAG	5010	1999.001	2006.351	8.0	2908	1256	43.2	1099	157	-0.75
CHA1	4555	1995.242	2003.320	8.2	3001	2295	76.5	1150	1144	-0.00
CHAT	3400	1995.277	2006.365	11.2	4107	3588	87.4	1572	2015	0.12
CHL1	4556	1995.166	2001.365	6.5	2392	1681	70.3	859	822	-0.02
CHL2	4557	1996.143	2000.247	4.3	1566	70	4.5	30	40	0.14
CHPI	5510	2003.169	2006.365	3.5	1293	755	58.4	217	538	0.43
CHR1	4558	1995.343	1999.169	3.5	1288	825	64.1	293	532	0.29
CHUM	2438	1997.298	2006.365	9.2	3355	2462	73.4	1009	1452	0.18
CHUR	4040	1995.176	2006.365	11.5	4208	3182	75.6	1198	1984	0.25
CIC1	4211	1999.086	2006.365	7.8	2837	1423	50.2	410	1012	0.42
CKIS	7428	2003.041	2006.365	3.9	1421	844	59.4	337	506	0.20
COCO	3500	1996.165	2006.365	10.6	3854	2887	74.9	1079	1808	0.25
CONZ	5012	2002.336	2006.365	4.1	1491	1295	86.9	582	712	0.10
CORD	5550	1999.212	2006.121	6.8	2467	1079	43.7	334	745	0.38
CREU	1296	1998.350	2006.364	8.0	2937	2151	73.2	898	1252	0.16
CRO1	5800	1994.014	2006.365	13.0	4735	3271	69.1	1419	1851	0.13
DAEJ	2030	1999.078	2006.365	7.8	2845	2347	82.5	1028	1318	0.12
DAKA	6910	2003.259	2006.365	3.3	1203	547	45.5	305	241	-0.12
DARW	3230	1998.039	2006.365	8.9	3249	2280	70.2	798	1481	0.30
DAV1	8100	1994.186	2006.365	12.5	4563	3378	74.0	1335	2043	0.21
DGAR	3600	1996.136	2006.365	10.6	3883	1967	50.7	970	997	0.01
DRAG	1021	2000.039	2006.365	6.9	2519	1394	55.3	223	1170	0.68

DOI: 10.2312/GFZ.b103-08037

Table 7: (*cont.*)

name	No.	yd_from	yd_to	L_{TS}/y	L_{TS}/d	N_{DP}	ρ_{TS}	N_{1h}	N_{2h}	n_{BI}
DRAO	4750	1994.001	2006.365	13.0	4748	4200	88.5	2060	2140	0.02
DUBO	4045	1996.293	2006.365	10.2	3726	3230	86.7	1392	1838	0.14
DUBR	1558	2000.267	2005.347	5.2	1908	1103	57.8	473	630	0.14
DUCK	4559	1997.242	2004.103	6.6	2418	1870	77.3	829	1041	0.11
DUM1	8015	1995.030	2002.357	7.9	2885	705	24.4	43	661	0.88
DUNT	3013	1999.273	2006.329	7.2	2614	1643	62.9	588	1055	0.28
DWH1	4771	2002.293	2006.350	4.2	1519	1347	88.7	599	747	0.11
DWH1	4771	2002.293	2006.350	4.2	1519	1347	88.7	599	747	0.11
EIJS	1115	2002.035	2006.365	4.9	1792	1722	96.1	846	876	0.02
EISL	7200	1994.041	2004.063	10.1	3675	2334	63.5	1235	1098	-0.06
EPRT	4025	1998.275	2006.290	8.0	2938	2198	74.8	1091	1107	0.01
ESTI	5011	2002.306	2003.056	0.3	116	107	92.2	56	51	-0.05
FAIR	4200	1994.001	2006.365	13.0	4748	3855	81.2	1839	2016	0.05
FLIN	4030	1996.157	2006.365	10.6	3862	3232	83.7	1411	1821	0.13
FMC1	4560	1995.336	2000.359	5.1	1850	411	22.2	38	373	0.82
FMC2	4561	1995.206	2000.062	4.6	1683	1041	61.9	539	501	-0.04
FORT	5200	1994.001	2006.098	12.3	4481	3191	71.2	1899	1292	-0.19
FREE	4835	1999.159	2001.294	2.4	867	385	44.4	183	202	0.05
FTS1	4562	1996.020	2006.365	10.9	3999	3285	82.1	1371	1913	0.16
GAL1	4563	1995.273	2003.190	7.8	2840	2163	76.2	1080	1083	0.00
GALA	7250	1996.034	2002.313	6.8	2472	1513	61.2	774	739	-0.02
GENO	1315	1998.204	2006.365	8.4	3084	2601	84.3	1172	1429	0.10
GETI	2015	1999.001	2002.263	3.7	1359	557	41.0	336	221	-0.21
GLPS	7251	2003.193	2006.365	3.5	1269	1106	87.2	560	545	-0.01
GLPT	4564	1995.290	2006.206	10.8	3935	2948	74.9	1204	1744	0.18
GLSV	1022	1998.080	2006.365	8.8	3208	2128	66.3	641	1487	0.40
GODE	4440	1994.002	2006.365	13.0	4747	3948	83.2	1992	1956	-0.01
GOLD	4100	1994.060	2006.365	12.8	4689	3217	68.6	1137	2079	0.29
GOPE	9077	2002.317	2006.365	4.1	1510	1383	91.6	650	733	0.06
GOUG	6800	1998.226	2006.335	8.3	3032	1730	57.1	1007	723	-0.16
GRAS	1290	1995.061	2006.365	11.8	4323	3408	78.8	1511	1897	0.11
GRAZ	1630	1994.001	2006.362	13.0	4745	2843	59.9	1821	1022	-0.28
GUAM	7300	1995.018	2006.365	12.0	4366	3208	73.5	1412	1796	0.12
GUAT	5130	2000.211	2006.365	6.4	2347	1903	81.1	886	1016	0.07
HARB	6010	2000.239	2006.365	6.3	2319	1874	80.8	887	986	0.05
HARK	6001	1997.186	2000.219	3.1	1129	740	65.5	438	301	-0.19
HARV	4165	1994.001	2006.365	13.0	4748	3135	66.0	2002	1133	-0.28
HELG	9600	1999.313	2006.365	7.1	2610	2231	85.5	968	1263	0.13
HILO	7011	1999.001	2006.365	8.0	2922	1359	46.5	399	960	0.41
HLFX	4005	2002.355	2006.365	4.0	1472	1229	83.5	510	719	0.17

DOI: 10.2312/GFZ.b103-08037

Table 7: (*cont.*)

name	No.	yd_from	yd_to	L_{TS}/y	L_{TS}/d	N_{DP}	ρ_{TS}	N_{1h}	N_{2h}	n_{BI}
HNLC	7510	1999.001	2006.365	8.0	2922	2260	77.3	1112	1148	0.02
HNPT	4450	1995.348	2006.365	11.0	4036	3177	78.7	1478	1699	0.07
HOB2	3210	1994.187	2006.365	12.5	4562	3422	75.0	1395	2027	0.18
HOFN	4920	1997.270	2006.343	9.2	3361	2938	87.4	1277	1660	0.13
HOLB	4720	1994.128	2006.323	12.5	4579	3775	82.4	1717	2058	0.09
HOLM	4591	2001.241	2006.365	5.3	1951	1795	92.0	852	942	0.05
HRAO	6700	1996.274	2006.361	10.2	3741	2889	77.2	1112	1776	0.23
IISC	2700	1994.286	2006.365	12.2	4463	3047	68.3	1257	1790	0.17
INEG	4880	1999.334	2002.081	2.3	844	382	45.3	62	320	0.68
INVK	4710	2003.193	2006.365	3.5	1269	1257	99.1	627	629	0.00
IRKT	2800	1995.264	2006.365	11.3	4120	3293	79.9	1540	1753	0.06
JAB1	3011	1998.202	2006.365	8.4	3086	1354	43.9	317	1037	0.53
JAMA	5140	1999.266	2006.365	7.3	2657	1030	38.8	842	187	-0.64
JOZE	1342	1994.001	2006.365	13.0	4748	3216	67.7	1756	1460	-0.09
JPLM	4150	1994.001	2006.365	13.0	4748	4153	87.5	2006	2147	0.03
KARR	3750	1997.220	2006.365	9.4	3433	2746	80.0	1152	1593	0.16
KELS	4565	1997.298	2006.365	9.2	3355	2964	88.3	1370	1593	0.08
KELY	4930	1995.212	2006.365	11.4	4172	2389	57.3	1058	1331	0.11
KEN1	4566	1996.032	2006.365	10.9	3987	3167	79.4	1366	1800	0.14
KERG	8500	1994.320	2006.365	12.1	4429	3584	80.9	1599	1985	0.11
KGNO	2012	2002.293	2006.090	3.4	1259	1162	92.3	547	614	0.06
KIRI	7429	2003.041	2006.364	3.9	1420	528	37.2	235	293	0.11
KIRU	1550	1994.001	2006.363	13.0	4746	3944	83.1	1894	2050	0.04
KIT3	2351	1994.238	2006.344	12.3	4490	3018	67.2	1507	1511	0.00
KODK	4250	1999.342	2006.206	6.6	2422	1181	48.8	809	372	-0.37
KOKB	7000	1994.001	2006.365	13.0	4748	3720	78.3	1872	1848	-0.01
KOSG	1100	1994.001	2006.365	13.0	4748	3665	77.2	1990	1675	-0.09
KOUR	5100	1994.001	2006.365	13.0	4748	2848	60.0	1067	1781	0.25
KSTU	2500	1997.271	2004.263	7.0	2549	1369	53.7	609	760	0.11
KUNM	2450	1998.281	2006.365	8.2	3007	2512	83.5	1107	1404	0.12
KUUJ	4019	2003.063	2006.365	3.8	1399	875	62.5	291	584	0.33
KWJ1	7400	1996.077	2002.203	6.3	2319	1375	59.3	877	497	-0.28
LAE1	3550	2001.014	2006.202	5.5	2015	1230	61.0	716	514	-0.16
LAGO	1559	2000.099	2006.365	6.7	2459	1822	74.1	727	1094	0.20
LAMP	1320	1999.086	2006.365	7.8	2837	2323	81.9	1038	1284	0.11
LAUT	7420	2003.041	2006.365	3.9	1421	854	60.1	269	584	0.37
LHAS	2400	1995.141	2006.364	11.6	4242	2945	69.4	1323	1622	0.10
LHUE	7012	1999.001	2004.203	5.6	2029	913	45.0	372	541	0.19
LPAL	6530	2001.179	2006.365	5.5	2013	1839	91.4	952	886	-0.04
LPGS	5643	1995.157	2006.360	11.6	4222	3159	74.8	1272	1887	0.19

DOI: 10.2312/GFZ.b103-08037

Table 7: (*cont.*)

name	No.	yd_from	yd_to	L_{TS}/y	L_{TS}/d	N_{DP}	ρ_{TS}	N_{1h}	N_{2h}	n_{BI}
LROC	1210	2001.325	2006.365	5.1	1867	1730	92.7	866	863	-0.00
LYTT	3014	1999.319	2006.329	7.0	2568	1442	56.2	489	953	0.32
MAC1	3300	1994.186	2006.365	12.5	4563	3518	77.1	1458	2060	0.17
MADR	1200	1994.033	2006.365	12.9	4716	3262	69.2	1152	2110	0.29
MAGO	2862	1997.318	2006.132	8.5	3102	2542	81.9	1086	1456	0.15
MALD	2730	1999.225	2006.162	6.8	2495	959	38.4	654	304	-0.36
MALI	6300	1995.321	2006.365	11.1	4063	2726	67.1	1182	1544	0.13
MALL	1560	2001.014	2006.365	6.0	2178	2048	94.0	991	1057	0.03
MANA	5420	2002.293	2006.333	4.1	1502	1028	68.4	591	437	-0.15
MANZ	4890	1999.110	2005.250	6.4	2333	833	35.7	473	359	-0.14
MAR6	1053	1999.060	2006.365	7.8	2863	2520	88.0	1126	1393	0.11
MARS	1561	1998.200	2006.365	8.5	3088	2234	72.3	951	1283	0.15
MAS1	6101	1994.155	2006.363	12.6	4592	3674	80.0	1605	2069	0.13
MATE	1300	1994.001	2006.365	13.0	4748	3987	84.0	1942	2045	0.03
MAUI	7013	1999.001	2006.364	8.0	2921	1542	52.8	430	1111	0.44
MAW1	8600	1997.220	2006.352	9.4	3420	2780	81.3	1218	1562	0.12
MBAR	6350	2001.198	2006.365	5.5	1994	1247	62.5	329	918	0.47
MCM4	8002	1995.025	2006.365	11.9	4359	3626	83.2	1688	1938	0.07
MDO1	4180	1994.001	2006.365	13.0	4748	4121	86.8	2029	2092	0.02
METS	1800	1994.002	2006.365	13.0	4747	4018	84.6	1924	2093	0.04
MIA1	4567	1995.237	1998.161	2.8	1021	718	70.3	335	382	0.07
MIA3	4568	1998.153	2006.365	8.6	3135	2580	82.3	1133	1446	0.12
MIL1	4569	1995.277	2006.317	11.1	4059	3208	79.0	1322	1886	0.18
MIZU	2010	2002.068	2006.365	4.8	1759	1625	92.4	819	805	-0.01
MKEA	7500	1996.275	2006.365	10.3	3744	3145	84.0	1344	1801	0.15
MNP1	4570	1995.139	1998.268	3.4	1226	680	55.5	418	262	-0.23
MOB1	4571	1996.101	2006.365	10.7	3918	3214	82.0	1321	1893	0.18
MORP	1295	1996.319	2006.365	10.1	3700	1806	48.8	456	1350	0.50
MPLA	5013	2002.296	2003.191	0.7	261	65	24.9	23	42	0.29
MQZG	3015	1999.270	2006.365	7.3	2653	1780	67.1	521	1258	0.41
MSKU	6960	2001.144	2006.358	5.6	2041	1166	57.1	447	719	0.23
NAIN	4772	2003.001	2006.365	4.0	1461	1341	91.8	630	710	0.06
NANO	4755	1995.133	2006.365	11.6	4251	3549	83.5	1552	1997	0.13
NAUR	7421	2003.182	2006.279	3.3	1194	179	15.0	92	87	-0.03
NEAH	4572	1998.058	2006.365	8.8	3230	2405	74.5	1179	1226	0.02
NEWL	1150	1998.273	2006.365	8.3	3015	1388	46.0	499	889	0.28
NEWP	4740	1996.158	2006.365	10.6	3861	2609	67.6	829	1779	0.36
NICO	6510	1997.247	2006.165	8.8	3206	2233	69.7	949	1284	0.15
NJI2	4573	2001.139	2006.365	5.6	2053	1900	92.5	924	975	0.03
NKLG	6950	2000.092	2006.356	6.7	2457	1963	79.9	919	1043	0.06

DOI: 10.2312/GFZ.b103-08037

Table 7: (*cont.*)

name	No.	yd_from	yd_to	L_{TS}/y	L_{TS}/d	N_{DP}	ρ_{TS}	N_{1h}	N_{2h}	n_{BI}
NLIB	4090	1994.001	2006.365	13.0	4748	4018	84.6	2009	2009	0.00
NOUM	3810	1998.001	2006.364	9.0	3286	2194	66.8	886	1308	0.19
NPLD	1701	2002.293	2006.364	4.2	1533	1215	79.3	548	667	0.10
NPRI	4574	1999.217	2006.365	7.4	2706	2339	86.4	1023	1316	0.13
NRC1	4010	1995.176	2006.365	11.5	4208	3130	74.4	1099	2031	0.30
NRIL	2810	2000.267	2006.365	6.3	2291	2065	90.1	957	1107	0.07
NSTG	1152	1998.183	2006.364	8.5	3104	871	28.1	71	800	0.84
NTUS	2900	1997.242	2006.304	9.2	3350	2216	66.1	817	1399	0.26
NVSK	2510	2000.211	2006.361	6.4	2343	1454	62.1	878	575	-0.21
NYA1	1401	1998.071	2006.365	8.8	3217	2745	85.3	1177	1567	0.14
NYAL	1400	1994.002	2006.365	13.0	4747	3696	77.9	1581	2114	0.14
OBE2	1611	2001.217	2006.365	5.4	1975	1860	94.2	932	927	-0.00
OBER	1610	1995.283	2001.147	5.6	2057	1341	65.2	628	712	0.06
OBET	1612	2003.187	2005.129	1.8	674	606	89.9	310	296	-0.02
OHI2	8302	2003.193	2006.365	3.5	1269	996	78.5	461	534	0.07
OHIG	8300	1995.045	2002.050	7.0	2563	1266	49.4	700	565	-0.11
ONSA	1050	1994.001	2006.365	13.0	4748	4116	86.7	1983	2133	0.04
OUS2	3880	2000.127	2006.365	6.7	2431	1704	70.1	607	1096	0.29
OUSD	3016	1995.084	2006.330	11.7	4265	2880	67.5	1318	1562	0.08
PALM	8310	1998.189	2006.365	8.5	3099	2679	86.4	1169	1509	0.13
PARC	5620	1999.001	2006.365	8.0	2922	976	33.4	790	186	-0.62
PBL1	4575	1995.193	2004.068	8.7	3163	2296	72.6	1091	1205	0.05
PDEL	1563	2000.109	2006.365	6.7	2449	1958	80.0	805	1152	0.18
PERT	3700	1994.001	2006.365	13.0	4748	3726	78.5	1831	1895	0.02
PETP	2851	1998.283	2006.365	8.2	3005	2355	78.4	941	1413	0.20
PGC5	4016	2000.323	2006.365	6.1	2235	1647	73.7	545	1101	0.34
PICL	4014	2003.063	2006.365	3.8	1399	806	57.6	170	635	0.58
PIE1	4212	1994.001	2006.247	12.7	4630	3236	69.9	1909	1327	-0.18
PIMO	2110	1999.074	2006.365	7.8	2849	1673	58.7	489	1183	0.41
PLO1	4576	1995.201	1996.168	0.9	333	195	58.6	130	65	-0.33
PLO3	4577	1996.274	2006.188	9.8	3568	2985	83.7	1301	1684	0.13
PMON	5720	1995.124	2004.155	9.1	3319	909	27.4	217	692	0.52
PNGM	7422	2003.043	2006.326	3.8	1380	572	41.4	214	358	0.25
POHN	7423	2003.122	2006.365	3.7	1340	803	59.9	244	559	0.39
POLV	1940	2001.170	2006.365	5.5	2022	1880	93.0	926	954	0.01
POR2	4578	1995.174	1999.059	3.7	1347	989	73.4	480	508	0.03
POR4	4579	1999.120	2004.308	5.5	2015	1508	74.8	587	920	0.22
POTS	1650	1994.199	2006.365	12.5	4550	3902	85.8	1828	2074	0.06
PRDS	4213	1997.049	2006.365	9.9	3604	2114	58.7	792	1322	0.25
QAQ1	1056	2002.143	2006.365	4.6	1684	1560	92.6	762	798	0.02

DOI: 10.2312/GFZ.b103-08037

Table 7: (*cont.*)

name	No.	yd_from	yd_to	L_{TS}/y	L_{TS}/d	N_{DP}	ρ_{TS}	N_{1h}	N_{2h}	n_{BI}
RABT	6120	2000.155	2006.361	6.6	2399	1993	83.1	852	1140	0.14
RAMO	6520	1998.162	2006.365	8.6	3126	2603	83.3	1174	1429	0.10
RBAY	6750	2000.295	2006.362	6.2	2260	1099	48.6	451	648	0.18
RED1	4580	1999.040	2006.365	7.9	2883	2448	84.9	1047	1400	0.14
RESO	4760	2003.193	2006.365	3.5	1269	1059	83.5	508	550	0.04
REUN	6210	2003.202	2006.321	3.3	1216	1074	88.3	522	552	0.03
REYK	4910	1995.306	2006.365	11.2	4078	3286	80.6	1425	1861	0.13
RIGA	1564	1999.060	2006.363	7.8	2861	2495	87.2	1102	1392	0.12
RIOG	5610	1995.196	2006.365	11.5	4188	2883	68.8	978	1905	0.32
RIOP	5410	1998.326	2001.362	3.1	1133	542	47.8	317	224	-0.17
RWSN	5630	2000.026	2003.192	3.5	1263	373	29.5	124	248	0.33
SACH	4773	2002.323	2005.289	2.9	1063	892	83.9	419	472	0.06
SAG1	4581	1995.237	2006.365	11.4	4147	3453	83.3	1440	2013	0.17
SAMO	7424	2003.041	2006.351	3.9	1407	627	44.6	248	379	0.21
SANT	5000	1994.001	2006.365	13.0	4748	3658	77.0	1600	2058	0.13
SASS	1119	2003.029	2006.365	3.9	1433	1211	84.5	520	690	0.14
SCH2	4060	1997.244	2006.365	9.3	3409	3002	88.1	1331	1670	0.11
SCUB	4950	1995.196	2006.364	11.5	4187	2018	48.2	532	1486	0.47
SEAT	4582	1998.058	2006.365	8.8	3230	2747	85.0	1253	1494	0.09
SELD	2017	2000.323	2006.365	6.1	2235	1078	48.2	599	479	-0.11
SEY1	6200	1995.136	2006.323	11.5	4206	1045	24.8	246	799	0.53
SFER	1220	1996.087	2006.365	10.8	3932	2722	69.2	875	1847	0.36
SHAO	2060	1996.001	2006.237	10.7	3890	1323	34.0	701	622	-0.06
SHEE	1151	1998.002	2006.360	9.0	3281	1566	47.7	758	808	0.03
SHK1	4583	1995.139	2006.157	11.1	4037	3297	81.7	1473	1823	0.11
SIMO	6620	2001.221	2006.365	5.4	1971	864	43.8	769	95	-0.78
SIO3	4160	1994.004	2006.365	13.0	4745	4086	86.1	2054	2031	-0.01
SOFI	1390	1997.186	2006.365	9.5	3467	1863	53.7	611	1252	0.34
SOL1	4035	1995.191	2006.365	11.5	4193	3376	80.5	1583	1793	0.06
SSIA	5120	2000.272	2006.232	5.9	2153	947	44.0	602	344	-0.27
STAS	1505	2000.323	2006.365	6.1	2235	2012	90.0	964	1047	0.04
STB1	4584	1996.020	2006.365	10.9	3999	3226	80.7	1305	1920	0.19
STJO	4050	1994.001	2006.365	13.0	4748	4131	87.0	2019	2112	0.02
SUTH	6600	1998.106	2006.365	8.7	3182	2520	79.2	1111	1409	0.12
SUTM	6610	2003.193	2006.365	3.5	1269	1123	88.5	543	579	0.03
SUVA	3820	1999.001	2001.233	2.6	964	466	48.3	359	107	-0.54
SUWN	2011	1997.334	2006.365	9.1	3319	1864	56.2	706	1158	0.24
SYOG	8400	1999.136	2006.365	7.6	2787	2369	85.0	1017	1351	0.14
TAIW	2200	1994.001	1997.336	3.9	1432	1149	80.2	648	501	-0.13
TAKL	3017	2001.192	2006.364	5.5	1999	1063	53.2	630	433	-0.19

DOI: 10.2312/GFZ.b103-08037

Table 7: (*cont.*)

name	No.	yd_from	yd_to	L_{TS}/y	L_{TS}/d	N_{DP}	ρ_{TS}	N_{1h}	N_{2h}	n_{BI}
TERS	1117	2002.035	2006.365	4.9	1792	1733	96.7	852	881	0.02
TGCV	6110	2000.120	2003.124	3.0	1101	117	10.6	31	86	0.47
THTI	7121	1998.153	2006.365	8.6	3135	2332	74.4	912	1419	0.22
THU1	4900	1995.123	2003.012	7.7	2812	1546	55.0	1068	478	-0.38
THU3	4903	2003.193	2006.365	3.5	1269	1225	96.5	600	624	0.02
TID1	3051	1997.220	2006.365	9.4	3433	2387	69.5	1099	1287	0.08
TID2	3052	1994.247	2006.361	12.3	4498	3353	74.5	1398	1955	0.17
TIDB	3050	1994.060	2006.365	12.8	4689	3367	71.8	1252	2114	0.26
TIXI	2860	1998.283	2006.365	8.2	3005	2538	84.5	1125	1412	0.11
TLSE	1023	2002.293	2006.365	4.2	1534	1439	93.8	697	742	0.03
TONG	7425	2003.041	2006.365	3.9	1421	651	45.8	276	375	0.15
TORP	4585	1997.059	2006.365	9.8	3594	3102	86.3	1361	1741	0.12
TORS	1060	2001.176	2004.108	2.8	1028	365	35.5	253	112	-0.39
TOW2	3020	1995.255	2006.365	11.3	4129	2810	68.1	820	1989	0.42
TRAB	1960	1999.347	2006.364	7.0	2575	1995	77.5	864	1130	0.13
TRDS	1503	2000.323	2006.365	6.1	2235	2032	90.9	972	1059	0.04
TRO1	1501	1998.071	2006.365	8.8	3217	2789	86.7	1213	1575	0.13
TRON	1565	1999.063	2000.055	1.0	358	160	44.7	103	57	-0.29
TSEA	4586	1999.180	2006.365	7.5	2743	1748	63.7	760	987	0.13
TSKB	2050	1994.001	2006.365	13.0	4748	4015	84.6	2035	1980	-0.01
TUVA	7426	2003.073	2006.351	3.8	1375	373	27.1	126	247	0.32
TWTF	2210	2003.193	2006.365	3.5	1269	1176	92.7	554	621	0.06
UCLU	4592	1994.128	2006.349	12.6	4605	3824	83.0	1801	2022	0.06
ULAB	2452	2000.323	2006.365	6.1	2235	1411	63.1	526	884	0.25
UNB1	4015	2006.184	2006.232	0.1	49	49	100.0	24	24	0.00
UNSA	5645	1995.196	2006.363	11.5	4186	2210	52.8	411	1799	0.63
URUM	2431	524 .199	2006.365	10.7	3905	2148	55.0	733	1414	0.32
USNA	4460	1995.191	2005.334	10.4	3797	3081	81.1	1463	1618	0.05
USNO	4587	1997.122	2006.365	9.7	3531	2908	82.4	1275	1632	0.12
USUD	2000	1994.001	2006.365	13.0	4748	3994	84.1	1969	2025	0.01
UZHL	1930	1999.185	2006.364	7.5	2737	1991	72.7	887	1103	0.11
VAAS	1803	1999.060	2006.365	7.8	2863	2418	84.5	1061	1356	0.12
VALD	4018	2003.063	2006.365	3.8	1399	1028	73.5	346	681	0.33
VALE	1566	2001.014	2006.365	6.0	2178	1647	75.6	846	801	-0.03
VALP	5020	1999.118	2002.302	3.5	1281	349	27.2	111	238	0.36
VANU	7427	2003.041	2006.365	3.9	1421	713	50.2	219	494	0.39
VARD	1567	1999.060	2000.055	1.0	361	257	71.2	152	104	-0.19
VARS	1506	2000.323	2006.364	6.1	2234	1987	88.9	958	1029	0.04
VBCA	5635	2000.068	2003.169	3.3	1198	327	27.3	99	228	0.39
VENE	1305	1996.251	2006.365	10.3	3768	2860	75.9	1133	1727	0.21

DOI: 10.2312/GFZ.b103-08037

Table 7: (*cont.*)

name	No.	yd_from	yd_to	L_{TS}/y	L_{TS}/d	N_{DP}	ρ_{TS}	N_{1h}	N_{2h}	n_{BI}
VESL	8800	1998.225	2006.308	8.2	3006	1442	48.0	601	841	0.17
VILL	1250	1994.327	2006.365	12.1	4422	3621	81.9	1657	1964	0.08
VIMS	4588	1995.211	2006.365	11.4	4173	2845	68.2	1241	1604	0.13
VISO	1052	1999.060	2006.365	7.8	2863	2502	87.4	1119	1382	0.11
WARN	1120	2003.043	2006.365	3.9	1419	1262	88.9	582	679	0.08
WES2	4080	1994.001	2006.365	13.0	4748	3918	82.5	2000	1918	-0.02
WGTN	3019	1999.270	2006.365	7.3	2653	1956	73.7	700	1255	0.28
WGTT	3018	1999.356	2006.365	7.0	2567	1658	64.6	708	949	0.15
WHIT	4260	1995.161	2006.365	11.6	4223	3398	80.5	1370	2028	0.19
WILL	4214	1994.036	2006.365	12.9	4713	3053	64.8	1766	1287	-0.16
WILR	4589	2001.098	2001.350	0.7	253	177	70.0	102	74	-0.16
WIS1	4590	1996.101	2006.365	10.7	3918	3235	82.6	1368	1867	0.15
WSRT	1110	1997.186	2006.365	9.5	3467	2969	85.6	1322	1646	0.11
WTZR	1601	1995.038	2006.365	11.9	4346	3780	87.0	1734	2046	0.08
WUHN	2070	1996.003	2006.364	11.0	4015	3288	81.9	1374	1913	0.16
XIAN	2080	1996.201	2001.174	4.9	1801	819	45.5	561	257	-0.37
YAKT	2864	1996.202	2006.362	10.4	3814	1893	49.6	173	1720	0.82
YAR1	3100	1994.001	2002.131	8.4	3053	2333	76.4	1229	1103	-0.05
YAR2	3102	1997.298	2006.365	9.2	3355	2182	65.0	578	1604	0.47
YELL	4700	1994.001	2006.365	13.0	4748	3916	82.5	1774	2142	0.09
YKRO	6900	1999.211	2004.244	5.1	1860	184	9.9	78	106	0.15
YSSK	2870	1999.212	2006.362	7.4	2708	2327	85.9	1003	1324	0.14
ZAMB	6650	2003.193	2006.365	3.5	1269	553	43.6	401	152	-0.45
ZECK	1950	1997.270	2006.365	9.3	3383	2274	67.2	1281	992	-0.13
ZIMM	1645	1994.001	2006.365	13.0	4748	3339	70.3	1850	1489	-0.11
ZWEN	1900	1994.328	2004.309	9.9	3634	2494	68.6	1417	1077	-0.14

DOI: 10.2312/GFZ.b103-08037

B Parameters of linear regression analysis between GPS and ATML induced vertical motion

Table 8 gives the parameters from linear regression analysis between GPS and atmospheric loading time series for the analyzed stations. In the table, N is the number of common data points, r the correlation coefficient, σ_r the standard deviation of r, α the significance factor (1 for significant; 0 for non-significant), R_{amp} is amplitude ratio.

Table 8: Linear regression analysis between GPS measured and atmospheric pressure loading induced vertical motion time series.

site	N	r	σ_r	α	R_{amp}	site	N	r	σ_r	α	R_{amp}
ABER	752	0.211	0.000	1	0.054	ACOR	1014	-0.015	0.623	0	-0.003
AJAC	1129	0.022	0.467	0	0.006	ALAC	1592	0.247	0.000	1	0.073
ALBH	3455	0.101	0.000	1	0.035	ALGO	3482	0.330	0.000	1	0.153
ALIC	2131	0.339	0.000	1	0.122	ALME	1308	0.086	0.002	1	0.022
ALRT	663	0.410	0.000	1	0.125	AMC2	1883	0.455	0.000	1	0.189
ANKR	1678	0.310	0.000	1	0.096	ANP2	95	0.078	0.453	0	0.013
AOML	1912	0.025	0.270	0	0.002	AREQ	2739	0.195	0.000	1	0.016
ARTU	1614	0.668	0.000	1	0.457	ASC1	1898	0.143	0.000	1	0.009
ASPA	282	0.068	0.257	0	0.004	AUCK	2853	0.245	0.000	1	0.027
BAHR	2558	0.647	0.000	1	0.147	BAIE	329	0.329	0.000	1	0.173
BAKE	284	0.554	0.000	1	0.323	BAKO	1808	0.111	0.000	1	0.007
BAN2	513	0.029	0.519	0	0.004	BARB	367	-0.005	0.927	0	-0.000
BARH	1891	0.246	0.000	1	0.087	BAY2	758	0.388	0.000	1	0.079
BILI	1418	0.426	0.000	1	0.210	BINT	363	0.008	0.873	0	0.000
BISH	1742	0.463	0.000	1	0.197	BJFS	1356	0.670	0.000	1	0.291
BOGT	1732	0.103	0.000	1	0.003	BOR1	756	0.616	0.000	1	0.447
BORK	672	0.154	0.000	1	0.065	BRAZ	2117	0.175	0.000	1	0.020
BRMU	3265	0.033	0.057	0	0.002	BRST	1510	-0.098	0.000	0	-0.032
BRUS	2628	0.202	0.000	1	0.073	CABL	2291	-0.081	0.000	0	-0.018
CAGL	2571	0.125	0.000	1	0.025	CANT	1253	0.071	0.012	0	0.018
CART	236	-0.041	0.530	0	-0.002	CAS1	2749	0.334	0.000	1	0.123
CASC	1745	0.017	0.475	0	0.003	CCV1	602	0.135	0.001	1	0.020
CCV3	1830	0.044	0.057	0	0.005	CEDU	1937	0.506	0.000	1	0.164
CEUT	1016	-0.131	0.000	0	-0.023	CFAG	1252	0.347	0.000	1	0.071
CHA1	2243	0.125	0.000	1	0.024	CHAT	2860	0.110	0.000	1	0.007
CHL1	1626	-0.015	0.542	0	-0.000	CHL2	69	-0.053	0.664	0	-0.011
CHPI	212	0.204	0.003	1	0.031	CHR1	825	0.183	0.000	1	0.045
CHUM	1766	0.476	0.000	1	0.169	CHUR	2512	0.549	0.000	1	0.268
CIC1	1065	0.137	0.000	1	0.022	CKIS	322	0.259	0.000	1	0.016
COCO	2215	0.134	0.000	1	0.010	CONZ	598	-0.050	0.222	0	-0.007

DOI: 10.2312/GFZ.b103-08037

Table 8: (*cont.*)

site	N	r	σ_r	α	R_{amp}	site	N	r	σ_r	α	R_{amp}
CORD	707	0.291	0.000	1	0.063	CREU	1473	0.031	0.242	0	0.008
CRO1	2781	0.016	0.405	0	0.001	DAEJ	1669	0.421	0.000	1	0.115
DAKA	203	0.203	0.004	1	0.016	DARW	1600	0.026	0.304	0	0.004
DAV1	2384	0.288	0.000	1	0.108	DGAR	1281	0.163	0.000	1	0.010
DRAG	631	0.496	0.000	1	0.116	DRAO	3479	0.366	0.000	1	0.164
DUBO	2503	0.550	0.000	1	0.319	DUBR	813	0.299	0.000	1	0.077
DUCK	1785	0.107	0.000	1	0.019	DUM1	683	0.388	0.000	1	0.110
DUNT	1101	0.095	0.002	1	0.017	DWH1	644	0.254	0.000	1	0.075
EIJS	1003	0.295	0.000	1	0.190	EISL	2325	0.022	0.279	0	0.001
EPRT	1738	0.295	0.000	1	0.108	ESTI	107	0.077	0.428	0	0.004
FAIR	3127	0.399	0.000	1	0.184	FLIN	2566	0.519	0.000	1	0.287
FMC1	411	0.054	0.271	0	0.008	FMC2	977	0.248	0.000	1	0.045
FORT	2862	0.177	0.000	1	0.010	FREE	385	0.014	0.787	0	0.001
FTS1	2359	0.029	0.155	0	0.008	GAL1	2111	0.177	0.000	1	0.038
GALA	1514	0.012	0.646	0	0.001	GENO	1974	0.341	0.000	1	0.131
GETI	551	0.162	0.000	1	0.010	GLPS	466	0.103	0.026	0	0.008
GLPT	2441	0.105	0.000	1	0.026	GLSV	1384	0.499	0.000	1	0.292
GODE	3239	-0.005	0.789	0	-0.000	GOLD	2530	0.152	0.000	1	0.025
GOPE	674	0.474	0.000	1	0.343	GOUG	1519	0.029	0.266	0	0.001
GRAS	2518	0.251	0.000	1	0.097	GRAZ	2247	0.342	0.000	1	0.159
GUAM	2536	-0.066	0.001	0	-0.003	GUAT	1237	0.243	0.000	1	0.021
HARB	1178	0.368	0.000	1	0.099	HARK	740	0.309	0.000	1	0.064
HARV	2763	-0.044	0.021	0	-0.005	HELG	1528	-0.007	0.798	0	-0.002
HILO	751	-0.099	0.007	0	-0.006	HLFX	515	0.125	0.004	1	0.048
HNLC	1617	-0.095	0.000	0	-0.005	HNPT	2641	0.183	0.000	1	0.051
HOB2	2745	0.138	0.000	1	0.012	HOFN	2239	0.427	0.000	1	0.122
HOLB	3091	0.193	0.000	1	0.056	HOLM	1094	0.394	0.000	1	0.146
HRAO	2217	0.198	0.000	1	0.039	IISC	2231	0.169	0.000	1	0.019
INEG	382	0.290	0.000	1	0.046	INVK	533	0.543	0.000	1	0.231
IRKT	2715	0.675	0.000	1	0.330	JAB1	885	-0.070	0.039	0	-0.012
JAMA	829	0.051	0.139	0	0.003	JOZE	2390	0.188	0.000	1	0.044
JPLM	3418	0.068	0.000	1	0.011	KARR	2076	0.313	0.000	1	0.064
KELS	2260	0.169	0.000	1	0.053	KELY	1924	0.544	0.000	1	0.267
KEN1	2322	0.505	0.000	1	0.221	KERG	2889	0.130	0.000	1	0.009
KGNO	716	0.196	0.000	1	0.040	KIRI	232	0.074	0.264	0	0.006
KIRU	3241	0.462	0.000	1	0.164	KIT3	2412	0.353	0.000	1	0.088
KODK	1043	0.533	0.000	1	0.210	KOKB	2897	-0.078	0.000	0	-0.004
KOSG	3348	0.257	0.000	1	0.127	KOUR	2159	0.234	0.000	1	0.012
KSTU	1370	0.635	0.000	1	0.337	KUNM	1843	0.291	0.000	1	0.061
KUUJ	291	0.210	0.000	1	0.089	KWJ1	1375	0.034	0.206	0	0.002

DOI: 10.2312/GFZ.b103-08037

Table 8: (*cont.*)

site	N	r	σ_r	α	R_{amp}	site	N	r	σ_r	α	R_{amp}
LAE1	1013	0.259	0.000	1	0.031	LAGO	1162	0.006	0.840	0	0.001
LAMP	1631	0.295	0.000	1	0.050	LAUT	252	0.393	0.000	1	0.029
LHAS	2451	0.139	0.000	1	0.019	LHUE	913	-0.025	0.456	0	-0.001
LPAL	1211	0.171	0.000	1	0.014	LPGS	2450	0.323	0.000	1	0.062
LROC	1065	-0.008	0.806	0	-0.003	LYTT	860	0.230	0.000	1	0.039
MAC1	2787	0.008	0.674	0	0.000	MADR	2376	0.060	0.004	1	0.015
MAGO	2094	0.358	0.000	1	0.155	MALD	792	0.002	0.959	0	0.000
MALI	2094	-0.008	0.725	0	-0.001	MALL	1336	0.075	0.006	1	0.015
MANA	613	0.162	0.000	1	0.010	MANZ	826	-0.021	0.548	0	-0.000
MAR6	1804	0.418	0.000	1	0.289	MARS	1570	0.213	0.000	1	0.068
MAS1	2949	-0.018	0.318	0	-0.002	MATE	3267	0.191	0.000	1	0.047
MAUI	919	-0.169	0.000	0	-0.013	MAW1	2116	0.255	0.000	1	0.083
MBAR	557	0.000	0.992	0	0.000	MCM4	2871	0.308	0.000	1	0.072
MDO1	3385	0.262	0.000	1	0.078	METS	3293	0.380	0.000	1	0.231
MIA1	710	0.067	0.075	0	0.007	MIA3	1711	-0.020	0.419	0	-0.002
MIL1	2432	0.339	0.000	1	0.149	MIZU	965	0.277	0.000	1	0.049
MKEA	2418	-0.080	0.000	0	-0.005	MNP1	678	0.060	0.118	0	0.015
MOB1	2413	0.099	0.000	1	0.019	MORP	1150	0.273	0.000	1	0.090
MPLA	65	0.291	0.019	0	0.056	MQZG	1057	0.212	0.000	1	0.043
MSKU	518	-0.106	0.016	0	-0.010	NAIN	631	0.408	0.000	1	0.201
NANO	2825	0.212	0.000	1	0.078	NAUR	85	0.127	0.246	0	0.011
NEAH	1830	0.021	0.364	0	0.007	NEWL	766	-0.121	0.001	0	-0.025
NEWP	1901	0.104	0.000	1	0.029	NICO	1927	0.452	0.000	1	0.104
NJI2	1204	0.239	0.000	1	0.091	NKLG	1338	0.096	0.000	1	0.011
NLIB	3348	0.302	0.000	1	0.116	NOUM	1625	0.390	0.000	1	0.037
NPLD	584	0.313	0.000	1	0.179	NPRI	1624	0.205	0.000	1	0.060
NRC1	2401	0.364	0.000	1	0.188	NRIL	1364	0.579	0.000	1	0.356
NSTG	292	0.218	0.000	1	0.063	NTUS	1667	0.001	0.954	0	0.000
NVSK	1040	0.435	0.000	1	0.213	NYA1	2031	0.365	0.000	1	0.082
NYAL	2973	0.342	0.000	1	0.066	OBE2	1184	0.387	0.000	1	0.214
OBER	1311	0.403	0.000	1	0.242	OBET	449	0.271	0.000	1	0.164
OHI2	335	0.352	0.000	1	0.049	OHIG	1253	0.242	0.000	1	0.022
ONSA	3387	0.254	0.000	1	0.142	OUS2	1068	0.091	0.003	1	0.021
OUSD	2253	0.095	0.000	1	0.013	PALM	1963	0.127	0.000	1	0.022
PARC	950	-0.104	0.001	0	-0.026	PBL1	2169	-0.056	0.010	0	-0.010
PDEL	1264	-0.026	0.356	0	-0.002	PERT	2082	0.391	0.000	1	0.094
PETP	1650	0.266	0.000	1	0.093	PGC5	924	0.218	0.000	1	0.099
PICL	141	0.484	0.000	1	0.285	PIE1	2545	0.256	0.000	1	0.082
PIMO	1148	0.139	0.000	1	0.008	PLO1	194	-0.089	0.217	0	-0.006
PLO3	2387	-0.026	0.210	0	-0.004	PMON	909	-0.150	0.000	0	-0.032

DOI: 10.2312/GFZ.b103-08037

Table 8: (*cont.*)

site	N	r	σ_r	α	R_{amp}	site	N	r	σ_r	α	R_{amp}
PNGM	214	0.438	0.000	1	0.040	POHN	219	0.148	0.028	0	0.011
POLV	1178	0.600	0.000	1	0.354	POR2	890	0.025	0.460	0	0.001
POR4	1379	0.144	0.000	1	0.045	POTS	3173	0.392	0.000	1	0.232
PRDS	1399	0.565	0.000	1	0.339	QAQ1	874	0.549	0.000	1	0.211
RABT	1277	0.172	0.000	1	0.032	RAMO	1912	0.698	0.000	1	0.148
RBAY	564	0.259	0.000	1	0.044	RED1	1657	0.144	0.000	1	0.042
RESO	413	0.429	0.000	1	0.211	REUN	452	0.171	0.000	1	0.022
REYK	2627	0.470	0.000	1	0.107	RIGA	1777	0.481	0.000	1	0.272
RIOG	2176	0.119	0.000	1	0.030	RIOP	535	0.002	0.958	0	0.000
RWSN	373	0.244	0.000	1	0.047	SACH	605	0.430	0.000	1	0.166
SAG1	2674	0.339	0.000	1	0.130	SAMO	248	0.198	0.002	1	0.012
SANT	2943	0.136	0.000	1	0.018	SASS	510	0.458	0.000	1	0.202
SCH2	2276	0.447	0.000	1	0.228	SCUB	1540	-0.099	0.000	0	-0.006
SEAT	2062	0.181	0.000	1	0.067	SELD	602	0.458	0.000	1	0.116
SEY1	789	-0.044	0.213	0	-0.001	SFER	2018	0.145	0.000	1	0.031
SHAO	936	0.161	0.000	1	0.044	SHEE	989	0.308	0.000	1	0.111
SHK1	2637	0.195	0.000	1	0.051	SIMO	769	0.241	0.000	1	0.029
SIO3	3303	0.078	0.000	1	0.011	SOFI	1310	0.223	0.000	1	0.073
SOL1	2732	0.073	0.000	1	0.019	SSIA	691	-0.015	0.701	0	-0.001
STAS	1316	0.180	0.000	1	0.085	STB1	2411	0.214	0.000	1	0.077
STJO	3408	0.066	0.000	1	0.014	SUTH	1888	0.348	0.000	1	0.063
SUTM	497	0.545	0.000	1	0.110	SUVA	466	0.236	0.000	1	0.015
SUWN	1383	0.214	0.000	1	0.053	SYOG	1641	0.347	0.000	1	0.140
TAIW	1125	0.102	0.001	1	0.009	TAKL	766	0.246	0.000	1	0.029
TERS	1015	0.084	0.007	1	0.031	TGCV	117	0.267	0.004	1	0.027
THTI	1677	0.073	0.003	1	0.003	THU1	1546	0.280	0.000	1	0.079
THU3	505	0.412	0.000	1	0.168	TID1	1710	0.377	0.000	1	0.113
TID2	2628	0.349	0.000	1	0.099	TIDB	2632	0.348	0.000	1	0.090
TIXI	1847	0.538	0.000	1	0.240	TLSE	731	0.265	0.000	1	0.126
TONG	276	0.314	0.000	1	0.024	TORP	2380	-0.025	0.214	0	-0.004
TORS	365	0.055	0.291	0	0.006	TOW2	2112	0.206	0.000	1	0.038
TRAB	1386	0.316	0.000	1	0.115	TRDS	1327	0.403	0.000	1	0.220
TRO1	2067	0.371	0.000	1	0.164	TRON	160	-0.025	0.750	0	-0.005
TSEA	1163	0.612	0.000	1	0.301	TSKB	3260	0.045	0.010	0	0.005
TUVA	126	0.229	0.010	0	0.009	TWTF	460	-0.027	0.560	0	-0.004
UCLU	3116	0.159	0.000	1	0.050	ULAB	713	0.095	0.011	0	0.005
UNSA	1548	0.273	0.000	1	0.040	URUM	1801	0.040	0.087	0	0.000
USNA	2754	0.189	0.000	1	0.042	USNO	2228	0.244	0.000	1	0.085
USUD	3291	0.034	0.053	0	0.004	UZHL	1411	0.470	0.000	1	0.235
VAAS	1698	0.413	0.000	1	0.185	VALD	316	0.385	0.000	1	0.228

DOI: 10.2312/GFZ.b103-08037

Table 8: (*cont.*)

site	N	r	σ_r	α	R_{amp}	site	N	r	σ_r	α	R_{amp}
VALE	1105	0.220	0.000	1	0.076	VALP	349	0.098	0.068	0	0.015
VANU	211	0.453	0.000	1	0.035	VARD	257	0.357	0.000	1	0.131
VARS	1313	0.326	0.000	1	0.144	VBCA	327	0.258	0.000	1	0.047
VENE	2242	0.215	0.000	1	0.059	VESL	1146	0.482	0.000	1	0.190
VILL	2915	0.239	0.000	1	0.075	VIMS	2186	0.132	0.000	1	0.028
VIS0	1789	0.348	0.000	1	0.165	WARN	564	0.450	0.000	1	0.259
WES2	3210	0.189	0.000	1	0.054	WGTN	1237	0.003	0.926	0	0.000
WGTT	1158	-0.054	0.065	0	-0.007	WHIT	2668	0.604	0.000	1	0.316
WILL	2228	0.431	0.000	1	0.263	WILR	177	0.191	0.011	0	0.025
WIS1	2392	0.426	0.000	1	0.206	WSRT	2274	0.305	0.000	1	0.168
WTZR	3060	0.372	0.000	1	0.216	WUHN	2588	0.033	0.088	0	0.015
XIAN	819	0.364	0.000	1	0.144	YAKT	1255	0.369	0.000	1	0.167
YAR1	2331	0.167	0.000	1	0.015	YAR2	1497	0.512	0.000	1	0.127
YELL	3184	0.553	0.000	1	0.320	YKRO	184	0.209	0.004	1	0.020
YSSK	1611	0.395	0.000	1	0.086	ZAMB	370	0.349	0.000	1	0.069
ZECK	2053	0.533	0.000	1	0.231	ZIMM	2618	0.189	0.000	1	0.061
ZWEN	2397	0.525	0.000	1	0.323						

DOI: 10.2312/GFZ.b103-08037

C Estimated velocities of the GPS stations

This appendix lists the estimated vertical and horizontal velocities of the analyzed GPS stations (see Table 9).

Table 9: Estimated station velocities for up, east and north components (Unit: mm/a). Longitude and latitude are in degrees. Negative longitude indicates western hemisphere. Negative latitude indicates southern hemisphere.

name	No.	Long.	Lat.	v_h	σ_h	v_e	σ_e	v_n	σ_n
ABER	1153	-2.08	57.14	2.535	0.020	14.889	0.012	14.886	0.012
ACOR	1551	-8.40	43.36	-1.406	0.054	21.542	0.015	14.934	0.016
AIS1	4730	-131.60	55.07	-	-	-	-	-	-
AJAC	1552	8.76	41.93	0.248	0.031	21.357	0.022	14.775	0.022
ALAC	1553	-0.48	38.34	-0.090	0.029	19.841	0.016	15.369	0.014
ALBH	4120	-123.49	48.20	-0.227	0.013	-7.753	0.007	-8.807	0.006
ALGO	4000	-78.08	45.95	2.927	0.008	-16.470	0.006	1.396	0.006
ALIC	3070	133.89	-23.53	3.438	0.028	31.878	0.012	57.428	0.010
ALME	1554	-2.46	36.85	0.606	0.027	18.906	0.019	14.505	0.018
ALRT	4770	-62.35	82.48	8.955	0.052	-20.801	0.034	6.053	0.035
AMC2	4130	-104.52	38.62	1.614	0.026	-15.200	0.012	-6.815	0.012
ANKR	1020	32.76	39.70	1.307	0.013	-0.684	0.011	11.816	0.009
ANP2	4551	-76.61	39.01	15.815	0.237	-15.806	0.089	3.152	0.094
AOML	4840	-80.17	25.73	-0.215	0.027	-10.306	0.017	1.740	0.018
AREQ	5300	-71.83	-15.23	1.954	0.031	10.377	0.029	13.031	0.026
ARTU	1980	58.56	56.25	0.543	0.019	25.019	0.013	4.998	0.014
ASC1	5700	-14.42	-6.05	0.878	0.020	-5.235	0.014	9.278	0.013
ASPA	7130	-170.72	-14.33	2.735	0.119	-64.676	0.071	33.570	0.065
AUCK	3800	174.83	-36.42	1.718	0.011	4.090	0.009	38.351	0.008
BAHR	6500	50.61	26.06	0.279	0.014	31.322	0.010	28.501	0.008
BAIE	4013	-68.26	49.19	0.812	0.063	-16.007	0.040	5.354	0.042
BAKE	4215	-96.00	64.32	8.453	0.075	-18.957	0.044	-3.663	0.047
BAKO	2910	106.85	-6.45	0.180	0.021	23.789	0.015	-8.031	0.013
BAN2	2720	77.51	13.03	-2.741	0.088	40.716	0.110	32.607	0.050
BARB	5110	-59.61	13.00	-0.379	0.158	15.261	0.124	15.130	0.095
BARH	4020	-68.23	44.38	-0.890	0.018	-15.417	0.011	5.733	0.011
BAY2	4210	162.71	55.19	-1.276	0.032	-9.331	0.022	-23.272	0.024
BILI	2890	166.44	67.94	0.894	0.022	8.447	0.014	-21.248	0.015
BINT	2016	113.07	3.26	5.230	0.140	27.643	0.078	-12.408	0.073
BISH	2399	74.59	42.68	-1.442	0.024	27.398	0.017	2.570	0.016

DOI: 10.2312/GFZ.b103-08037

Table 9: (*cont.*)

name	No.	Long.	Lat.	v_h	σ_h	v_e	σ_e	v_n	σ_n
BJFS	2880	115.89	39.42	2.375	0.023	30.376	0.016	-12.309	0.017
BOGT	5400	-74.08	4.63	-36.202	0.022	0.289	0.011	12.652	0.011
BOR1	9048	17.07	52.10	1.004	0.039	20.715	0.027	13.424	0.028
BORK	9638	6.75	53.56	-0.188	0.133	16.187	0.081	14.360	0.085
BRAZ	5500	-47.88	-14.07	0.450	0.021	-3.725	0.011	10.390	0.012
BRMU	4850	-64.70	32.37	-1.263	0.009	-12.078	0.006	7.193	0.007
BRST	1270	-4.50	48.38	0.724	0.020	16.621	0.014	15.930	0.014
BRUS	1130	4.36	50.61	1.317	0.008	17.540	0.006	14.517	0.006
CABL	4552	-124.56	42.84	1.906	0.014	-6.880	0.010	0.218	0.010
CAGL	1310	8.97	39.13	-0.126	0.011	22.118	0.008	14.512	0.008
CANT	1555	-3.80	43.47	-0.465	0.027	17.735	0.018	16.085	0.021
CART	5150	-75.53	10.39	-2.138	0.183	10.854	0.115	9.206	0.112
CAS1	8200	110.52	-66.14	4.986	0.036	2.136	0.007	-10.353	0.008
CASC	1556	-9.42	38.69	1.155	0.019	17.717	0.013	15.548	0.012
CCV1	4553	-80.54	28.46	1.875	0.115	-12.589	0.079	-0.248	0.077
CCV3	4554	-80.55	28.30	-3.487	0.054	-12.857	0.012	1.288	0.011
CEDU	3710	133.81	-31.69	3.092	0.022	29.143	0.014	57.624	0.011
CEUT	1557	-5.31	35.90	-2.228	0.046	15.297	0.027	17.285	0.034
CFAG	5010	-68.23	-30.40	-0.930	0.045	6.818	0.035	9.800	0.031
CHA1	4555	-79.84	32.58	-1.181	0.085	-13.039	0.014	2.188	0.012
CHAT	3400	-176.57	-43.76	2.563	0.011	-40.724	0.009	32.424	0.008
CHL1	4556	-75.09	38.59	0.278	0.042	-14.780	0.020	2.822	0.018
CHL2	4557	-75.09	38.59	1.122	0.372	-17.735	0.274	0.647	0.246
CHPI	5510	-45.00	-21.32	3.165	0.076	-5.070	0.055	8.743	0.054
CHR1	4558	-76.01	36.74	-0.334	0.192	-14.463	0.044	-0.770	0.046
CHUM	2438	74.75	42.98	0.158	0.018	26.893	0.013	1.101	0.012
CHUR	4040	-94.10	58.75	10.799	0.035	-18.047	0.008	-3.914	0.009
CIC1	4211	-116.67	31.70	-0.349	0.026	-40.471	0.019	19.621	0.017
CKIS	7428	-159.80	-21.20	4.304	0.075	-62.593	0.054	34.272	0.048
COCO	3500	96.83	-12.11	1.435	0.018	45.775	0.021	48.004	0.012
CONZ	5012	-73.03	-35.17	7.649	0.054	32.788	0.037	16.852	0.036
CORD	5550	-64.48	-30.30	3.404	0.041	0.276	0.025	9.563	0.023
CREU	1296	3.32	42.32	2.015	0.040	20.390	0.028	16.148	0.032
CRO1	5800	-64.60	17.75	-0.813	0.013	10.621	0.009	11.614	0.009
DAEJ	2030	127.37	36.38	1.169	0.021	26.369	0.014	-13.767	0.013
DAKA	6910	-17.47	14.68	-2.096	0.094	18.051	0.064	16.294	0.060
DARW	3230	131.13	-12.76	2.413	0.023	35.939	0.018	56.671	0.017
DAV1	8100	77.97	-68.45	2.191	0.019	-2.224	0.008	-5.884	0.008
DGAR	3600	72.62	-6.57	2.048	0.017	46.342	0.019	31.139	0.010
DRAG	1021	35.39	31.42	7.528	0.110	22.998	0.033	18.088	0.032

DOI: 10.2312/GFZ.b103-08037

Table 9: (*cont.*)

name	No.	Long.	Lat.	v_h	σ_h	v_e	σ_e	v_n	σ_n
DRAO	4750	-119.62	49.13	0.593	0.008	-13.403	0.006	-11.264	0.006
DUBO	4045	-95.87	50.25	-1.814	0.020	-17.379	0.008	-5.547	0.013
DUBR	1558	18.11	42.65	0.034	0.040	23.238	0.033	16.589	0.030
DUCK	4559	-75.75	36.00	-1.240	0.095	-12.567	0.022	5.013	0.059
DUM1	8015	140.00	-66.67	1.156	0.060	7.558	0.046	-11.193	0.046
DUNT	3013	170.63	-45.81	0.807	0.029	-31.760	0.022	31.485	0.022
DWH1	4771	-122.08	47.77	-3.427	0.056	-12.325	0.037	-7.678	0.039
EIJS	1115	5.68	50.76	2.118	0.033	18.328	0.021	15.033	0.022
EISL	7200	-109.38	-26.99	-0.636	0.036	67.997	0.015	-8.291	0.013
EPRT	4025	-67.00	44.90	-1.630	0.039	-14.692	0.012	6.118	0.013
ESTI	5011	-86.37	13.08	-	-	-	-	-	-
FAIR	4200	-147.49	64.83	0.051	0.024	-8.639	0.012	-21.683	0.013
FLIN	4030	-101.98	54.54	1.205	0.012	-17.601	0.008	-7.740	0.008
FMC1	4560	-76.68	34.52	-1.538	0.095	-13.861	0.075	5.696	0.084
FMC2	4561	-76.68	34.52	2.890	0.061	-17.087	0.043	4.299	0.044
FORT	5200	-38.43	-2.13	1.815	0.048	-4.258	0.009	10.842	0.009
FREE	4835	-79.00	26.70	2.107	0.145	-10.821	0.090	3.332	0.088
FTS1	4562	-123.96	46.01	-0.887	0.033	-4.188	0.008	-4.632	0.009
GAL1	4563	-94.74	29.17	-4.391	0.045	-11.552	0.014	-4.449	0.015
GALA	7250	-90.32	0.73	-0.041	0.032	51.193	0.021	8.539	0.027
GENO	1315	8.92	44.42	-0.018	0.021	20.630	0.011	14.632	0.011
GETI	2015	102.11	6.23	6.677	0.093	32.541	0.063	-6.964	0.055
GLPS	7251	-90.30	-0.74	1.112	0.065	50.078	0.045	6.321	0.045
GLPT	4564	-76.50	37.06	-3.646	0.015	-14.541	0.010	2.901	0.010
GLSV	1022	30.50	50.18	1.539	0.037	22.837	0.026	11.375	0.028
GODE	4440	-76.83	39.02	-2.012	0.009	-14.823	0.006	2.954	0.006
GOLD	4100	-116.88	35.24	-1.547	0.024	-19.425	0.008	-4.989	0.008
GOPE	9077	14.79	49.72	1.276	0.042	20.685	0.029	14.133	0.029
GOUG	6800	-9.88	-39.67	-10.853	0.033	20.983	0.020	17.507	0.020
GRAS	1290	6.92	43.75	0.805	0.009	20.902	0.007	15.033	0.008
GRAZ	1630	15.49	46.88	0.443	0.009	22.021	0.007	14.270	0.007
GUAM	7300	144.87	13.58	1.299	0.014	-9.345	0.010	2.935	0.017
GUAT	5130	-90.53	14.58	1.008	0.029	4.503	0.020	0.884	0.020
HARB	6010	27.71	-25.74	1.262	0.030	17.316	0.020	16.138	0.019
HARK	6001	27.72	-25.89	-2.516	0.120	20.265	0.091	17.148	0.083
HARV	4165	-120.68	34.29	-7.934	0.030	-43.299	0.008	22.611	0.009
HELG	9600	7.89	54.17	1.253	0.024	17.564	0.014	15.203	0.014
HILO	7011	-155.05	19.60	-1.391	0.026	-63.024	0.018	34.252	0.015
HLFX	4005	-63.61	44.68	-2.876	0.056	-14.923	0.033	7.265	0.036
HNLC	7510	-157.86	21.17	-4.317	0.038	-63.225	0.015	33.292	0.014

DOI: 10.2312/GFZ.b103-08037

Table 9: (*cont.*)

name	No.	Long.	Lat.	v_h	σ_h	v_e	σ_e	v_n	σ_n
HNPT	4450	-76.13	38.59	-3.598	0.012	-14.798	0.008	2.837	0.009
HOB2	3210	147.44	-42.61	2.201	0.011	13.731	0.009	54.657	0.008
HOFN	4920	-15.20	64.27	12.400	0.029	13.216	0.019	14.679	0.018
HOLB	4720	-128.13	50.45	0.328	0.019	-12.408	0.008	-11.359	0.007
HOLM	4591	-117.77	70.73	3.502	0.033	-18.193	0.020	-12.465	0.023
HRAO	6700	27.69	-25.74	0.804	0.017	18.218	0.012	16.110	0.012
IISC	2700	77.57	13.02	0.865	0.014	41.342	0.013	33.391	0.008
INEG	4880	-102.28	21.72	-87.293	0.199	-12.304	0.180	-3.044	0.165
INVK	4710	-133.53	68.31	1.888	0.060	-14.011	0.037	-16.049	0.041
IRKT	2800	104.32	52.03	-1.416	0.022	25.009	0.008	-7.897	0.008
JAB1	3011	132.89	-12.58	1.811	0.029	34.560	0.021	57.765	0.018
JAMA	5140	-76.78	17.93	-1.596	0.043	2.993	0.048	9.175	0.048
JOZE	1342	21.03	51.91	0.717	0.009	20.973	0.006	13.479	0.006
JPLM	4150	-118.17	34.02	-1.004	0.009	-37.784	0.006	12.646	0.006
KARR	3750	117.10	-20.85	3.384	0.052	38.275	0.018	56.376	0.017
KELS	4565	-122.90	45.93	-0.057	0.014	-9.971	0.010	-6.988	0.010
KELY	4930	-50.95	66.98	-0.126	0.030	-17.430	0.017	11.097	0.017
KEN1	4566	-151.35	60.51	12.662	0.044	-9.263	0.032	-29.994	0.034
KERG	8500	70.26	-49.16	2.864	0.012	5.258	0.009	-3.855	0.008
KGNO	2012	139.48	35.70	2.686	0.059	-2.577	0.040	-7.270	0.039
KIRI	7429	172.92	1.35	0.824	0.086	-66.438	0.065	31.671	0.058
KIRU	1550	20.97	67.86	5.732	0.017	15.919	0.006	14.469	0.006
KIT3	2351	66.88	38.94	-2.295	0.013	28.022	0.008	4.309	0.008
KODK	4250	-152.50	57.56	9.265	0.049	-16.655	0.040	-12.024	0.043
KOKB	7000	-159.66	21.99	0.901	0.031	-62.224	0.027	33.133	0.023
KOSG	1100	5.80	52.17	-0.263	0.009	17.632	0.006	15.523	0.009
KOUR	5100	-52.80	5.21	1.340	0.029	-4.952	0.009	10.888	0.009
KSTU	2500	92.79	55.99	0.020	0.026	24.761	0.018	-5.300	0.019
KUNM	2450	102.78	25.02	0.835	0.020	30.173	0.015	-21.223	0.016
KUUJ	4019	-77.75	55.28	9.688	0.072	-18.113	0.042	0.417	0.045
KWJ1	7400	167.72	8.72	-1.119	0.044	-70.303	0.033	27.924	0.025
LAE1	3550	146.99	-6.67	-3.019	0.046	27.917	0.030	51.111	0.031
LAGO	1559	-8.67	37.10	0.892	0.026	17.552	0.017	15.863	0.016
LAMP	1320	12.61	35.50	-0.200	0.027	19.855	0.012	17.195	0.013
LAUT	7420	177.45	-17.61	1.998	0.076	17.311	0.054	30.819	0.048
LHAS	2400	91.10	29.65	1.880	0.023	45.831	0.009	13.893	0.008
LHUE	7012	-159.35	21.98	-1.849	0.038	-62.177	0.026	34.038	0.025
LPAL	6530	-17.53	28.46	-1.992	0.035	16.314	0.021	14.759	0.021
LPGS	5643	-57.93	-33.10	3.927	0.018	-1.377	0.011	9.588	0.012
LROC	1210	-1.23	46.15	0.204	0.032	18.471	0.020	14.952	0.020

DOI: 10.2312/GFZ.b103-08037

Table 9: (*cont.*)

name	No.	Long.	Lat.	v_h	σ_h	v_e	σ_e	v_n	σ_n
LYTT	3014	172.72	-43.61	0.853	0.033	-33.234	0.026	30.684	0.025
MAC1	3300	158.94	-54.32	0.564	0.011	-12.619	0.011	31.161	0.011
MADR	1200	-4.25	40.42	3.422	0.039	18.398	0.016	14.505	0.017
MAGO	2862	150.77	59.57	0.430	0.015	7.474	0.018	-21.872	0.013
MALD	2730	73.52	4.18	-0.739	0.061	48.451	0.045	32.571	0.034
MALI	6300	40.19	-2.98	0.142	0.026	26.757	0.014	13.936	0.012
MALL	1560	2.62	39.55	-0.258	0.028	17.805	0.040	15.471	0.034
MANA	5420	-86.25	12.13	-0.782	0.068	2.045	0.044	-2.187	0.050
MANZ	4890	-104.30	19.06	4.913	0.067	-4.701	0.049	-2.614	0.050
MAR6	1053	17.26	60.60	8.172	0.018	17.665	0.011	13.228	0.012
MARS	1561	5.35	43.28	1.262	0.027	19.132	0.018	15.687	0.020
MAS1	6101	-15.63	27.75	-0.728	0.025	16.382	0.007	15.920	0.007
MATE	1300	16.70	40.63	0.710	0.021	23.556	0.014	17.757	0.014
MAUI	7013	-156.26	20.58	-3.359	0.036	-62.406	0.026	33.273	0.022
MAW1	8600	62.87	-67.47	3.199	0.016	-2.916	0.013	-3.176	0.013
MBAR	6350	30.74	-0.60	2.449	0.041	24.702	0.028	15.202	0.026
MCM4	8002	166.67	-77.76	-0.281	0.024	10.062	0.014	-11.654	0.013
MDO1	4180	-104.02	30.51	-0.220	0.009	-12.475	0.007	-6.834	0.006
METS	1800	24.68	60.22	4.816	0.009	19.993	0.006	11.891	0.006
MIA1	4567	-80.16	25.58	-0.956	0.111	-12.285	0.068	2.017	0.064
MIA3	4568	-80.16	25.58	-4.199	0.030	-9.912	0.013	2.308	0.014
MIL1	4569	-87.89	42.81	-4.705	0.038	-15.314	0.008	-1.194	0.008
MIZU	2010	141.13	38.95	4.965	0.044	-6.264	0.033	-10.221	0.032
MKEA	7500	-155.46	19.68	-0.980	0.014	-63.048	0.010	33.450	0.009
MNP1	4570	-116.42	32.72	2.045	0.203	-17.118	0.056	5.591	0.051
MOB1	4571	-88.02	30.23	-2.449	0.039	-13.626	0.009	-2.097	0.009
MORP	1295	-1.69	55.21	1.564	0.019	15.544	0.012	15.893	0.013
MPLA	5013	-57.53	-38.04	100.062	13.899	-29.709	10.222	23.343	9.034
MQZG	3015	172.65	-43.70	-0.134	0.047	-32.675	0.027	30.967	0.020
MSKU	6960	13.55	-1.62	2.998	0.038	20.850	0.029	18.088	0.027
NAIN	4772	-61.69	56.54	3.076	0.044	-16.007	0.029	9.643	0.032
NANO	4755	-124.09	49.10	0.460	0.010	-8.722	0.007	-8.648	0.007
NAUR	7421	166.93	-0.55	-0.048	0.234	-66.572	0.152	31.014	0.160
NEAH	4572	-124.62	48.30	2.929	0.017	-3.380	0.011	-5.485	0.011
NEWL	1150	-5.54	50.10	0.309	0.018	15.859	0.012	15.752	0.012
NEWP	4740	-124.07	44.39	1.344	0.014	-5.985	0.012	-3.985	0.010
NICO	6510	33.40	34.96	-0.336	0.018	18.875	0.014	14.091	0.012
NJI2	4573	-74.18	40.74	-3.760	0.029	-15.805	0.019	3.009	0.019
NKLG	6950	9.67	0.35	0.594	0.029	22.129	0.022	16.769	0.019
NLIB	4090	-91.58	41.77	-2.230	0.021	-15.601	0.006	-2.550	0.006

DOI: 10.2312/GFZ.b103-08037

Table 9: (*cont.*)

name	No.	Long.	Lat.	v_h	σ_h	v_e	σ_e	v_n	σ_n
NOUM	3810	166.41	-22.14	-0.045	0.018	20.519	0.012	44.929	0.012
NPLD	1701	-0.35	51.42	2.388	0.050	15.562	0.037	11.819	0.034
NPRI	4574	-71.33	41.51	-3.067	0.023	-15.333	0.014	4.515	0.013
NRC1	4010	-75.63	45.45	2.906	0.012	-16.156	0.008	2.723	0.008
NRIL	2810	88.36	69.23	2.113	0.027	21.982	0.017	-2.987	0.018
NSTG	1152	-1.44	55.01	0.704	0.042	16.571	0.027	15.114	0.025
NTUS	2900	103.68	1.34	0.862	0.020	30.489	0.020	-7.009	0.017
NVSK	2510	83.23	54.83	-8.647	0.106	25.941	0.024	-2.018	0.024
NYA1	1401	11.85	78.92	9.212	0.016	10.289	0.011	14.333	0.010
NYAL	1400	11.87	78.92	8.322	0.011	10.447	0.006	13.897	0.006
OBE2	1611	11.30	48.10	1.049	0.032	20.760	0.023	14.332	0.022
OBER	1610	11.28	48.09	-0.866	0.039	20.438	0.026	14.650	0.028
OBET	1612	11.27	48.08	-0.110	0.166	19.876	0.119	15.559	0.113
OHI2	8302	-57.90	-63.32	11.730	0.082	14.407	0.051	8.680	0.057
OHIG	8300	-57.90	-63.17	6.265	0.033	14.714	0.023	9.611	0.024
ONSA	1050	11.93	57.22	1.456	0.009	17.140	0.005	13.886	0.006
OUS2	3880	170.50	-44.33	-0.469	0.036	-30.986	0.029	31.801	0.025
OUSD	3016	170.51	-45.87	0.559	0.034	-32.437	0.011	29.991	0.010
PALM	8310	-64.05	-64.63	8.882	0.033	12.952	0.014	9.025	0.014
PARC	5620	-70.88	-52.87	0.659	0.051	4.477	0.033	9.779	0.031
PBL1	4575	-122.42	37.85	-4.073	0.052	-33.769	0.014	9.187	0.012
PDEL	1563	-25.66	37.75	-1.619	0.029	12.142	0.018	14.343	0.018
PERT	3700	115.89	-31.63	-3.881	0.015	39.392	0.011	56.340	0.010
PETP	2851	158.61	52.88	-3.912	0.024	-5.620	0.017	-8.280	0.017
PGC5	4016	-123.45	48.65	0.772	0.043	-10.007	0.025	-9.474	0.025
PICL	4014	-90.16	51.48	4.290	0.153	-16.622	0.046	-3.002	0.055
PIE1	4212	-108.12	34.12	1.671	0.010	-13.167	0.007	-8.700	0.007
PIMO	2110	121.07	14.63	1.771	0.030	-29.779	0.019	3.616	0.023
PLO1	4576	-116.76	32.67	-28.354	1.891	-14.677	1.361	-40.763	1.142
PLO3	4577	-117.24	32.67	-5.021	0.045	-39.820	0.010	18.346	0.010
PMON	5720	-72.92	-41.28	4.931	0.045	-0.225	0.034	11.798	0.037
PNGM	7422	147.37	-2.04	-2.313	0.083	-65.858	0.051	22.805	0.055
POHN	7423	158.21	6.96	-3.580	0.117	-70.021	0.074	27.014	0.062
POLV	1940	34.53	49.60	-0.011	0.026	22.832	0.018	11.134	0.019
POR2	4578	-69.29	43.07	3.356	0.064	-16.372	0.043	4.941	0.045
POR4	4579	-70.71	43.07	-1.289	0.092	-15.889	0.025	4.001	0.025
POTS	1650	13.07	52.37	0.405	0.009	19.208	0.006	14.165	0.006
PRDS	4213	-114.29	50.68	-1.992	0.051	-14.939	0.009	-12.572	0.011
QAQ1	1056	-46.05	60.70	4.373	0.036	-17.198	0.023	14.416	0.025
RABT	6120	-6.87	33.97	-0.276	0.028	16.432	0.018	16.018	0.017

DOI: 10.2312/GFZ.b103-08037

Table 9: (*cont.*)

name	No.	Long.	Lat.	v_h	σ_h	v_e	σ_e	v_n	σ_n
RAMO	6520	34.76	30.43	0.838	0.015	25.912	0.027	19.710	0.019
RBAY	6750	32.08	-28.63	0.493	0.051	16.859	0.033	15.458	0.031
RED1	4580	-75.57	39.56	-3.755	0.041	-14.761	0.013	2.529	0.013
RESO	4760	-94.89	74.69	7.615	0.066	-20.545	0.042	-4.498	0.048
REUN	6210	55.57	-21.21	0.169	0.075	18.810	0.052	9.813	0.047
REYK	4910	-21.97	64.13	-1.863	0.019	-10.224	0.016	18.813	0.014
RIGA	1564	24.06	56.95	1.735	0.018	20.377	0.014	12.458	0.012
RIOG	5610	-67.75	-52.22	5.499	0.023	3.350	0.010	10.144	0.011
RIOP	5410	-78.67	-0.35	3.897	0.119	-4.988	0.080	-1.084	0.077
RWSN	5630	-65.11	43.30	0.228	0.151	-3.328	0.109	8.248	0.118
SACH	4773	-125.25	71.98	2.443	0.078	-17.009	0.051	-14.706	0.059
SAG1	4581	-83.84	43.63	-2.716	0.031	-18.198	0.008	-0.818	0.007
SAMO	7424	-171.74	-13.85	1.922	0.093	-63.789	0.065	32.886	0.056
SANT	5000	-70.68	-32.85	5.012	0.010	20.371	0.009	14.388	0.008
SASS	1119	13.64	54.51	8.286	0.057	18.461	0.034	13.747	0.037
SCH2	4060	-66.83	54.82	10.054	0.013	-17.625	0.009	6.596	0.010
SCUB	4950	-75.77	20.00	-0.182	0.037	-5.517	0.013	2.970	0.013
SEAT	4582	-122.31	47.65	-0.975	0.015	-10.016	0.011	-9.783	0.011
SELD	2017	-151.71	59.28	6.048	0.041	-6.911	0.033	-32.480	0.027
SEY1	6200	55.48	-4.64	-2.016	0.040	26.417	0.023	9.856	0.021
SFER	1220	-6.22	36.45	1.996	0.018	14.757	0.013	15.437	0.011
SHAO	2060	121.20	31.08	-0.611	0.020	31.576	0.014	-15.089	0.015
SHEE	1151	0.74	51.45	0.729	0.016	17.021	0.010	15.186	0.011
SHK1	4583	-74.01	40.47	-2.189	0.033	-11.480	0.009	4.291	0.010
SIMO	6620	18.43	-33.82	0.786	0.056	16.433	0.039	17.010	0.039
SIO3	4160	-117.25	32.69	2.113	0.012	-38.144	0.008	17.559	0.007
SOFI	1390	23.38	42.55	0.148	0.017	24.264	0.012	10.679	0.011
SOL1	4035	-76.47	38.32	-3.458	0.019	-14.703	0.007	2.920	0.007
SSIA	5120	-89.12	13.68	3.739	0.043	4.019	0.028	6.939	0.029
STAS	1505	5.60	59.02	2.135	0.027	15.340	0.017	15.022	0.017
STB1	4584	-87.31	44.80	2.979	0.027	-16.543	0.008	-1.450	0.008
STJO	4050	-52.68	47.58	-0.302	0.009	-14.708	0.006	11.554	0.006
SUTH	6600	20.81	-32.21	3.368	0.019	17.009	0.013	17.617	0.013
SUTM	6610	20.81	-32.38	3.871	0.061	17.972	0.045	17.042	0.041
SUVA	3820	178.42	-17.87	-1.571	0.158	16.035	0.120	33.203	0.103
SUWN	2011	127.05	37.27	2.540	0.081	26.996	0.013	-13.654	0.012
SYOG	8400	39.58	-69.00	3.453	0.020	-3.382	0.014	1.333	0.015
TAIW	2200	121.54	24.87	-4.254	0.080	37.355	0.060	-13.483	0.082
TAKL	3017	174.77	-36.84	2.076	0.042	4.635	0.030	39.337	0.027
TERS	1117	5.22	53.36	-0.265	0.035	18.933	0.021	13.623	0.022

DOI: 10.2312/GFZ.b103-08037

Table 9: (*cont.*)

name	No.	Long.	Lat.	v_h	σ_h	v_e	σ_e	v_n	σ_n
TGCV	6110	-22.98	16.75	-1.268	0.311	18.487	0.200	14.408	0.253
THTI	7121	-149.62	-16.43	1.234	0.026	-66.386	0.017	33.214	0.015
THU1	4900	-68.80	76.53	-0.027	0.032	-22.215	0.019	4.187	0.019
THU3	4903	-68.83	76.53	6.883	0.058	-21.924	0.034	5.549	0.035
TID1	3051	148.98	-35.21	2.983	0.016	17.879	0.012	53.869	0.010
TID2	3052	148.98	-35.21	2.296	0.013	17.933	0.010	53.947	0.008
TIDB	3050	148.98	-35.21	3.250	0.014	17.637	0.011	53.812	0.008
TIXI	2860	128.87	71.52	1.401	0.017	16.803	0.011	-12.276	0.012
TLSE	1023	1.47	43.55	0.425	0.041	20.084	0.027	14.804	0.028
TONG	7425	-175.18	-21.14	-0.612	0.088	95.644	0.109	-7.895	0.069
TORP	4585	-118.33	33.62	0.441	0.015	-39.516	0.009	17.797	0.009
TORS	1060	-6.76	62.02	-3.491	0.161	10.104	0.119	16.992	0.116
TOW2	3020	147.06	-19.15	2.730	0.017	28.423	0.012	54.102	0.011
TRAB	1960	39.77	40.98	0.661	0.025	25.384	0.016	12.058	0.016
TRDS	1503	10.32	63.37	5.853	0.027	14.164	0.017	15.115	0.018
TRO1	1501	18.93	69.65	3.954	0.015	16.753	0.019	14.377	0.011
TRON	1565	8.97	39.14	5.308	1.074	15.114	0.853	12.397	0.768
TSEA	4586	-149.89	61.19	5.100	0.052	-16.469	0.037	-15.893	0.039
TSKB	2050	140.09	35.92	1.278	0.011	-3.624	0.007	-8.894	0.007
TUVA	7426	179.20	-8.53	2.044	0.109	-62.324	0.070	32.101	0.068
TWTF	2210	121.16	24.95	5.681	0.069	30.896	0.046	-14.592	0.043
UCLU	4592	-125.54	48.73	1.202	0.030	-4.577	0.017	-6.938	0.018
ULAB	2452	107.05	47.67	1.451	0.027	28.108	0.020	-9.918	0.021
UNB1	4015	-66.65	45.95	-	-	-	-	-	-
UNSA	5645	-65.42	-23.28	2.245	0.024	4.986	0.016	8.792	0.017
URUM	2431	87.63	43.59	1.861	0.021	30.215	0.014	5.693	0.013
USNA	4460	-76.48	38.97	-0.597	0.018	-14.896	0.012	2.437	0.012
USNO	4587	-77.07	38.92	-3.210	0.042	-14.477	0.017	2.919	0.017
USUD	2000	138.36	35.95	0.493	0.024	-0.508	0.016	-11.643	0.022
UZHL	1930	22.30	48.44	-0.458	0.022	21.893	0.014	12.791	0.015
VAAS	1803	21.77	62.96	8.864	0.020	18.433	0.011	12.558	0.012
VALD	4018	-77.56	48.10	3.806	0.068	-17.294	0.039	1.513	0.040
VALE	1566	-0.34	39.48	-0.139	0.029	20.787	0.020	13.845	0.021
VALP	5020	-71.63	-32.98	-6.296	0.110	28.240	0.083	18.875	0.078
VANU	7427	168.32	-17.74	-1.322	0.079	-58.600	0.056	8.857	0.051
VARD	1567	31.03	70.34	-4.728	0.740	18.103	0.547	14.221	0.635
VARS	1506	31.03	70.34	4.043	0.028	17.672	0.016	11.367	0.018
VBCA	5635	-62.27	-38.70	-3.269	0.210	-0.686	0.174	5.990	0.152
VENE	1305	12.33	45.24	-1.420	0.030	21.762	0.010	16.279	0.010
VESL	8800	-2.85	-70.33	3.175	0.024	-0.283	0.015	9.340	0.016

DOI: 10.2312/GFZ.b103-08037

Table 9: (*cont.*)

name	No.	Long.	Lat.	v_{h}	σ_{h}	v_{e}	σ_{e}	v_{n}	σ_{n}
VILL	1250	-3.97	40.43	-2.637	0.025	19.204	0.014	15.520	0.007
VIMS	4588	-75.69	37.61	-3.779	0.012	-14.736	0.008	3.354	0.008
VIS0	1052	18.37	57.65	3.744	0.019	18.886	0.011	12.936	0.012
WARN	1120	12.10	54.17	5.176	0.052	19.311	0.034	14.334	0.037
WES2	4080	-71.50	42.60	-1.399	0.021	-15.326	0.018	4.098	0.019
WGTN	3019	174.81	-41.32	0.661	0.037	-24.581	0.021	33.154	0.018
WGTT	3018	174.78	-41.29	-1.637	0.032	-22.798	0.025	34.115	0.022
WHIT	4260	-135.22	60.59	0.134	0.027	-12.124	0.014	-14.095	0.016
WILL	4214	-122.17	52.05	-0.328	0.022	-14.519	0.006	-12.464	0.007
WILR	4589	-77.93	34.24	7.594	9.050	-30.408	7.351	-20.834	6.751
WIS1	4590	-92.02	46.71	-2.612	0.034	-16.887	0.008	-3.475	0.008
WSRT	1110	6.60	52.90	-0.371	0.013	17.615	0.008	15.400	0.008
WTZR	1601	12.87	49.13	-0.331	0.016	20.404	0.006	14.499	0.006
WUHN	2070	114.35	30.52	1.860	0.031	31.974	0.009	-13.094	0.009
XIAN	2080	109.22	34.37	3.093	0.086	33.046	0.055	-11.657	0.053
YAKT	2864	129.68	61.87	0.746	0.044	17.743	0.032	-13.382	0.036
YAR1	3100	115.34	-28.88	0.322	0.023	42.157	0.021	55.392	0.015
YAR2	3102	115.33	-28.97	3.241	0.037	39.250	0.013	56.375	0.011
YELL	4700	-114.48	62.32	6.237	0.022	-16.921	0.006	-11.714	0.006
YKRO	6900	-5.25	6.83	3.545	0.099	21.394	0.073	17.090	0.066
YSSK	2870	142.72	47.02	1.418	0.021	12.244	0.027	-14.773	0.027
ZAMB	6650	28.31	-15.42	2.899	0.072	20.924	0.062	15.589	0.054
ZECK	1950	41.57	43.60	1.260	0.017	26.130	0.012	10.430	0.012
ZIMM	1645	7.47	46.69	0.564	0.008	20.315	0.006	14.648	0.006
ZWEN	1900	36.76	55.52	-0.258	0.030	23.014	0.022	11.244	0.023

DOI: 10.2312/GFZ.b103-08037

D Inter-annual variations in GPS height time series

This appendix demonstrates the height time series of those GPS stations with inter-annual variations. These time series are still fitted with seasonal waves and linear trend.

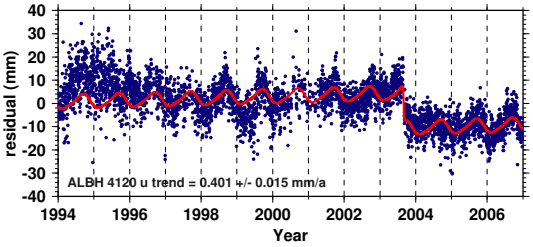

Figure 53: ALBH height time series. Inter-annual.

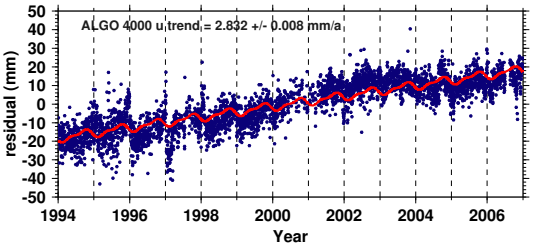

Figure 54: ALGO height time series. Inter-annual.

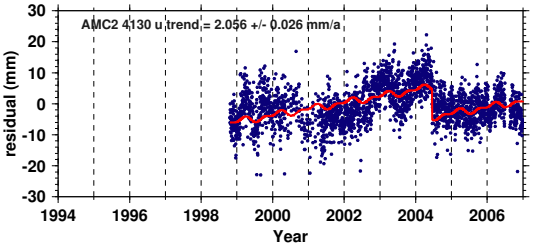

Figure 55: AMC2 height time series. Inter-annual, velocity change, or specious offset at about 2003.0.

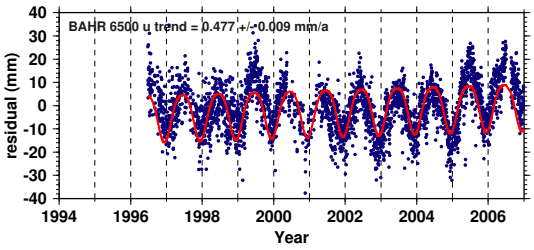

Figure 56: BAHR height time series. Inter-annual.

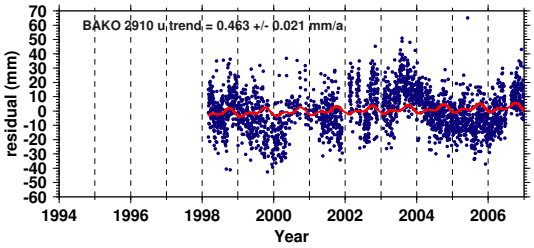

Figure 57: BAKO height time series. Inter-annual.

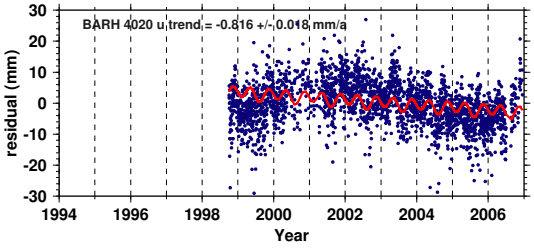

Figure 58: BARH height time series. Inter-annual.

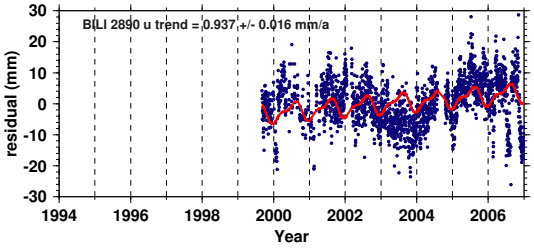

Figure 59: BILI height time series. Inter-annual.

DOI: 10.2312/GFZ.b103-08037

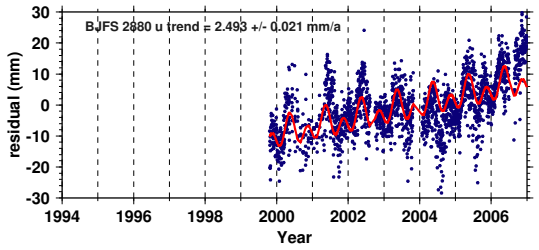

Figure 60: BJFS height time series. Inter-annual.

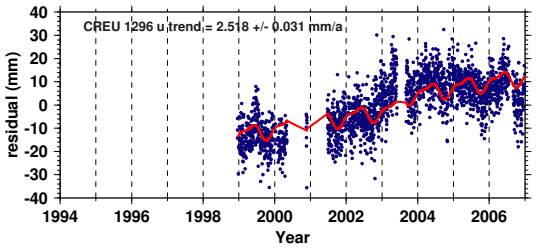

Figure 64: CREU height time series. Inter-annual.

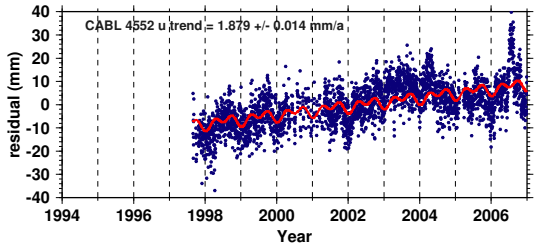

Figure 61: CABL height time series. Inter-annual.

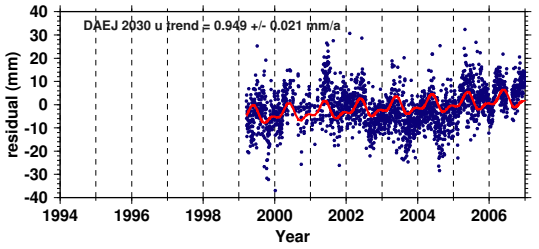

Figure 65: DAEJ height time series. Inter-annual.

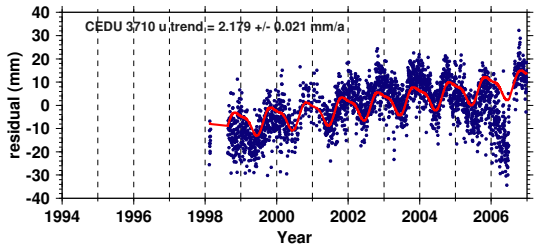

Figure 62: CEDU height time series. Inter-annual, followed with offset.

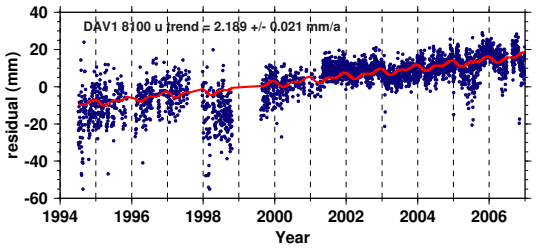

Figure 66: DAV1 height time series. Inter-annual.

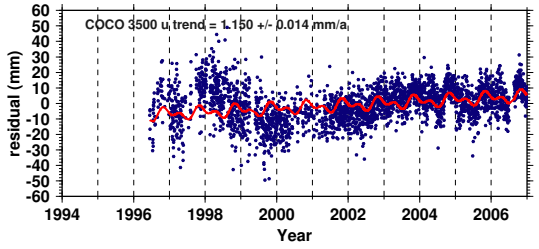

Figure 63: COCO height time series. Inter-annual.

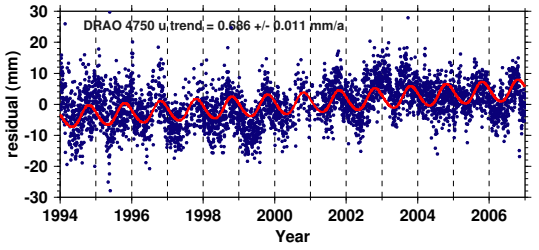

Figure 67: DRAO height time series. Inter-annual, slight, long-term.

DOI: 10.2312/GFZ.b103-08037

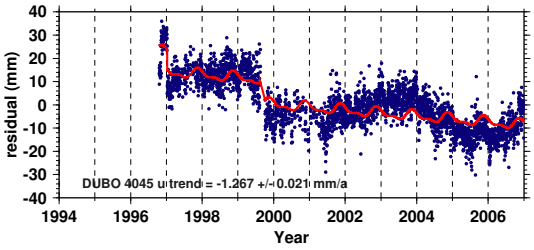

Figure 68: DUBO height time series. Inter-annual, obvious.

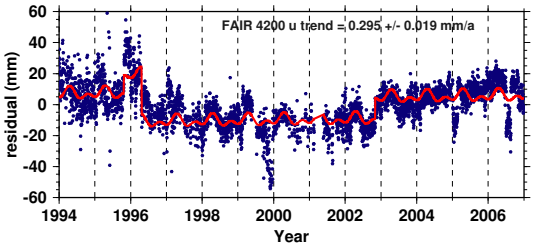

Figure 69: FAIR height time series. Inter-annual.

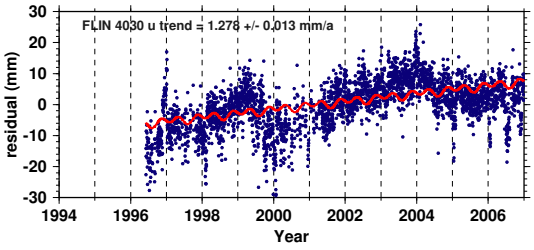

Figure 70: FLIN height time series. Inter-annual.

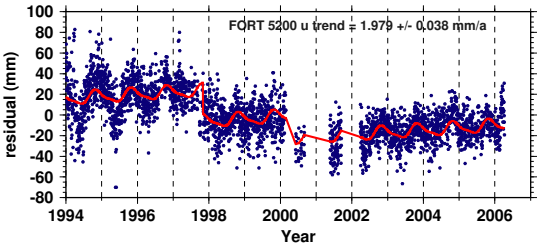

Figure 71: FORT height time series. Inter-annual.

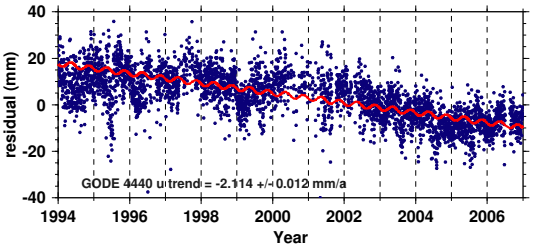

Figure 72: GODE height time series. Inter-annual, slight, long-term.

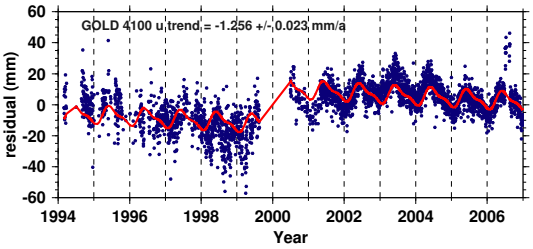

Figure 73: GOLD height time series. Inter-annual, velocity change followed with offset after a data gap.

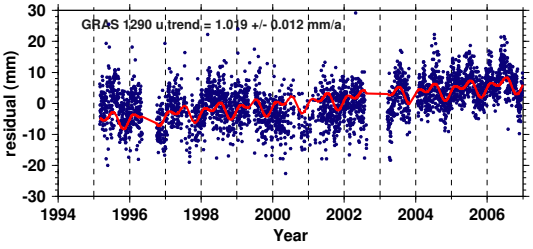

Figure 74: GRAS height time series. Inter-annual, slight, long-term.

DOI: 10.2312/GFZ.b103-08037

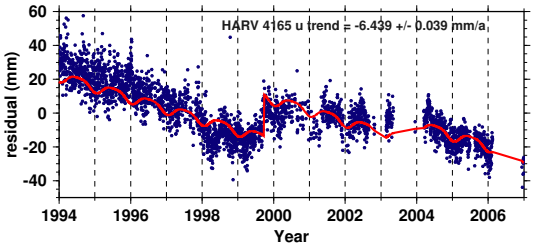

Figure 75: HARV height time series. Inter-annual, velocity change; after the velocity change, a slower subsidence.

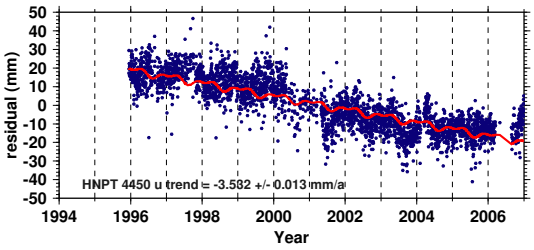

Figure 76: HNPT height time series. Inter-annual, or specious offset.

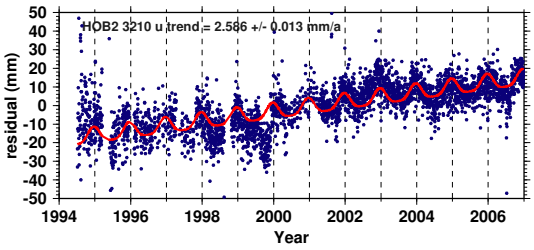

Figure 77: HOB2 height time series. Inter-annual, and velocity change.

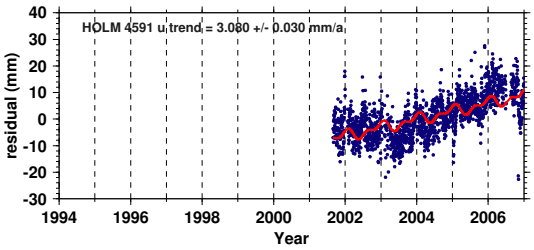

Figure 78: HOLM height time series. Inter-annual.

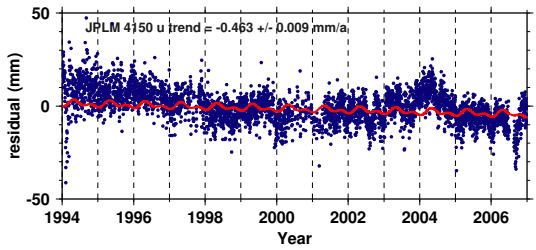

Figure 79: JPLM height time series. Inter-annual.

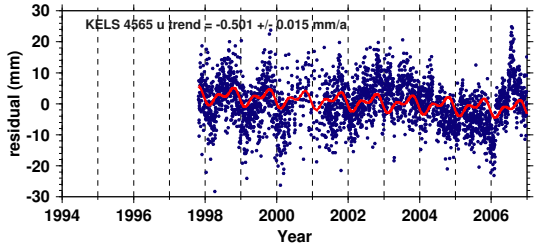

Figure 80: KELS height time series. Inter-annual.

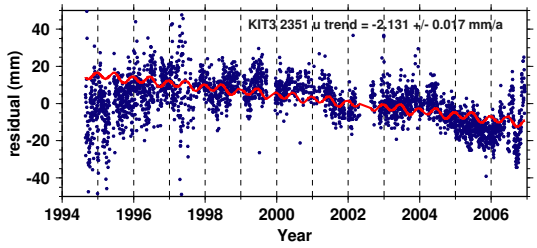

Figure 81: KIT3 height time series. Velocity (sign) change after offset.

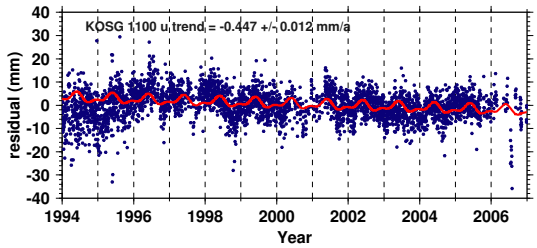

Figure 82: KOSG height time series. Inter-annual, slight.

DOI: 10.2312/GFZ.b103-08037

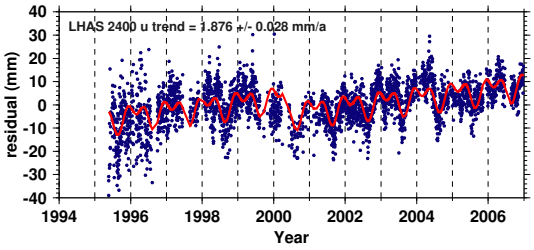

Figure 83: LHAS height time series. Inter-annual.

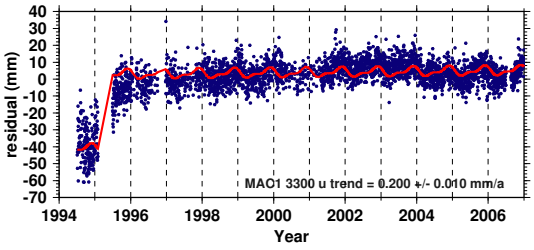

Figure 84: MAC1 height time series. Inter-annual.

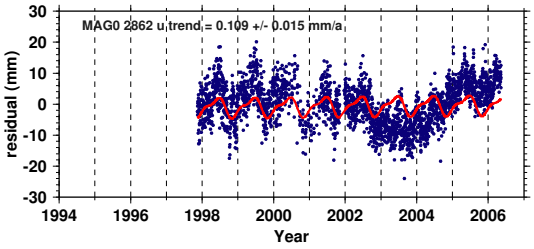

Figure 85: MAG0 height time series. Inter-annual.

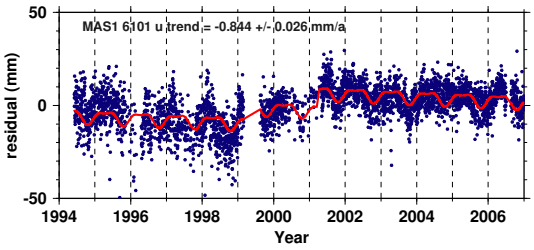

Figure 86: MAS1 height time series. Velocity change.

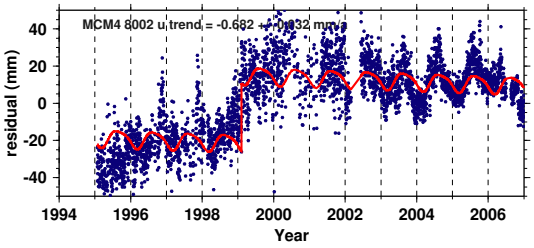

Figure 87: MCM4 height time series. Velocity change after offset.

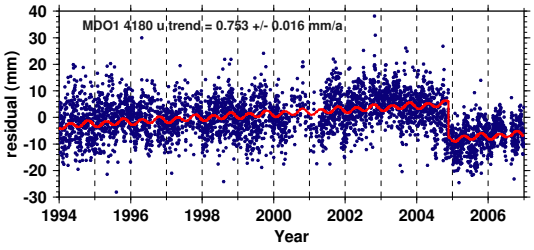

Figure 88: MDO1 height time series. Inter-annual, specious offset.

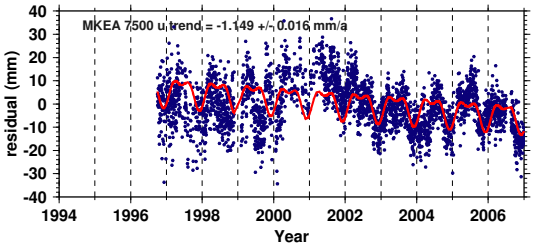

Figure 89: MKEA height time series. Inter-annual.

DOI: 10.2312/GFZ.b103-08037

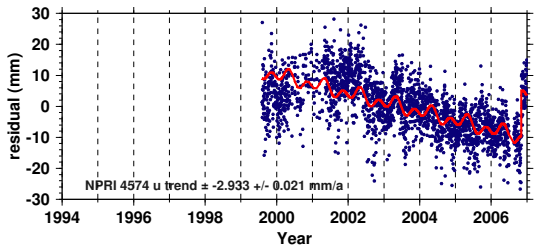

Figure 90: NPRI height time series. Inter-annual.

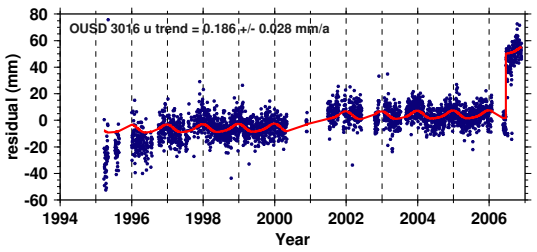

Figure 94: OUSD height time series. Inter-annual, or velocity change.

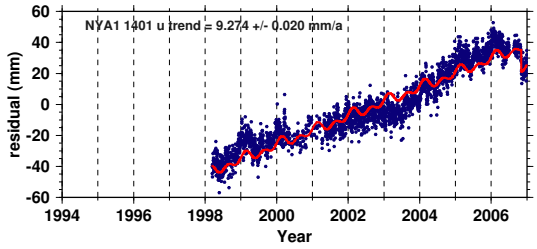

Figure 91: NYA1 height time series. Inter-annual.

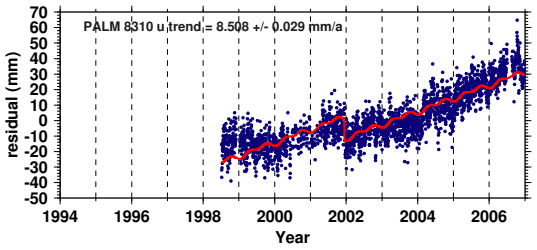

Figure 95: PALM height time series. Inter-annual.

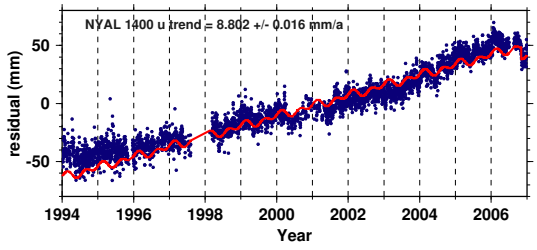

Figure 92: NYAL height time series. Inter-annual, long-term.

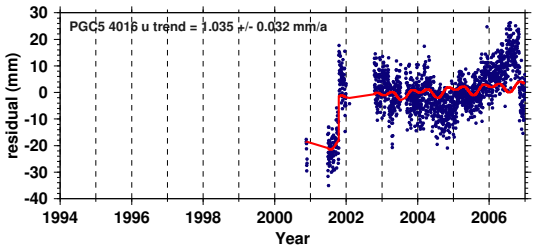

Figure 96: PGC5 height time series. Inter-annual.

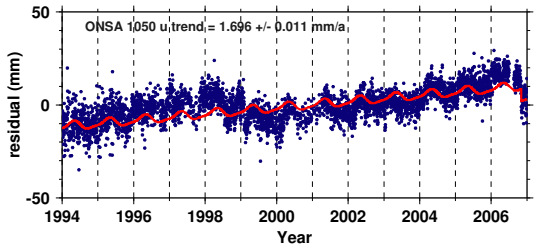

Figure 93: ONSA height time series. Inter-annual, long-term.

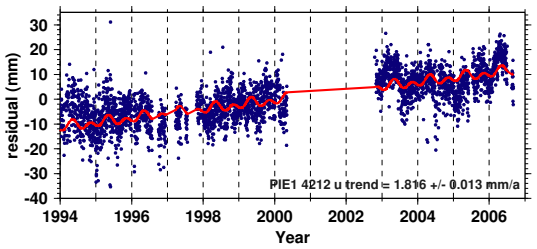

Figure 97: PIE1 height time series. Inter-annual.

DOI: 10.2312/GFZ.b103-08037

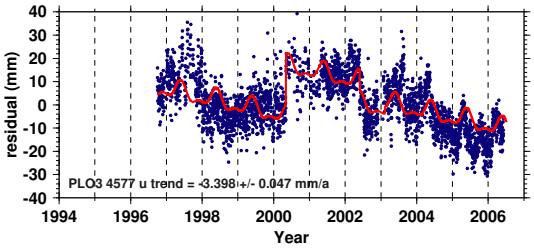

Figure 98: PLO3 height time series. Inter-annual, velocity change.

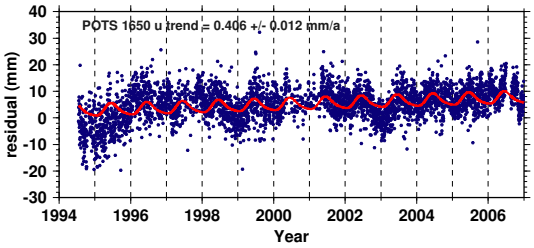

Figure 99: POTS height time series. Inter-annual.

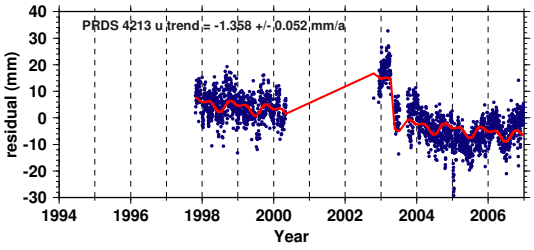

Figure 100: PRDS height time series. Inter-annual.

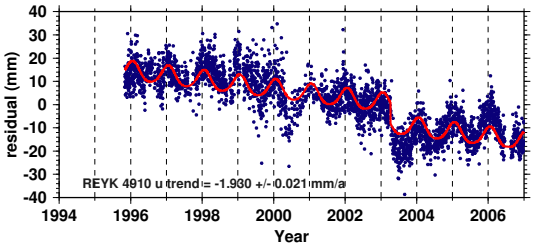

Figure 101: REYK height time series. Velocity change after offset.

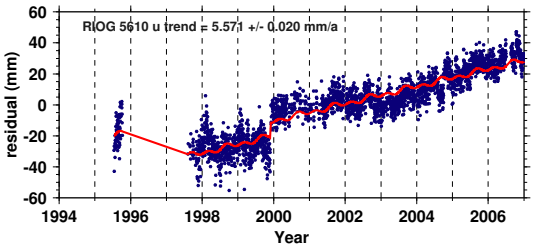

Figure 102: RIOG height time series. Inter-annual, or un-identified offset.

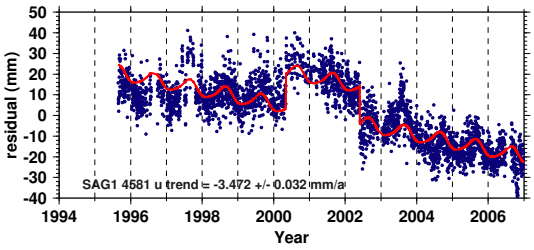

Figure 103: SAG1 height time series. Inter-annual, velocity change, or un-identified offset.

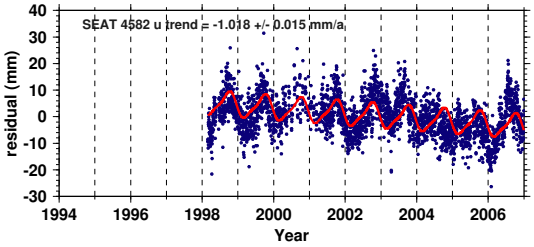

Figure 104: SEAT height time series. Inter-annual, or un-identified offset.

DOI: 10.2312/GFZ.b103-08037

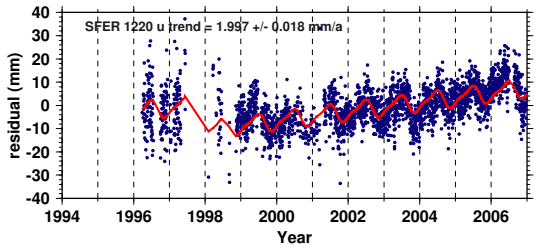

Figure 105: SFER height time series. Inter-annual.

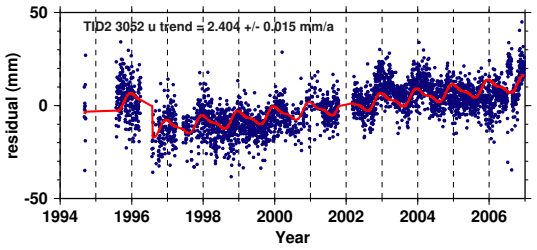

Figure 109: TID2 height time series. Inter-annual.

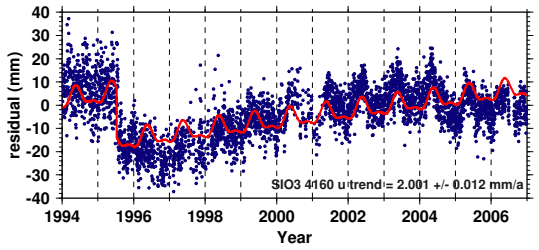

Figure 106: SIO3 height time series. Inter-annual, long-term.

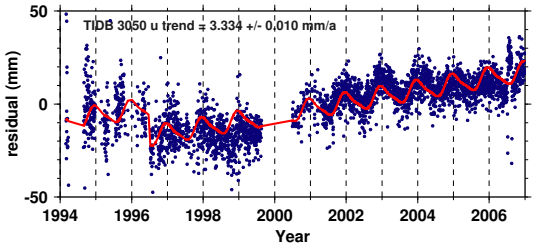

Figure 110: TIDB height time series. Inter-annual, or velocity change after offset.

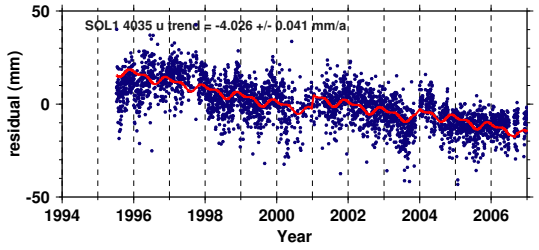

Figure 107: SOL1 height time series. Inter-annual, or un-identified offsets.

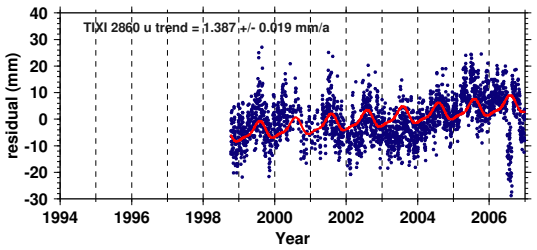

Figure 111: TIXI height time series. Inter-annual, long-term.

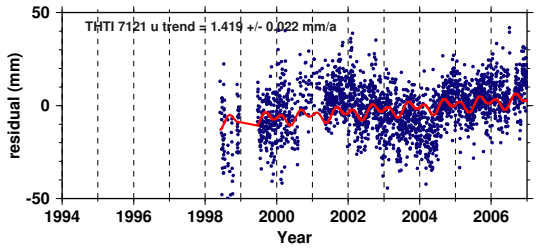

Figure 108: THTI height time series. Velocity change from mid-2000 to mid-2004.

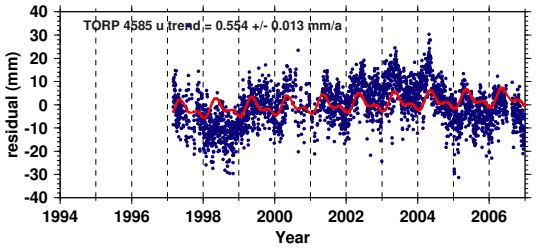

Figure 112: TORP height time series. Inter-annual, long-term.

DOI: 10.2312/GFZ.b103-08037

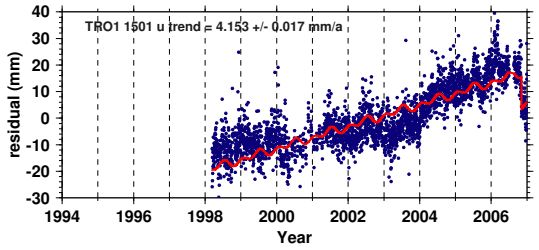

Figure 113: TRO1 height time series. Inter-annual.

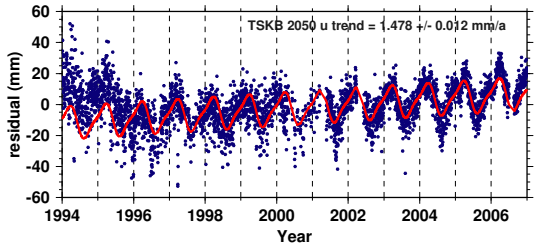

Figure 114: TSKB height time series. Inter-annual.

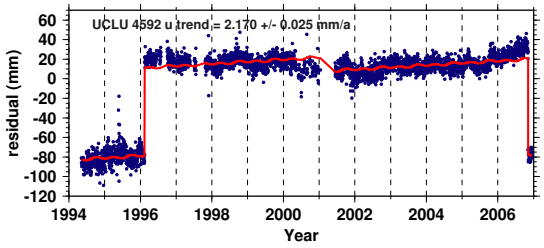

Figure 115: UCLU height time series. Inter-annual.

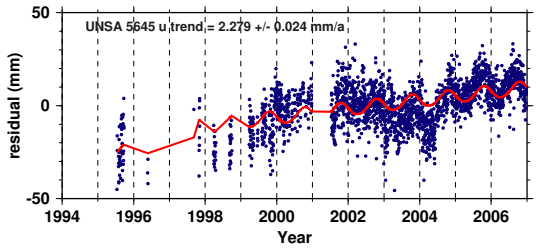

Figure 116: UNSA height time series. Inter-annual.

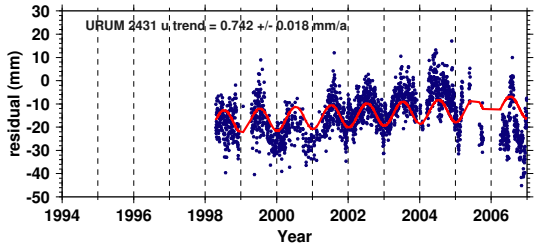

Figure 117: URUM height time series. Inter-annual.

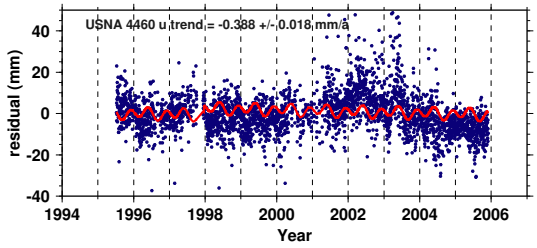

Figure 118: USNA height time series. Inter-annual.

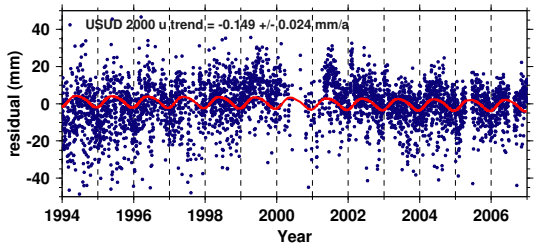

Figure 119: USUD height time series. Inter-annual.

DOI: 10.2312/GFZ.b103-08037

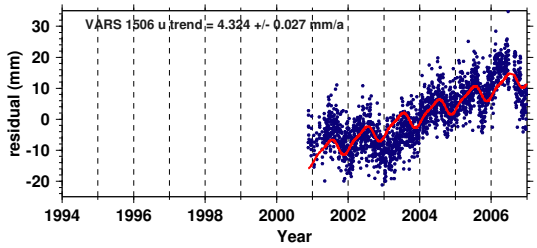

Figure 120: VARS height time series. Inter-annual, velocity (sign) change after 2003.0.

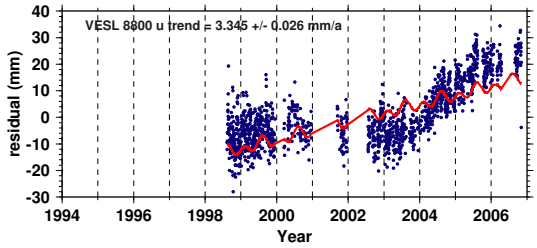

Figure 121: VESL height time series. Inter-annual, velocity change.

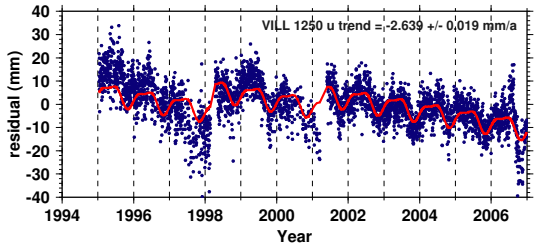

Figure 122: VILL height time series. Three intervals with different subsiding velocities, slower and slower subsidence.

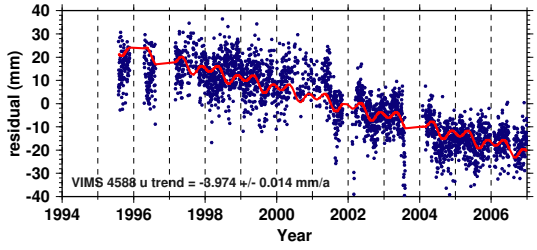

Figure 123: VIMS height time series. Inter-annual.

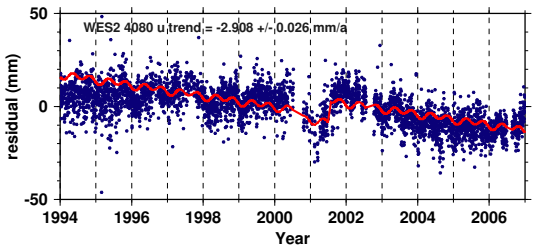

Figure 124: WES2 height time series. Inter-annual, velocity change after mid-2001.

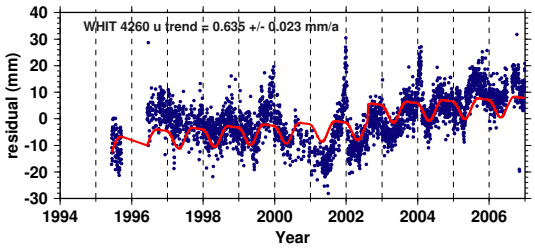

Figure 125: WHIT height time series. Inter-annual, velocity (sign) change after 2001.0.

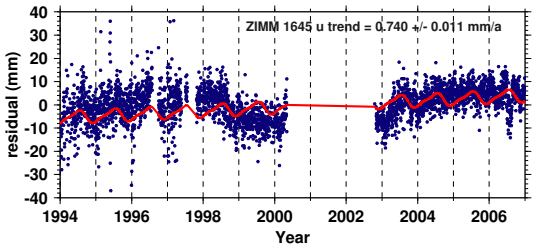

Figure 126: ZIMM height time series. Inter-annual, or un-identified offset.

DOI: 10.2312/GFZ.b103-08037

References

[1] Altamimi, Z., P. Sillard, and C. Boucher, 2002. ITRF2000: A new release of the International Terrestrial Reference Frame for earth science applications. Journal of Geophysical Research, Vol. 107, No. B10, 2214, doi:10.1029/2001JB000561, 2002.

[2] Altamimi, Z., X. Collilieux, J. Legrand, B. Garayt, and C. Boucher, ITRF2005: A new release of the International Terrestrial Reference Frame based on time series of station positions and Earth Orientation Parameters, JOURNAL OF GEOPHYSICAL RESEARCH, VOL. 112, B09401, doi:10.1029/2007JB004949, 2007.

[3] Blewitt, G., An automatic editing algorithm for GPS data. Geophysical Research Letters, Vol. 17, No. 3, p. 199-202, 1990.

[4] Blewitt, G. and D. Lavallée, Effect of annual signals on geodetic velocity. Journal of Geophysical research, Vol. 107, No. B7, 10.1029/2001JB000570, 2002.

[5] Brondeel, M. and T. Willems, Atmospheric pressure loading in GPS height estimates. Adv. Space Res. Vol. 31, No. 8, pp. 1959-1964, 2003.

[6] Cardellach, E., P. Elósegui, and J. L. Davis, Global distortion of GPS networks associated with satellite antenna model errors, JOURNAL OF GEOPHYSICAL RESEARCH, VOL. 112, B07405, doi:10.1029/2006JB004675, 2007.

[7] Crétaux, J.-F., L Soudarin, et al., Seasonal and interannual geocenter motion from SLR and DORIS measurements: Comparison with surface loading data. Journal of Geophysical Research, Vol. 107, No. B12, 2374, doi:10.1029/2002JB001820, 2002.

[8] Dong, D., J. O. Dickey, Y. Chao, and M. K. Cheng, Geocenter variations caused by atmosphere, ocean and surface ground water, Geophysical Research Letters, Vol. 24, No. 15, pp 1867-1870, 1997.

[9] Dong, D., P. Fang, Y. Bock, M. K. Cheng, and S. Miyazaki, Anatomy of apparent seasonal variations from GPS-derived site position time series. Journal of Geophysical Research, Vol. 107, No. B4, 10.1029/2001JB000573, 2002.

[10] Doodson, A. T., The Analysis of Tidal Observations, Phil. Trans. Roy. Soc. Lond., 227, pp. 223 - 279, 1928.

[11] Eanes, R. J. Diurnal and semidiurnal tides from TOPEX/POSEIDON altimetry. Eos Trans. AGU, 75(16):108, 1994.

[12] Egbert, G. D., Bennett, A. F., and Foreman, M. G. G. TOPEX/POSEIDON tides estimated using a global inverse model. J. Geophys. Res., 99(C12):24,821-24,852, 1994.

[13] Farrell, W.E., Deformation of the Earth by surface loads, Rev. Geophys., 10, 761-797, 1972.

DOI: 10.2312/GFZ.b103-08037

[14] Ge, M., G. Gendt, G. Dick, F. P. Zhang, and C. Reigber, Impact of GPS satellite antenna offsets on scale changes in global network solutions. GEOPHYSICAL RESEARCH LETTERS, VOL. 32, L06310, doi:10.1029/2004GL022224, 2005

[15] Ge, M., G. Gendt, G. Dick and F.P. Zhang, Improving carrier-phase ambiguity resolution in global GPS network solutions, Journal of Geodesy, vol 79, No. 1-3, 2005. doi:10.1007/s00190-005-0447-0

[16] Ge, M., G. Gendt, G. Dick, F.P. Zhang and M. Rothacher, A New Data Processing Strategy for Huge GNSS Global Networks, Journal of Geodesy, Vol. 80, No.4, pages 199-203, 2006. doi:10.1007/s00190-006-0044-x

[17] Gendt, G., G. Dick, W. Mai, T. Nischan, W. Sommerfeld, Nutzerhandbuch zum Programmsystem EPOS.P.V2 (Earth Parameters and Orbit determination System) für die Analyse von GPS-daten. GeoForschungsZentrum Potsdam, Bereich "Rezente Kinematik und Dynamik der Erde", February 18, 1994.

[18] Guo, J. Y., 2001, Fundamentals of Geophysics, Publishing House of Surveying and Mapping, Beijing. (in Chinese)

[19] Jacobs, G. A., G. H. Born, M. E. Parke, and P. C. Allen, The global structure of the annual and semiannual sea surface height variability from Geosat altimeter data, J. Geophys. Res., 97, 17,813C 17,828, 1992.

[20] Kostoglodov, V., S. K. Singh, J. A. Santiago, S. I. Franco, K. M. Larson, A. R. Lowry, and R. Bilham, A large silent earthquake in the Guerrero seismic gap, Mexico, Geophys. Res. Lett., 30(15), 1807, doi:10.1029/2003GL017219, 2003.

[21] Lambert, A., S. D. Pagiatakis, A. P. Billyard, and H. Dragert, Improved ocean tide loading correctins for gravity and displacement: Canada and northern United States, J. Geophys. Res., 103, 30,231 - 30,244, 1998.

[22] Lefèvre, F., Lyard, F. H., and Le Provost, C. FES98: A new global tide finite element solution independent of altimetry. Geophys. Res. Letters, 27(17):2717-2720, 2000.

[23] Le Provost, C., Genco, M. L., Lyard, F., Vincent, P., and Canceil, P. Spectroscopy of the world ocean tides from a finite-element hydrodynamic model. J. Geophys. Res., 99(C12):24,777-24,797, 1994.

[24] Le Provost, C., Lyard, F., Molines, J. M., Genco, M. L., and Rabilloud, F. A hydrodynamic ocean tide model improved by assimilating a satellite altimeter-derived data set. J. Geophys. Res., 103(C3):5513-5529, 1998.

[25] MacMillan, D. S., and J. M. Gipson (1994), Atmospheric pressure loading parameters from very long baseline interferometry observations, J. Geophys. Res., 99(B9), 18,08118,087.

DOI: 10.2312/GFZ.b103-08037

[26] Mangiarotti, S., A. Cazenave, L. Soudarin, and J. F. Crtaux (2001), Annual vertical crustal motions predicted from surface mass redistribution and observed by space geodesy, J. Geophys. Res., 106(B3), 42774291.

[27] Matsumoto, K., Takanezawa, T. and Ooe, M. Ocean Tide Models Developed by Assimilating TOPEX/POSEIDON Altimeter Data into Hydrodynamical Model: A Global Model and a Regional Model Around Japan. J. of Oceanog., 56, 567-581, 2000.

[28] Matt King, 2002, comments, http://www.oso.chalmers.se/∼loading/notesncomments.html.

[29] Melchior, P., The tides of the planet Earth, 2nd Ed., Pergamon Press, 1983.

[30] McCarthy, D. D., G. Petit (ed.), 2003, IERS Conventions (2003), IERS Technical Note 32, U.S. Naval Observatory (http://maia.usno.navy.mil/conv2000.html).

[31] NOAA (1988), Digital relief of the Surface of the Earth, Data Announcement 88-MGG-02, NOAA, National Geophysical Data Center, Boulder, Colorado.

[32] http://en.wikipedia.org/wiki/Nyquist-Shannon_sampling_theorem

[33] Pagiatakis, S.D. (1988), "Ocean tide loading on a self-gravitating, compressible, layered, anisotropic, viscoelastic and rotating earth with solid inner core and fluid outer core," Technical Report No. 139, Dept. of Surveying Engineering, University of New Brunswick, Fredericton, Canada.

[34] Pagiatakis, S.D. (1990), "The response of a realistic earth to ocean tide loading," Geophysical Journal International, 103, 541-560.

[35] Parke, M. E., R. H. Stewart, and D. L. Farless, On the choice of orbits for an altimetric satellite to study ocean circulation and tides, Journal of Geophysical Research, Vol. 92, No. C11, pages 11,693-11,707, 1987.

[36] Penna, N. T., and M. P. Stewart, Aliased tidal signatures in continuous GPS height time series, Geophys. Res. Lett., 30(23), 2184, doi:10.1029/2003GL018828, 2003.

[37] Petrov, L., J.-P. Boy, Study of the atmospheric pressure loading signal in VLBI observations, Journal of Geophysical Research, 10.1029/2003JB002500, Vol. 109, No. B03405, 2004.

[38] Petrov, L., and C. Ma, Study of harmonic site position variations determined by very long baseline interferometry, J. Geophys. Res., 108(B4), 2190, doi:10.1029/2002JB001801, 2003.

[39] Press, W. H., S. A. Teukolsky, W. T. Vetterling, and B. P. Flannery, "§14.5 Linear Correlation" in Numerical Recipes in C++, The Art of Scientific Computing, 2nd Ed. Cambridge, England: Cambridge University Press, pp.641, 2002.

DOI: 10.2312/GFZ.b103-08037

[40] Ray, R. D. A Global Ocean Tide Model From TOPEX/POSEIDON Altimetry: GOT99.2. NASA Technical Memorandum 209478, 1999.

[41] Rabbel, W. and J. Zschau, Static deformations and gravity changes at the earth's surface due to atmospheric loading, J. Geophys., 56, 81-99, 1985.

[42] Schmid, R., M. Rothacher, Estimation of elevation-dependent satellite antenna phase center variations of GPS satellites, Journal of Geodesy, in press.

[43] T. Schueler, On Ground-Based GPS Tropospheric Delay Estimation, Schriftenreihe, Studiengang Geodaesie und Geoinformation Universitaet der Bundeswehr Muenchen, ISSN: 0173-1009, Neubiberg, pages 72-74, 2001.

[44] Van Dam, T. M., G. Blewitt, M. B. Heflin, Atmospheric pressure loading effects on Global Positioning System coordinate determinations, J. Geophys. Research, Vol. 99, No. B12, Pages 23,939-23,950, 1994.

[45] Van Dam, T. M. and J. M. Wahr, Displacement of the Earth's Surface Due to Atmospheric Loading: Effects on Gravity and Baseline Measurements. Journal of Geophysical Research, Vol.92, No.B2, Pages 1281-1286, 1987.

[46] Van Dam, T. M. and and J. Wahr, Modeling Environment Loading Effects: a Review, Phys. Chem. Earth, Vol. 23, No. 9-10, pp. 1077-1087, 1998.

[47] van Dam, T., J. Wahr, et al., Crustal displacements due to continental water loading. Geophysical Research Letters, Vol. 28, No. 4, Pages 651-654, 2001.

[48] Wolf, D., V. Klemann, J. Wünsch and F.-P. Zhang, A Reanalysis and Reinterpretation of Geodetic and Geological Evidence of Glacial-Isostatic Adjustment in the Churchill Region, Hudson Bay. Surveys in Geophysics, 27:19-61, 2006. DOI 10.1007/s10712-005-0641-x

[49] Zhang, F.-P., D. Dong, et al, Seasonal vertical crustal motions in China detected by GPS. Chinese Science Bulletin, Vol.47, No.21, page1772-1779, 2002.

[50] Zhang, F.-P., G. Gendt, M.-R. Ge, GPS data processing at GFZ for monitoring the vertical motion of global tide gauge benchmarks, – technical report for projects TIGA and SEAL, GFZ-STR 07/02, GeoForschungsZentrum Potsdam, 2007.

[51] Zhang, J., Continuous GPS measurements of crustal deformation in southern California, Ph. D. dissertation, Univ. of Calif., San Diego, 1996.

[52] Zhu, S.Y., F.-H. Massmann, Y. Yu, Ch. Reigber, Satellite antenna phase center offsets and scale errors in GPS solutions, Journal of Geodesy, 76, 668-672, 2003.

DOI: 10.2312/GFZ.b103-08037